A&A 414, 235–243 (2004)
DOI: 10.1051/0004-6361:20031637

Astronomy & Astrophysics

Observations of hydroxyl ground state transitions in a complete sample of methanol sources⋆,⋆⋆

M. Szymczak[1] and E. Gérard[2]

[1] Torun Centre for Astronomy, Nicolaus Copernicus University, Gagarina 11, 87-100 Toruń, Poland
[2] GEPI, UMR 8111, Observatoire de Paris, 5 place J. Janssen, 92195 Meudon Cedex, France

Received 6 June 2003 / Accepted 1 October 2003

Abstract. High sensitivity observations of all four transitions of the ground state $^2\Pi_{3/2}$, $J = 3/2$ of OH in both senses of circular polarization have been carried out with the Nançay radio telescope. The sample was a set of 100 star forming regions detected in a recent unbiased survey of 6668 MHz CH_3OH masers. OH maser emission was found in 55 objects of which 31 were not previously catalogued. The 1665 MHz line was seen in almost all OH maser sources and was accompanied by the 1667 MHz line in about 75% of cases. Respectively 7% and 11% of OH 1665 MHz masers were accompanied by maser lines at 1612 and 1720 MHz. These two satellite line masers never occurred simultaneously in the same source nor at the same radial velocity, suggesting mutually exclusive physical conditions as predicted by models. OH maser emission usually shared the same velocity range as the 6668 MHz CH_3OH maser. The intensity ratio of the 6668 MHz and 1665 MHz lines clearly divides the sample into methanol- and hydroxyl-rich sources and could be controlled by the abundance of maser molecules and the kinetic temperature. The OH maser emission was substantially polarized with a mean fractional circular polarization of 0.30 and Zeeman pair candidates were found in 15 targets. 36 sources were found in OH absorption at the main lines and 24 of them were also accompanied by OH maser emission. OH absorption features were blueshifted with regard to the related OH masers, indicating that they were formed in front of the central continuum sources. Absorption at 1720 MHz was always accompanied by emission at 1612 MHz and vice versa. The behaviour of stimulated emission and absorption in both satellite lines was thus conjugated and the 1720 MHz emission features seem to be signatures of regions of low hydrogen density and OH column density. The correlation of OH and CH_3OH flux densities with the IRAS flux densities found for our sample appears to support pumping schemes of both molecules by infrared photons. Statistics of masers in the sample appear to be consistent with the scenario that the CH_3OH masers appeared earlier than the OH masers.

Key words. masers – surveys – stars: formation – ISM: molecules – radio lines: ISM – HII regions

1. Introduction

Since its discovery more than three decades ago, OH maser emission from the ground state transitions is a widely used tool to study the environments of ongoing or recently formed massive stars. The most extensive survey of all four 18 cm OH lines near the Galactic plane with various sampling densities, different areas and targeted to specific objects was carried out by Turner (1979). Subsequent systematic surveys of the main line OH masers in the Galactic plane extended to weaker sources of the southern sky (Caswell & Haynes 1983a, 1983b). Those surveys provided a large data set which revealed a close association of OH masers with other signs of star formation such as compact HII regions, infrared objects, and masers of other species.

An efficient way to search for OH masers was revealed with the release of IRAS all sky data. Observations of IRAS-selected ultra compact HII region candidates were successful in obtaining a more complete set of OH masers (Cohen et al. 1988; Moore et al. 1988; Slysh et al. 1994, 1997) and supported a far infrared pumping scheme of the main lines.

The detection of a very strong and widespread CH_3OH maser line at 6668 MHz (Menten 1991) has allowed more efficient investigation of star formation sites. The data sets resulting from various surveys of the 6668 MHz masers offered more complete samples of targets for OH maser studies (Gaylard et al. 1994; Szymczak & Kus 2000). Caswell (1997) suggested that CH_3OH masers probe the environment of young stars in a somewhat earlier phase than OH masers, so it follows that observations of OH lines arising from CH_3OH sources can be important for building a more general picture of maser properties and hosting sites.

Send offprint requests to: M. Szymczak,
e-mail: msz@astro.uni.torun.pl

⋆ Figure A1 is only available in electronic form via http://www.edpsciences.org

⋆⋆ Tables 1, 2, 4 are only, and Table 3 also, available at the CDS via anonymous ftp to cdsarc.u-strasbg.fr (130.79.128.5) or via http://cdsweb.u-strasbg.fr/cgi-bin/qcat?J/A+A/414/235

Unbiased surveys of the 6668 MHz CH_3OH masers (Caswell 1996; Ellingsen et al. 1996; Szymczak et al. 2002) significantly improved statistics on sites of star formation, providing excellent lists of targets for further observations. In this paper we report on the OH survey of a sample of CH_3OH masers detected in a blind survey of a 21 deg^2 region in the Galactic plane (Szymczak et al. 2002). Our aims are to derive the detection rate and to depict properties of all four ground state OH transitions. The OH data obtained allow us to diagnose the physical conditions in the environments of the target sites. Additionally this study provides some constraints for pumping schemes proposed for CH_3OH, notably the recent model by Cragg et al. (2002, hereafter CSG02). This investigates the conditions under which CH_3OH and OH masers can arise together from the same region, and the implications if only certain combinations of the possible lines are seen.

2. Observations

The measurements were carried out using the upgraded Nançay radio telescope (van Driel et al. 1996) from October 2001 to March 2002. At 18 cm the instrument had a half-power beamwidth of 3.′5 in the E−W direction and 19′ in the N−S direction. The beam efficiency was 0.65, the point source efficiency at $\delta = 0°$ was 1.4 K Jy^{-1} and the system temperature was about 35 K. All four transitions of the ground OH state ($^2\Pi_{3/2}$, $J = 3/2$) were observed simultaneously in both orientations of circular polarization using a 8192 channel autocorrelator configured into eight banks of 1024 channels. Each bank had a bandwidth of 1.5625 MHz yielding velocity resolutions of 0.284, 0.275, 0.274 and 0.266 km s^{-1} at 1612, 1665, 1667 and 1720 MHz, respectively. The total useful velocity coverage was about ±140 km s^{-1}. The radial velocities were measured with respect to the local standard of rest. The spectral bandwidth was centred at the middle velocity of the 6668 MHz CH_3OH emission range of each target. Spectra of each source were taken in the frequency switching mode with an integration time of about 18 min. A typical 1σ noise level for a single polarization was about 40 mJy. The data were calibrated by comparison observations of W12 and W3OH and the absolute flux density was determined with an accuracy better than 10%.

The sample of targets was a set of 100 CH_3OH sources found by Szymczak et al. (2002) in an unbiased survey for 6668 MHz maser emission. That survey was restricted to the Galactic plane between $20° \leq l \leq 40°$ and $|b| \leq 0.°52$, providing a large complete sample of young star forming regions.

3. Results

Tables 1 and 2 list the sources detected in the main and satellite OH lines, respectively. These tables and further discussion only refer to those features that appeared at velocities that differ by less than 5 km s^{-1} from the velocity range of 6668 MHz CH_3OH maser emission (Szymczak et al. 2002). This criterion results from observations; the typical velocity extent of previously known OH and CH_3OH masers in star forming regions is about 10 km s^{-1} (Caswell et al. 1995). OH emission and absorption of those objects in our sample which do not meet this criterion appear to come from objects unrelated to the CH_3OH sources. The first two columns of Tables 1 and 2 give the source name and date of observation. The line properties derived from the I Stokes parameter spectra are the velocity interval at zero intensity ΔV (all velocities in km s^{-1}) over which OH emission was detected, the centre V_c of this interval, the velocity V_p and the flux density S_p (in Jy) of the strongest feature and the integrated flux density S_i (in Jy km s^{-1}). The 3σ noise level is given when no line was detected. A rich variety in the polarization characteristics of OH emission can be seen in the spectra themselves, while only the degree of circular polarization $m_c = (S_i(R) - S_i(L))/(S_i(R) + S_i(L))$ is given in Tables 1 and 2. Here $S_i(L)$ and $S_i(R)$ is the integrated flux density in left and right circular polarization, respectively. The degree of polarization is omitted for absorption and/or quasi-thermal emission features as they are unpolarized within the noise limits. The known OH sources are labelled to show where they were published. The spectra of most known sources, taken about twenty years ago, were published by Caswell & Haynes (1983b) and usually look very different from ours. Thus, we make the complete set of OH spectra available in electronic form (Fig. A1) in the whole velocity range observed. The spectra are the left-handed and right-handed circular polarization at 1612, 1665, 1667 and 1720 MHz, respectively, from top to bottom. Note that along the lines of sight towards several target sources there are several absorption and likely quasi-thermal emission features as well as the characteristic OH/IR star profiles seen at 1612 MHz (e.g. the source G20.08−0.14 in Fig. A1) unrelated to the CH_3OH sources. For the features related to the CH_3OH sources the velocity centroid of the Gaussian fitted line profile was measured rather than V_p determined for the OH maser emission. V_p is equal to V_c for almost all the non-maser lines. About 73% of entries in Table 1 and possibly all entries in Table 2 were not previously catalogued.

3.1. Variety of spectra

The spectra of representative sources are shown in Fig. 1. The source 24.79+0.09 shows the OH maser emission at both main lines superimposed on the broad and weak absorption feature centred near 109 km s^{-1}. At a similar velocity the satellite lines at 1612 and 1720 MHz show emission and absorption, respectively. There are 13 sources in our sample that exhibit such a morphology of OH emission and similarly 4 other sources but with absorption and emission at 1612 and 1720 MHz, respectively. In the group of sources typified by 24.79+0.09 the 6668 MHz CH_3OH maser coincides in velocity with the OH maser and quasi-thermal profiles.

The source 30.76−0.05 is typical of a group of 6 sources in the sample where the OH main line masers are superimposed on a deep and broad absorption profile (Fig. 1). The two satellite lines show conjugate behaviour. The 1612 MHz line shows absorption at velocities slightly blueshifted from the main line masers, while the 1720 MHz line shows emission. At redshifted velocities with respect to the absorption peak at main lines, the 1612 MHz line is seen in emission, while the 1720 MHz line in absorption. Generally, the two satellite lines have different

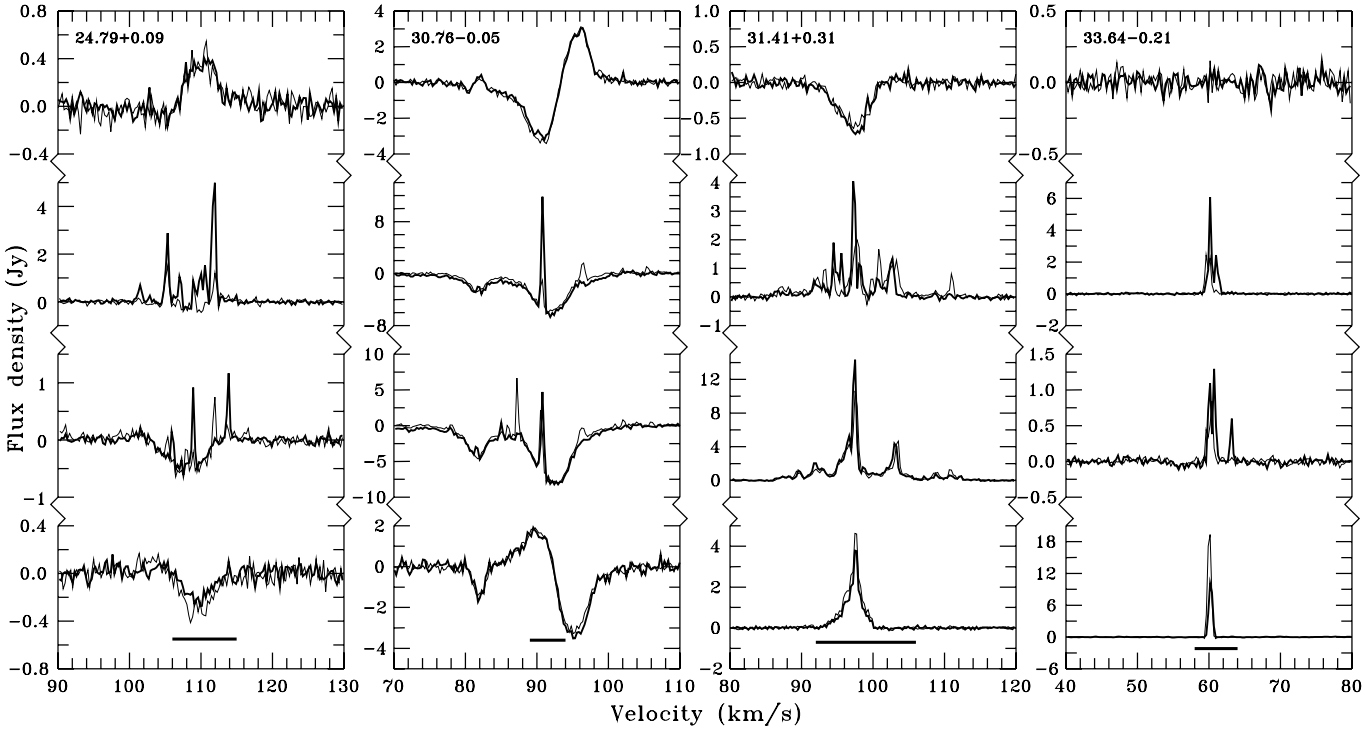

Fig. 1. OH spectra of the four selected sources 24.79+0.09, 30.76−0.05, 31.41+0.31 and 33.64−0.21. The ground state transitions at 1612, 1665, 1667 and 1720 MHz are shown from top to bottom. Light lines indicate left circularly polarized emission and heavy lines right circularly polarized emission. Horizontal bars above the velocity axis mark the ranges of the CH_3OH 6668 MHz maser emission as observed by Szymczak et al. (2002).

absolute intensities. The 6668 MHz CH_3OH maser emission is commonly centred at a transition velocity from 1720 MHz to 1612 MHz emission.

The 1612 MHz line of the source 31.41+0.31 is seen in absorption (Fig. 1). The 1720 MHz profile appears to be a superposition of narrow maser emission and broad quasi-thermal emission coinciding in velocity with the 1612 MHz absorption profile. Broad multi-feature spectra are observed in both OH main lines without any obvious absorption feature. The CH_3OH maser at 6668 MHz coincides well in velocity with the OH profiles.

The source 33.64−0.21 is typical for objects without the 1612 MHz line and without the absorption features at the OH main lines (Fig. 1). Strongly circularly polarized maser emission occurs at the main lines and 1720 MHz. The velocity interval of the 6668 MHz maser is the same as for the OH lines.

3.2. Detection rates

OH ground state masers were found at 55 of the 100 CH_3OH maser sites. 31 OH masers were found for the first time. A summary of the occurrence of maser lines is given in Table 3. The 1665 MHz maser occurs almost always (96%) in all OH sources studied and is accompanied at nearly 74% of sites by the 1667 MHz maser. Masers at 1720 MHz are detectable in 11% of 1665 MHz maser objects and occur only where both 1665 and 1667 MHz lines are also seen. The 1612 MHz masers are observed in 9% of OH sources and are usually accompanied by the main line masers. No objects are found with simultaneous maser emission or absorption at both satellite lines at the same velocity.

Table 3. Number of maser sources in the sample depending on the presence (+) and absence (−) of four OH transitions.

1612	+	+	+	−	−	−	−
1665	−	+	+	+	+	−	+
1667	−	−	+	−	+	+	+
1720	−	−	−	−	−	−	+
Frequency	1	3	1	11	32	1	6
(MHz)	Number of sources						

36 objects were detected in absorption in the main lines and 24 of them were also accompanied by maser emission (Table 1). 30 objects were detected in absorption in either satellite line and only 5 of them were possibly accompanied by maser emission (Table 2). No OH maser emission nor absorption and quasi-thermal emission features were detected towards 31 targets (Table 4).

3.3. Characteristics of OH maser lines

The OH maser velocity extent ranges from 1 to 26 km s^{-1} with the median values of 8.3 and 8.8 km s^{-1} at 1665 and 1667 MHz, respectively. On average the velocity range of both satellite OH maser lines is about a factor of four narrower than that for the main maser lines. The 6668 MHz CH_3OH maser emission in the sample studied extends from 1 to 20 km s^{-1}

(Szymczak et al. 2002) and the median velocity interval of 8.0 km s^{-1} is comparable to that observed for OH main lines.

On average, for 53 maser sources found in the 1665 MHz line, V_c differs from that at 6668 MHz only by -0.5 ± 4.1 km s^{-1}. The largest differences in V_c of both species are seen for sources 23.19−0.38 (-10.8 km s^{-1}) and 32.74−0.08 ($+11.2$ km s^{-1}).

The brightest source in our sample is 34.25+0.16 with S_p equal to 75 and 95 Jy at 1665 and 1667 MHz, respectively. The weakest source visible at both main lines is 23.49+0.08 (0.35 and 0.20 Jy respectively). The median peak flux density of 53 objects detected in 1665 MHz is 1.2 Jy, while that of 40 sources of 1667 MHz maser is 0.7 Jy. The latter value is very similar to the median S_p of the 1720 MHz masers. The 1612 MHz masers of median $S_p = 0.4$ Jy belong to the group of the weakest OH sources in the sample. The integrated flux densities follow the above described trends.

The great majority of the masers have the 1667 MHz emission weaker than the 1665 MHz emission. The median ratio of S_i of 1667 MHz and 1665 MHz is 0.45 for the 39 sources. The quartiles are at 1.0 and 0.23, i.e. there are 9(25%) objects for which S_i at 1667 MHz is greater than that at 1665 MHz, and 10(25%) objects with the 1667 MHz flux density weaker than 0.23 times the 1667 MHz flux density. The extreme low and high ratios are 0.016 (35.02+0.35) and 3.50 (31.41+0.31).

In order to estimate the intensity ratio of methanol and hydroxyl we have used the 6668 MHz CH_3OH data (Szymczak et al. 2002) obtained about half a year before the OH data presented here. The sum of S_i in all OH lines is taken into ratio $S_i(CH_3OH)/S_i(OH)$. For the sample of 55 sources with both CH_3OH and OH detected the median ratio is 10.7 with the quartiles at 34.2 and 4.6. This ratio is greater than 100 and lower than 1 for 7 and 6 sources, respectively. The source 36.11+0.55 belongs to the first group of methanol-rich sources and has the highest ratio 730. The source 20.08−0.14 is a member of the second group of hydroxyl-rich objects having the extremely low ratio 0.05. We notice that our estimate of the median intensity ratio of CH_3OH and OH is about 2 times higher than that obtained by Caswell et al. (1995). A plausible cause is a difference in sensitivity limits of OH and CH_3OH surveys. OH observations reported here are about one order of magnitude more sensitive than the 6668 MHz CH_3OH unbiased survey (Szymczak et al. 2002). Indeed, when we restrict the sample to the 28 OH sources with a peak flux density greater than 1.6 Jy, which corresponds to a 3σ detection level in the unbiased CH_3OH survey, then the median value of $S_i(CH_3OH)/S_i(OH)$ is 5.2. This agrees well with Caswell's et al. estimate.

3.4. Polarization properties

In the sample studied there are several OH masers which show considerable circular polarization (Tables 1 and 2). At 1667 MHz the degree of circular polarization m_c increases with a decrease in S_i. In contrast, at 1665 MHz no obvious relation between m_c and S_i is seen. Therefore, one can expect that at this frequency a statistical analysis of the polarization degree is not strongly biased by that effect. The median value of $|m_c|$ is 0.30 for 53 1665 MHz sources. The quartiles are at 0.51 and 0.17. There are 13 objects with $|m_c| \geq 0.55$. Two sources 23.44−0.18 and 31.27−0.08 exhibit high fractional circular polarization ($|m_c| > 0.8$) being relatively strong emitters with S_i of 3.9 and 9.7 Jy km s^{-1}, respectively.

Table 5. Possible Zeeman patterns.

Sources	Line (MHz)	V_c (km s^{-1})	Field (mG)
20.08−0.14	1667	41.76	−4.3
		46.70	−4.1
20.24+0.07	1665	71.83	−0.5
		73.23	−0.5
		75.31	−1.2
	1720	74.55	+3.0
21.87+0.01	1665	20.95	+2.9
22.34−0.16	1665	25.15	+0.3
22.35+0.06	1667	78.39	+0.6
23.01−0.41	1667	74.31	−0.2
23.26−0.24	1665	57.22	+3.8
30.76−0.05	1665	90.84	−0.3
	1667	90.79	−0.8
30.89+0.17	1667	107.18	+0.8
32.05+0.06	1665	92.10	−0.6
	1667	92.43	−0.6
32.74−0.08	1720	36.38	−1.3
32.98+0.04	1665	79.48	+0.3
33.64−0.21	1720	60.23	−1.0
34.25+0.16	1667	58.33	+0.6
35.79−0.17	1665	59.41	−4.2
	1667	59.45	−3.7

In our data we found sources with left and right circularly polarized features well separated in velocity. It is possible that some of those are Zeeman pairs. If features of opposite polarization come from the same spatial location then the velocity separation provides a direct measure of the component of the magnetic field in the maser region parallel to the line of sight. Table 5 lists the maser sources with possible Zeeman patterns and the field intensity estimates assuming that a 1 mG magnetic field produces velocity splittings of 0.59, 0.35, and 0.23 km s^{-1} at 1665, 1667, and 1720 MHz, respectively (see Davis 1974). The absolute field intensity along the line of sight ranges from 0.3 to 4.3 mG. The latter value is typical for the Galactic star forming regions (Reid & Silverstein 1990). The source 23.26−0.24 is a prominent example of object with the magnetic field of 3.8 mG and large fractional polarization of 0.55 at 1665 MHz. In the group of 15 objects there is neither a preference for the field direction towards nor away from the observer. Our candidate Zeeman pairs need to be confirmed by high angular resolution observations to check whether opposite circularly polarized components spatially coincide. Single telescope data (Table 5) can be a guide to select suitable targets for detailed studies.

3.5. OH absorption

44 sources in the sample are accompanied by absorption at main and/or satellite OH transitions at a velocity differing from the central velocity of the 6668 MHz CH_3OH maser emission by less than 5 km s^{-1}. The main OH lines dominate in absorption sources; 28 sources are seen in both main lines and 8 sources only in the 1667 MHz line. There are 30 objects accompanied by absorption at one of the satellite lines, 5 of them are only seen at one satellite line. We note that the satellite lines 1612 and 1720 MHz always behave complementarily to each other; if one shows emission the other is seen in absorption.

24 out of 36 absorption main line objects exhibit maser emission. The average width of absorption features at 1665 MHz of 14.3 ± 1.8 km s^{-1} is by 5.8 km s^{-1} larger than the average velocity interval of maser emission. The central velocity of absorption features are blueshifted with regard to that of the maser emission by 2.0 ± 1.2 km s^{-1} at 1665 MHz and by 3.8 ± 1.1 km s^{-1} at 1667 MHz.

In some of our sources, especially those with noisy spectra, the ratio of absorption depth at 1667 and 1665 MHz, R_m, depends on whether the flux density or the integrated flux density is used. In the analysis below we discuss the ratio taken as the mean of both values. This ratio ranges from 0.82 to 2.36 with the average value of 1.30 ± 0.09 for 20 objects with absorption at main and satellite lines. Only the source 31.06+0.09 has R_m close to 1.78 together with the intensity ratios 1665/1612 and 1667/1612 close to 6.3 and 10.2, respectively. These ratios are close to those expected for thermally excited optically thin OH transitions. In this case one can use the intensity ratios to derive the OH column density N_{OH} (Magnani et al. 1988, and reference therein). For the width of absorption feature at half intensity 3.6 and 3.2 km s^{-1} at 1665 and 1667 MHz respectively, we obtained $N_{OH} = 1.2 \times 10^{15}$ cm^{-2}. This value is similar to, or even slightly higher than, typical OH column densities estimated towards molecular clouds with continuum sources (Colgan et al. 1989).

In our sample there are two further sources, 23.19−0.38 and 23.44−0.18, with R_m equal to 1.32 and 1.50 respectively, and with the ratios of the main line to the satellite line deviating only by a factor of 2–3 from those expected for thermal excitation. However, the satellite lines exhibit conjugate S-shaped patterns with emission/absorption and it is unlikely that these are thermally excited OH lines. For the remaining sources in the sample the ratios of absorption depths are very different from the LTE value. We conclude that most (about 90%) CH_3OH sources at 6668 MHz accompanied by absorption features are possibly embedded in clouds where OH molecules are non thermally excited and the estimation of N_{OH} from the main line ratios can no longer be applied.

4. Properties of target sites

4.1. Location of OH and CH_3OH masers

As shown in Sect. 3.3 the OH and CH_3OH maser spectra in the sample are confined to a very similar velocity interval. It is therefore likely that both masers arise in close proximity, even if they do not arise in exactly the same volume of gas surrounding the newly formed star. This appears to be consistent with results of VLBI observations of the archetypical ultra compact HII region W3(OH) which showed that the general distribution of the 6668 MHz masers closely resembles that of the 1665 MHz masers (Menten et al. 1992). Caswell (1996) also reported the position coincidence of the CH_3OH and OH masers for about 80% of sources in his sample resulting from a blind search for 6668 MHz emission.

21 sources in our sample were observed in the CS (2−1) line by Bronfman et al. (1996). This thermal emission, being a tracer of high density gas, usually associated with embedded ultra compact HII regions, provides a reliable estimate of the systemic velocity. For 17 out of 21 sources the central velocity of the CH_3OH maser emission (11 sources are also OH masers) is confined to less than 4 km s^{-1} around the velocity of the CS peak, while for the remaining 4 sources: 30.82+0.27, 32.98+0.04, 35.02+0.35 and 38.12−0.24 it is as different as 10 km s^{-1}. This suggests that most CH_3OH and OH masers probably originate from the inner part of the cloud surrounding a central star. For a minority of the sources the maser emission of both molecules can arise in outflows. However, given a large uncertainty of position of the maser sources of about 30″ we cannot exclude, for these four objects, the possibility that the masers arise from objects different from those observed in the CS line.

4.2. Physical parameters

There are few objects in the sample that were observed in the CS lines (e.g. Olmi & Cesaroni 1999; Beuther et al. 2002) and their properties are discussed here in order to constrain the CSG02 model. This model deals with the origin of masers in OH and CH_3OH under identical conditions in regions of high-mass star formation.

Sources 29.95−0.02, 31.41+0.31 and 34.25+0.16 are common to Olmi & Cesaroni's sample and ours. For these targets they derived the density of molecular hydrogen gas n_{H_2} of $0.6-1.1 \times 10^6$ cm^{-3} (their Table 6) and the hydrogen column density of about 10^{24} cm^{-2} (their Table 7). These estimates generally agree with values derived for sources 22.35+0.06 and 32.98+0.04 (Beuther et al. 2002, their Table 3) assuming a CS abundance relative to hydrogen of $10^{-8}-10^{-9}$. We note that n_{H_2} derived from CS data falls in the lower limit of the gas density range required in the CSG02 model for the 6668 MHz CH_3OH and 1665 MHz OH masers.

Our estimate of N_{OH} from the absorption depth ratio at 1665 and 1667 MHz for source 31.06+0.09 (Sect. 3.5) of 1.2×10^{15} cm^{-2}, if typical for our sample, implies a fractional abundance of OH molecules of $10^{-8}-10^{-9}$. This agrees well with the minimum value of fractional abundance of $10^{-8.5}$ for OH which leads to an OH maser with a brightness temperature $T_b > 10^4$ K (CSG02). In the CSG02 model the brightest OH masers ($T_b = 10^{11}$ K) require an OH fractional abundance of $10^{-5}-10^{-6}$. Such high values can be easily reached due to evaporation of icy grain mantles (Hartquist et al. 1995).

There are six sources in our sample identified with IRAS counterparts that are also included in a sample of high-mass

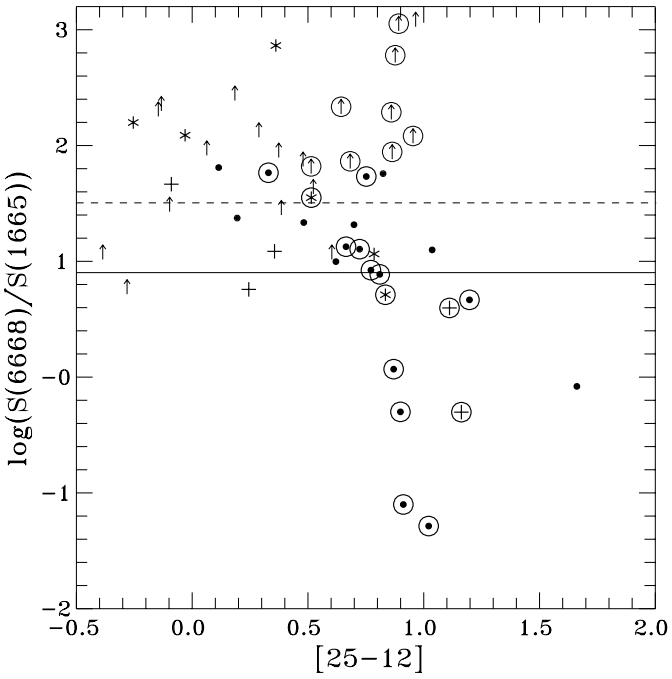

Fig. 2. Ratio of the integrated flux density for CH_3OH 6668 MHz and OH 1665 MHz lines versus [25−12] IRAS colour. The sources with 1720 MHz (crosses), 1665 and 1667 MHz (dots), only with 1665 MHz (stars) are shown. Upper limits for the ratio for sources with only the CH_3OH emission are marked by arrows. Circled symbols represent objects with well determined colour. The masers above the dashed line are methanol-rich, while those below the solid line are hydroxyl-rich.

protostellar candidates studied by Sridharan et al. (2002). They showed that the IRAS data supplemented by the 1.2 mm dust observation can be well reproduced by two component grey bodies. The temperature of the cold dust component which can represent a less evolved outer environment of young stars ranges from 23 to 65 K. The hot dust component which possibly represents a more evolved inner environment of the central object has a temperature ranging from 123 to 204 K.

The hot dust temperature estimate essentially relies on the flux densities at 12 and 25 μm. Figure 2 shows the ratio of the maser intensity versus [25−12] colour[1] for all 52 sources (22 sources without the OH maser emission) in the sample with IRAS counterparts within a radius of less than 58″. Note that there are 23 sources with high quality IRAS measurements (flags 3 and 2) at 12 and 25 μm, so that their colour can be well determined and we only consider those in the following discussion. The ratio R_m of the integrated flux density at 6668 and 1665 MHz maser transitions slightly increases with colour. For 9 OH objects called hydroxyl-rich with $R_m < 8$ (Caswell et al. 1995; CSG02) the mean colour is 0.98 ± 0.05, while for 6 OH objects with intermediate and methanol-rich ($R_m > 32$) ratios the mean colour is 0.62 ± 0.07. For 8 CH_3OH sources without OH masers the mean colour is 0.78 ± 0.05 being intermediate between those of the two groups of OH masers discussed. A significant increase of R_m with the dust temperature is generally predicted in the CSG02 model for the high kinetic temperature T_k regime. The appearance of either maser at 1665, 1667 and 1720 MHz, or the 1665 MHz alone, in a similar range of dust temperatures, can be explained by differences in T_k. For the three sources from the Olmi & Cesaroni (1999) sample, T_k shows a large scatter from 100 to 250 K (Kurtz et al. (2000).

[1] Colour is defined as $[\lambda_i - \lambda_j] = \log(S(\lambda_i)/S(\lambda_j))$, where $S(\lambda_i)$ and $S(\lambda_j)$ are the IRAS flux densities at wavelengths λ_i and λ_j.

5. Discussion

5.1. Maser occurrence and flux ratios

The present observations show that 55% of CH_3OH maser sites in the sample are accompanied by OH masers. This detection rate is broadly consistent with a 44% rate inferred by Caswell (1996) for southern hemisphere sources. However, our detection rate is biased by a sensitivity effect; the OH survey reported here is about one order of magnitude more sensitive than the 6668 MHz CH_3OH blind survey (Szymczak et al. 2002). The number of OH detections would then decrease to 28 sources if we apply a poorer common sensitivity limit of about 1.6 Jy for the surveys of both maser species. Furthermore, due to the low angular resolution of both surveys it is possible that in some sources the coincidence of the CH_3OH and OH masers is subject to position uncertainties up to 30″.

The prevalence of the 1665 MHz line in the sample documented here agrees well with findings by Caswell (1998). The occurrence of the 1667 MHz line in nearly 74% of the 1665 MHz sources is less frequent than in Caswell (1998). Furthermore, in our sample the median ratio of the 1665 and 1667 MHz flux density of 1.8 (Fig. 3) is about a factor of two higher than Caswell's ratio. Our detection rate of the 1720 MHz maser emission is nearly a factor of two higher than his rate. We suggest that these differences can be due to the selection of the samples; Caswell's sample is essentially based on an OH survey, while ours is taken from an unbiased search for the 6668 MHz CH_3OH emission.

The present study clearly shows that the 1612 and 1720 MHz masers behave complementarily to each other; no 1612 MHz maser line was found in the 1720 MHz maser source at the same velocity and vice versa. This observational finding is well explained with the CSG02 model where the 1612 MHz line needs $N_{OH} > 10^{14}$ cm^{-2} and $T_k > 100$ K, whereas the 1720 MHz line arises in regions with N_{OH} about 1.5 orders of magnitude lower for similar T_k. The scarcity of satellite OH masers strongly suggests that these conditions are less common.

The median ratio of the flux density of the 6668 MHz and 1665 MHz masers is 13.3 (Fig. 3) and is close to the typical value of 16 (Caswell 1996) that is expected if the CH_3OH and OH maser components are comparable in size and the ratio of the brightness temperatures of components at 6668 and 1665 MHz equals unity (CSG02). The average values of the 6668/1665 flux ratio for the sources with only 1665 MHz emission and with 1665/1667 MHz emission are 124.3 ± 56.1 and 33.1 ± 10.1 respectively. This difference is statistically significant at the 98.3% confidence level (t-test) and can be a result of differences in T_k at which the maser transitions are quenched. The CSG02 model predicts such a trend since the 1667 MHz transition is quenched at $T_k > 80$ K, the 1665 MHz transition

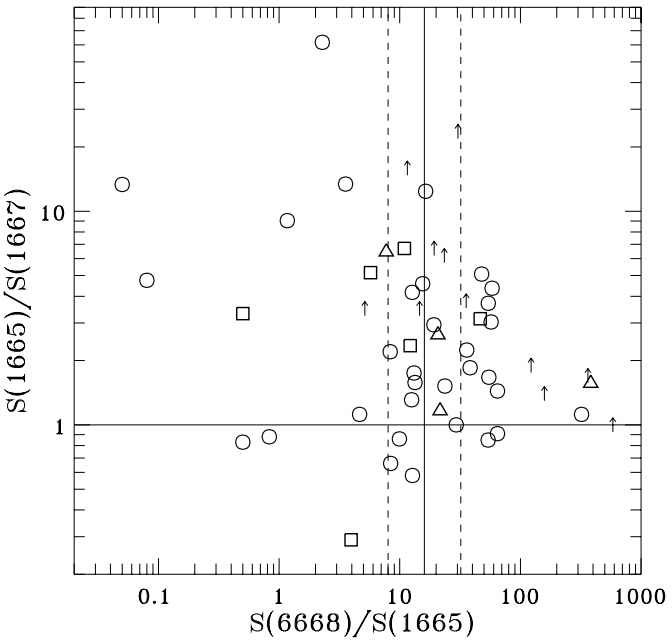

Fig. 3. Diagram of the ratios of the integrated flux density for OH 1665 and 1667 MHz and CH_3OH 6668 MHz masers. The objects with the maser emission at 1665 and 1667 MHz (circles), 1720 MHz (squares), 1612 MHz (triangles), only 1665 MHz (arrows) are shown. Note that arrows indicate only the upper limit to the 1665/1667 ratio as the 1667 MHz emission is not detected. The solid horizontal line marks the 1665/1667 ratio equals to unity. The solid vertical line marks the ratio 6668/1665 equals to 16, while the dashed vertical lines mark that ratio of 8 and 32.

is quenched at $T_k > 125$ K, while the 6668 MHz maser is still strong at T_k up to 200 K. There are no statistically significant differences in the flux density ratios (Fig. 3) for other groups of maser objects.

5.2. Abundances and timescales

Our study shows that 30 out of a total of 39 satellite sources listed in Table 2 exhibit absorption and/or quasi-thermal emission. The satellite lines show exclusively complementary behaviour, as they do in maser emission. Emission at 1612 MHz and absorption at 1720 MHz are seen in 5 objects, while the reverse case is observed in 18 sources. The remaining 6 objects exhibit a change from absorption to emission across the 1612 MHz profile and a change from emission to absorption across the 1720 MHz profile. This behaviour was predicted by the OH pumping model with non-local overlap (Lucas 1980). Absorption at 1612 MHz and emission at 1720 MHz is a signature of low column density of OH molecules ($<10^{15}$ cm^{-2}) and is seen for the blueshifted part of the profile, while the inverse case occurs for the redshifted part of the profile and marks the region of higher density (Elitzur 1992). The prevalence of emission at 1612 MHz and absorption at 1720 MHz suggests that the majority of sources have $n_{H_2} \geq 10^7$ cm^{-3}. More than 80% of sources with conjugate behaviour of satellite lines are associated with OH masers. This implies higher N_{OH} in CH_3OH/OH than in CH_3OH maser sources.

The main line absorption appears in more than one third of the sample sources. The absorption features are clearly blueshifted relative to the corresponding maser lines (Sect. 3.5). This can suggest that absorption forms in front of the central radio continuum source in expanding layers of molecular clouds. The depth ratio of the main line absorption profiles is almost always different to the LTE value, suggesting non-thermal excitation of OH molecules. The main line absorption features are preferentially associated with sources also supporting OH masers, but about 30% of them are seen in objects with only CH_3OH masers.

Our finding that no OH masers are observed towards many strong CH_3OH sources can be explained by N_{CH_3OH} of about an order of magnitude higher than N_{OH} (CSG02). A large CH_3OH column density can easily be reached in star forming regions due to a high abundance of methanol ice on grain mantles (Dartois et al. 1999). The detection of OH absorption in CH_3OH objects without OH masers supports the scenario in which both molecules enrich circumstellar gas due to injection from grain mantles (Hartquist et al. 1995) but, in those objects, the OH column density is insufficient to sustain maser emission. This appears to be consistent with the chemical models (Charnley et al. 1992, 1995) that predict a maximum of methanol abundance before a peak of OH abundance. If these models are proven, then in our sample the CH_3OH sources without OH absorption and OH masers could be at earlier phases of evolution than OH-rich sources. These chemical models predict a rapid drop of CH_3OH abundance between 10^5 and 10^6 yr as the CH_3OH is used up, while an abrupt drop of OH abundance occurs at a later time. In this phase a large dispersion of CH_3OH abundance is likely to occur from one source to another. We conclude that, under similar physical conditions (CSG02), the abundances and column densities of CH_3OH and OH control the occurrence of both maser species and their intensity ratios.

5.3. Maser pumping

Most theoretical models assume that IR pumping can account for both the OH and CH_3OH masers (e.g. CSG02, and references therein). However, there is no convincing observational evidence for correlation between the 6668 MHz maser and IR flux densities (van der Walt et al. 1995). IR pumping of the OH main line masers was found to be a feasible mechanism (Moore et al. 1988). The present study provides a new insight into the pumping problem. The correlation coefficient between the OH integrated flux density and IRAS 60 μm flux density is 0.72 for the objects with good quality IRAS measurements (Fig. 4). The ratio of the OH and 60 μm flux densities is lower than 0.025 for all but one object and higher than 0.0025. A similar correlation but with $r = 0.65$ is seen for the 100 μm IRAS band. This result confirms the correlation found for IRAS selected OH masers (Moore et al. 1988).

The CH_3OH maser and IRAS flux densities are also well correlated. The best correlation with $r = 0.68$ is seen for the 25 μm band (Fig. 4). The average ratio of the 6668 MHz and 25 μm flux densities is 0.04. We found that these correlations

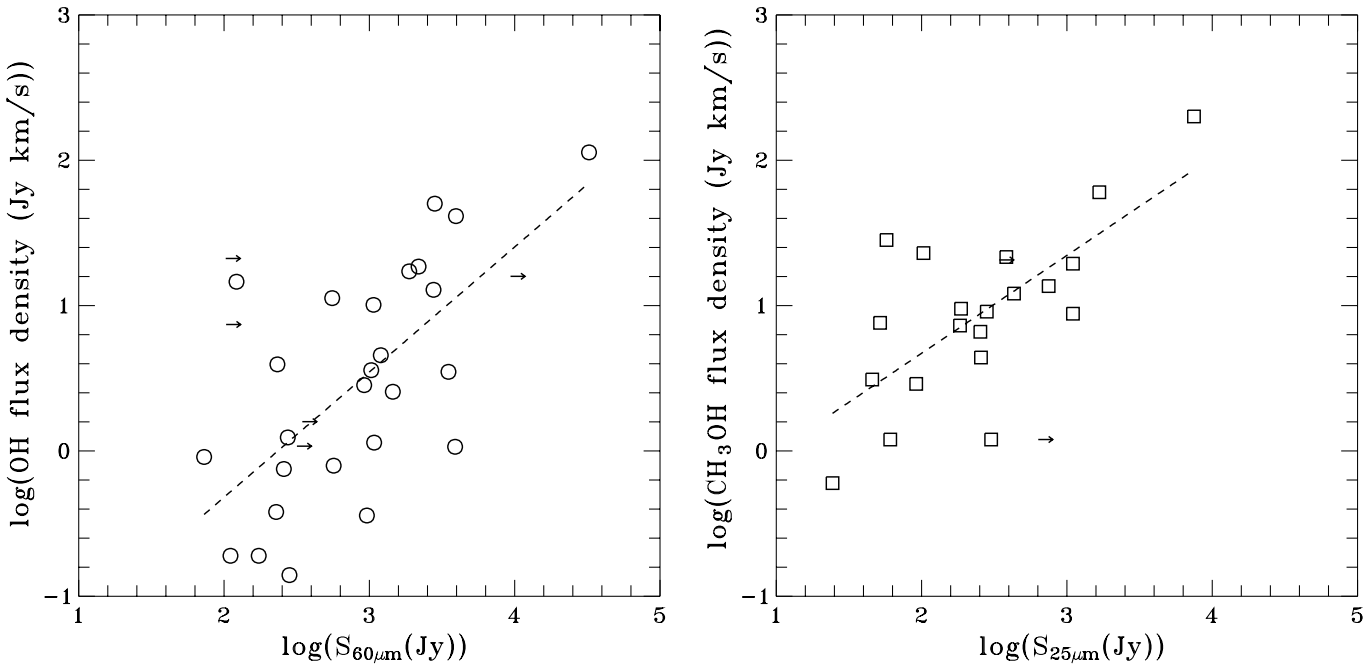

Fig. 4. Left: diagram of the OH integrated flux density versus IRAS 60 μm flux density for the sources with the OH maser emission. Right: diagram of the CH_3OH integrated flux density versus IRAS 25 μm flux density for the sources with only 6668 MHz maser line. The horizontal arrows indicate the upper limit for the IRAS flux densities. The dashed lines are the best least square fits for the sources represented by open symbols. Note that within noise, the regression lines are compatible with a slope of 1.

disappear when objects with OH maser emission are included and no other correlation between CH_3OH and IRAS flux densities are seen in objects showing maser emission of both species. This suggests an intrinsic difference between objects with just the CH_3OH maser and these with OH masers also. A plausible factor is a difference in CH_3OH abundance, with the abundances falling during the lifetimes of objects such as OH maser sources. This is discussed in Sect. 5.2. The issue of maser – IR flux correlation needs further study with much better positional accuracy to avoid mismatching of masers and IR sources.

6. Conclusions

We have made OH observations of a complete sample of 100 CH_3OH maser sources. The 1665 and 1667 MHz are dominant lines while the satellite lines at 1612 and 1720 MHz, almost always associated with the main line emission, are scarce and occur in different objects or in the same object but at different velocities. A large dispersion of the kinetic temperature (100−250 K) is deduced for the OH sources. The 1612 MHz OH line probes regions of $T_k > 150$ K, while the 1720 MHz line occurs in regions of $n_{H_2} < 10^7$ cm^{-3}. A substantial degree of circular polarization of OH maser emission is observed and Zeeman pair candidates identified in several sources, which deserve further investigation, imply the strength of the magnetic field in the line of sight to be up to 4 mG. About half of the targets show OH absorption and quasi-thermal emission. The conjugate behaviour of the satellite line absorption/emission features is related to the gas density and OH column density; the absorption at 1612 MHz and emission at 1720 MHz seen for the blueshifted part of the profile marks regions of $N_{OH} < 10^{15}$ cm^{-2}. The absorption features are blueshifted by 2−4 km s^{-1} relative to the maser profiles, indicating that absorption forms in slowly expanding layers of gas in front of the central continuum source.

The physical conditions inferred for methanol- and hydroxyl-rich sources appear to be very similar. The maser amplification of both molecular species can occur in common regions with $n_{H_2} < 10^{5-8}$ cm^{-3}, $N_{OH} \approx N_{CH_3OH} = 10^{14-16}$ cm^{-2} as predicted by the CSG02 model. We found evidence that the OH main lines and the 6668 MHz CH_3OH line can be efficiently pumped by infrared photons.

The two groups of objects: (1) without any OH emission and absorption, (2) without OH masers but accompanied by OH absorption can represent less evolved environments of young stars. There is evidence that the CH_3OH maser appears earlier than the OH maser. The studies of extreme CH_3OH and OH sources can provide more information about possible evolutionary scenarios of young central stars and their environments.

Acknowledgements. The Nançay Radio Observatory is operated by the Unité Scientifique de Nançay of the Observatoire de Paris, associated with the CNRS. This work was supported by the KBN grant 2P03D01122.

References

Argon, A. L., Reid, M. J., & Menten, K. M. 2000, ApJS, 129, 159
Beuther, H., Schilke, P., Menten, K. M., et al. 2002, ApJ, 566, 945
Braz, M. A., & Epchtein, N. 1983, A&AS, 54, 167
Bronfman, L., Nyman, L. A., & May, J. 1996, A&AS, 115, 81
Caswell, J. L. 1996, MNRAS, 279, 79

Caswell, J. L. 1997, MNRAS, 289, 203
Caswell, J. L. 1998, MNRAS, 297, 215
Caswell, J. L., & Haynes, R. F. 1983a, Aust. J. Phys., 36, 361
Caswell, J. L., & Haynes R. F. 1983b, Aust. J. Phys., 36, 417
Caswell, J. L., Vaile, R. A., Ellingsen, S. P., Whiteoak, J. B., & Norris, R. P. 1995, MNRAS, 272, 96
Charnley, S. B., Tielens, A. G. G. M., & Millar, T. J. 1992, ApJ, 399, L71
Charnley, S. B., Kress, M. E., Tielens A. G. G. M., & Millar, T. J. 1995, ApJ, 448, 232
Cohen, R. J., Baart, E. E., & Jonas, J. L. 1988, MNRAS, 231, 205
Colgan, S. W. J., Salpeter, E. E., & Terzian, Y. 1989, ApJ, 336, 231
Cragg, D. M., Sobolev, A. M., & Godfrey, P. D. 2002, MNRAS, 331, 521 (CSG02)
Dartois, E., Schutte, W., Geballe, T. R., et al. 1999, A&A, 342, L32
Davis, R. D. 1974, in Galactic Radio Astronomy, ed. E. J. Kerr & S. C. Simonson (Dordrecht: Reidel), 275
Elitzur, M. 1992, in Astronomical Masers (Kluwer Publishers), 234
Ellingsen, S. P., von Bibra, M. L., McCulloch, P. M., et al. 1996, MNRAS, 280, 378
Gaylard, M. J., MacLeod, G. C., & van der Walt, D. J. 1994, MNRAS, 269, 257
Hartquist, T. W., Menten, K. M., Lepp, S., & Dalgarno A. 1995, MNRAS, 272, 184
Hughes, V. A., & MacLeod, G. C. 1989, AJ, 97, 786
Kurtz, S., Cesaroni, R., Churchwell, E., Hofner, P., & Walmsley, C. M. 2000, in Protostars and Planets IV, ed. V. Mannings, A. P. Boss, & S. S. Russell (Univ. of Arizona Press), 299
Lucas, R. 1980, A&A, 84, 36
Magnani, L., Blitz, L., & Wouterloot, J. G. A. 1988, ApJ, 326, 909
Menten, K. M. 1991, ApJ, 380, L75
Menten, K. M., Reid, M. J., Pratap, P., Moran, J. M., & Wilson, T. L. 1992, ApJ, 401, L39
Moore, T. J. T., Cohen, R. J., & Mountain, C. M. 1988, MNRAS, 231, 887
Olmi, L., & Cesaroni, R. 1999, A&A, 352, 266
Reid, M. J., & Silverstein, E. M. 1990, ApJ, 361, 483
Sridharan, T. K., Beuther, H., Schilke, P., Menten, K. M., & Wyrowski, F. 2002, ApJ, 566, 931
Slysh, V. I., Dzura, A. M., Val'tts, I. E., & Gérard, E. 1994, A&AS, 106, 87
Slysh, V. I., Dzura, A. M., Val'tts, I. E., & Gérard, E. 1997, A&AS, 124, 85
Szymczak, M., & Kus, A. J. 2000, A&AS, 147, 181
Szymczak, M., Kus, A. J., Hrynek, G., Kepa, A., & Pazderski, E. 2002, A&A, 392, 277
Turner, B. E. 1979, A&AS, 37, 1
van Driel, W., Pezzani, J., & Gérard, E. 1996, in High Sensitivity Radio Astronomy, ed. N. Jackson, & R. J. Davis (Cambridge Univ. Press), 229
van der Walt, D. J., Gaylard, M. J., & MacLeod, G. C. 1995, A&AS, 110, 81
Wood, D. O. S., & Churchwell, E. 1989, ApJ, 340, 265

Online Material

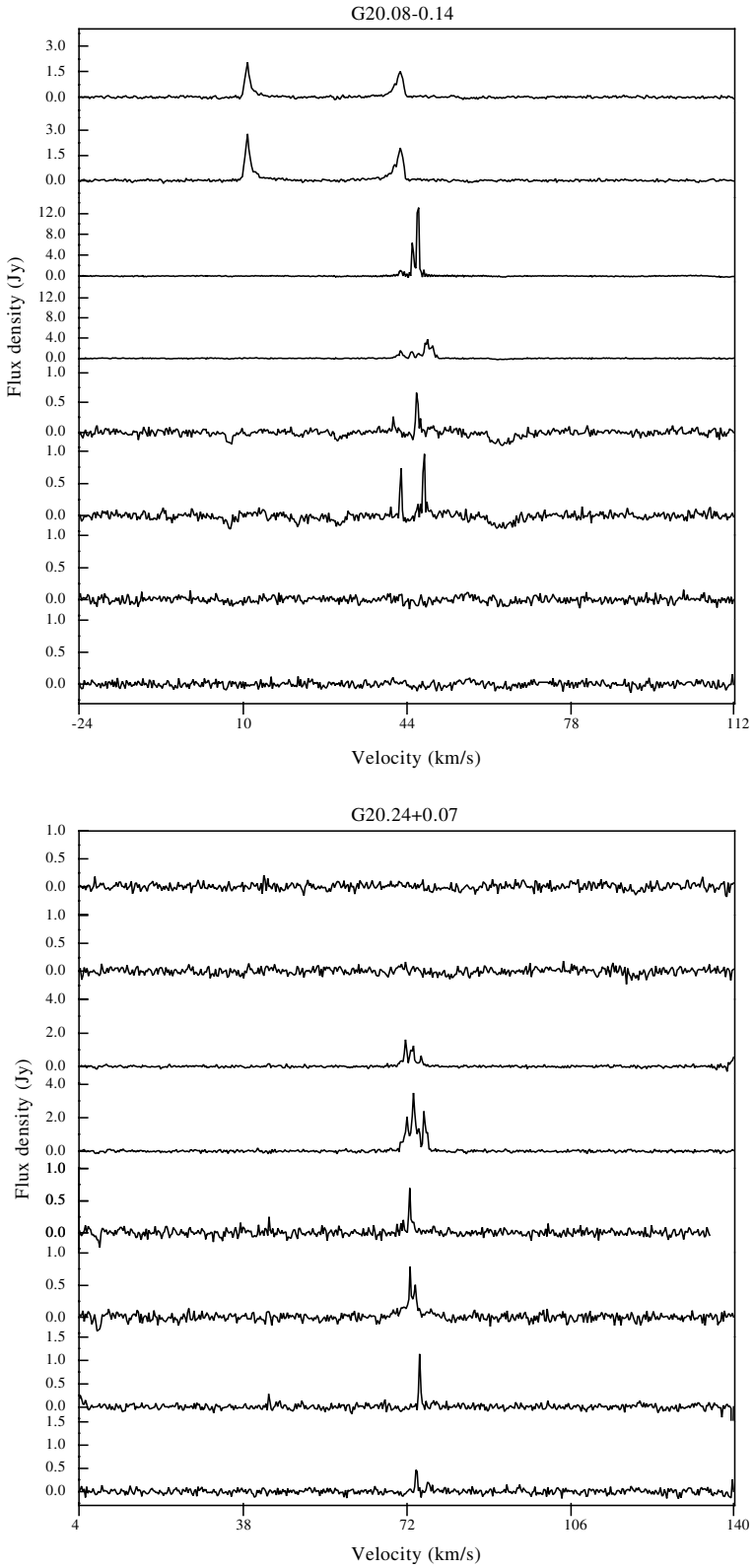

Fig. A.1. The OH spectra of the sources observed. The left and right circular polarization at 1612, 1665, 1667 and 1720 MHz are shown from top to bottom.

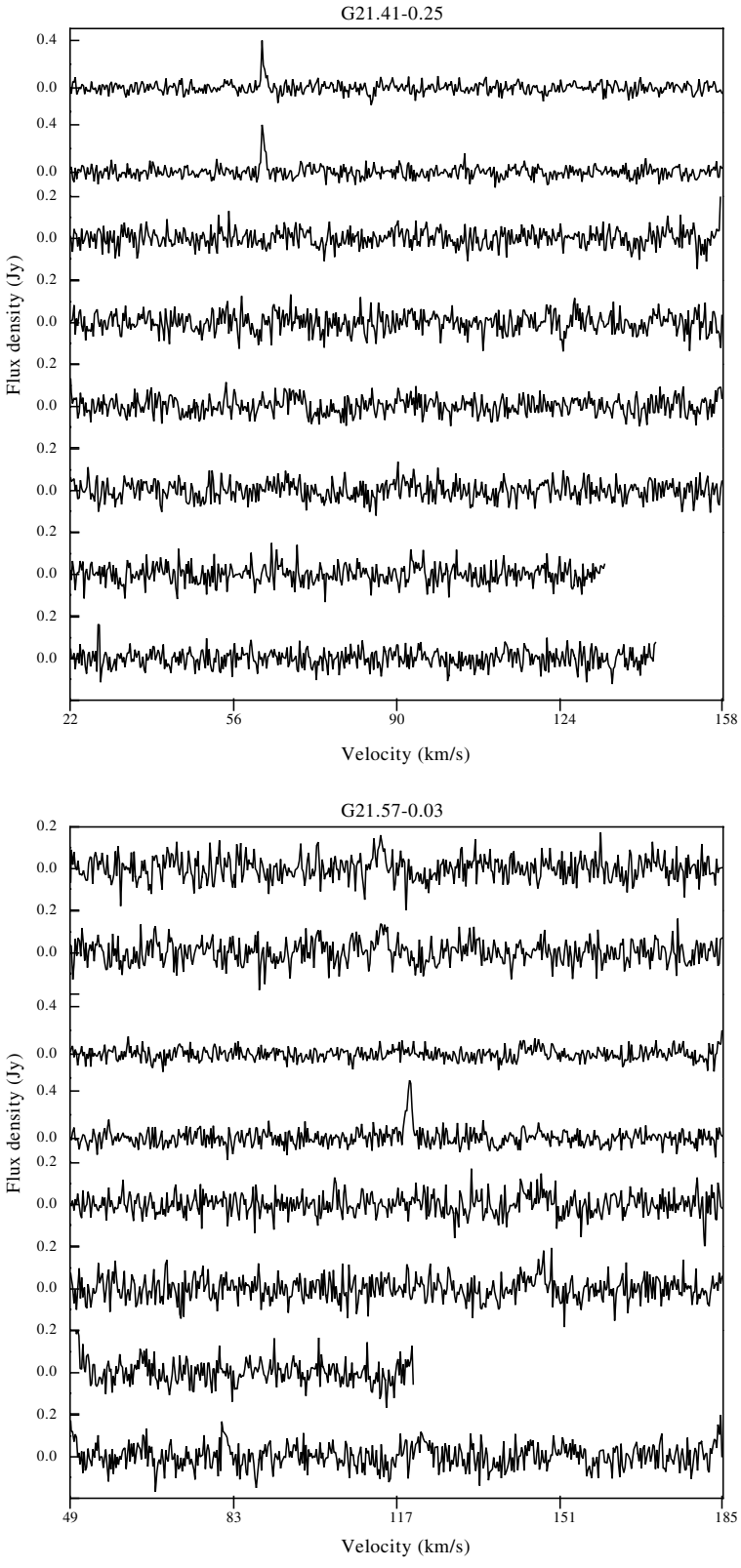

Fig. A.1. continued.

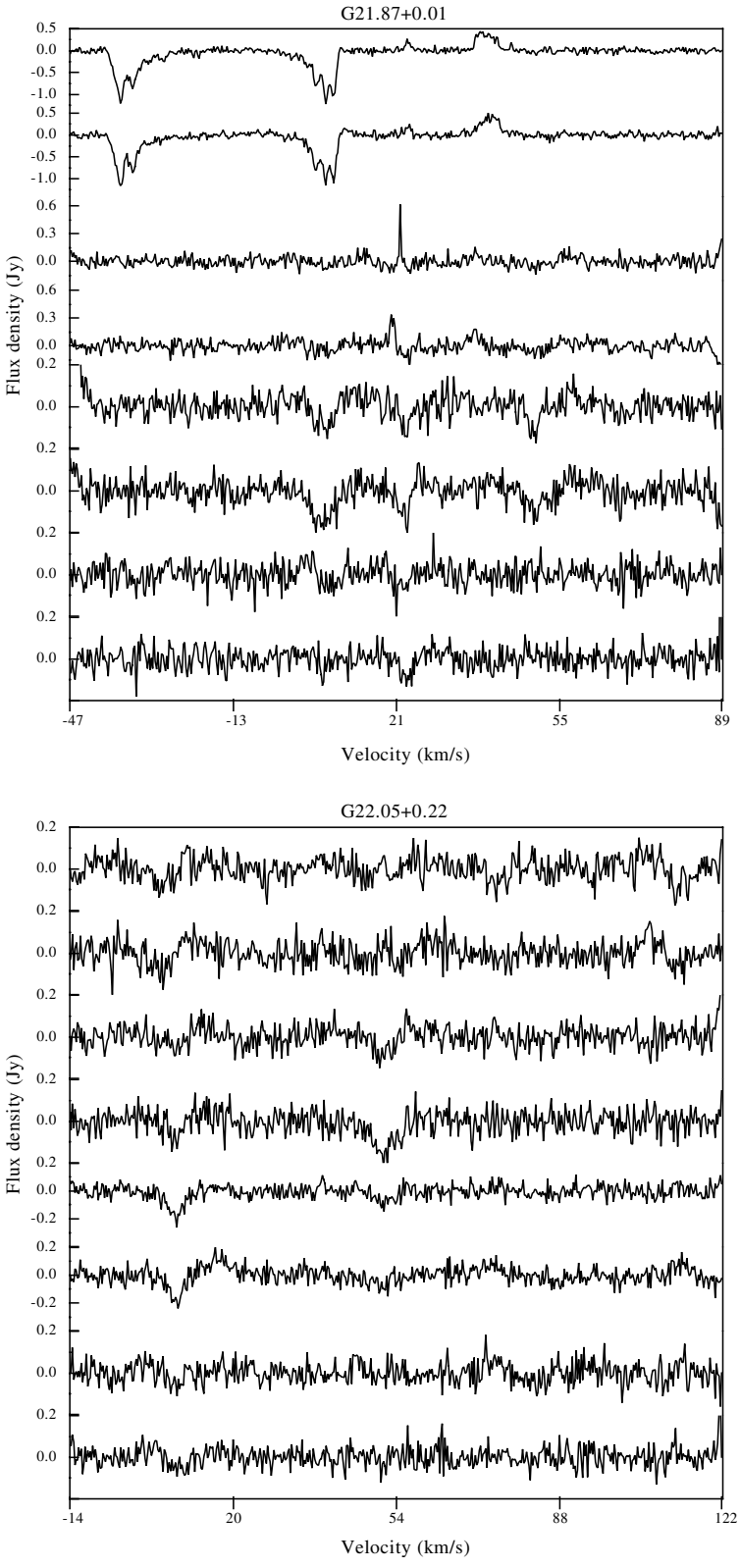

Fig. A.1. continued.

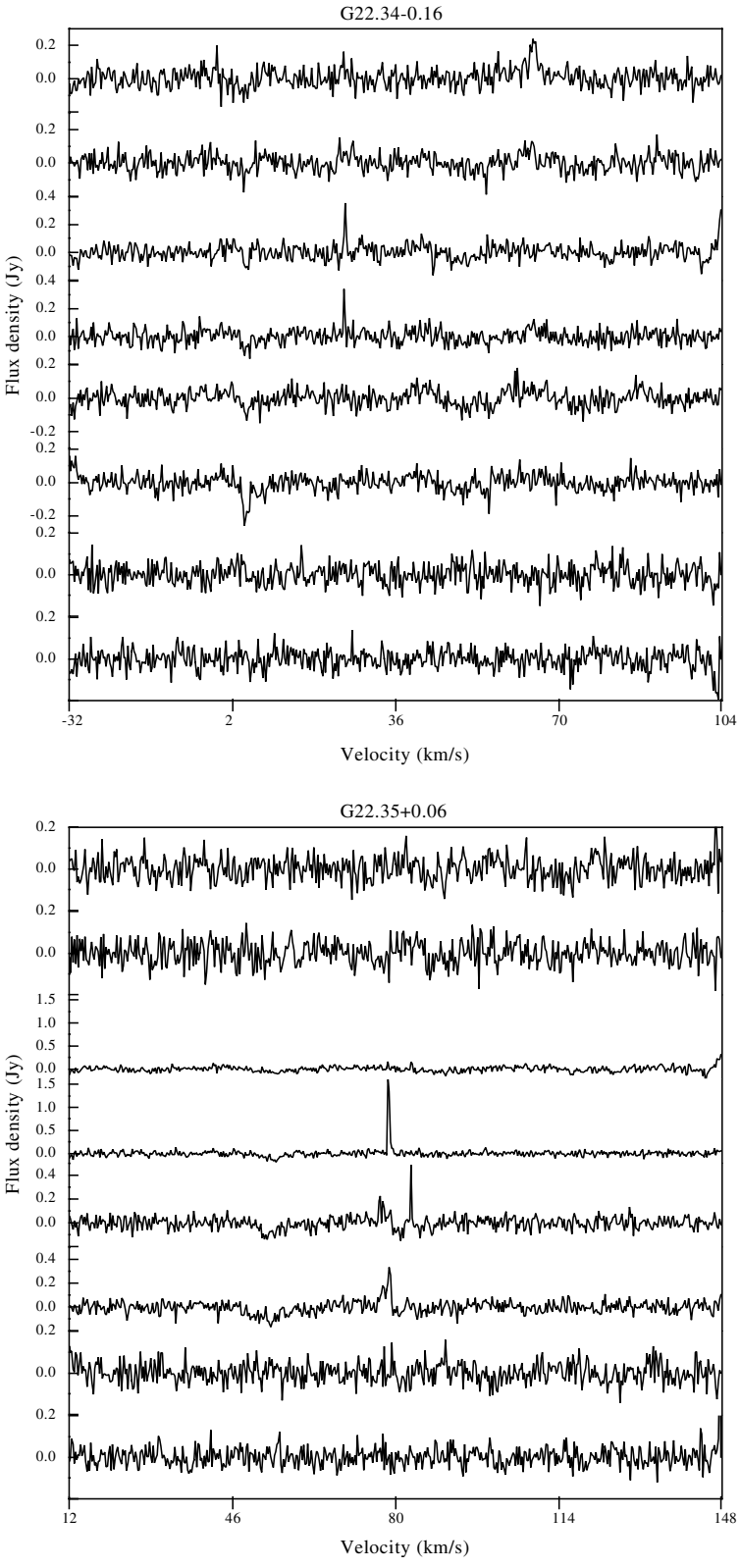

Fig. A.1. continued.

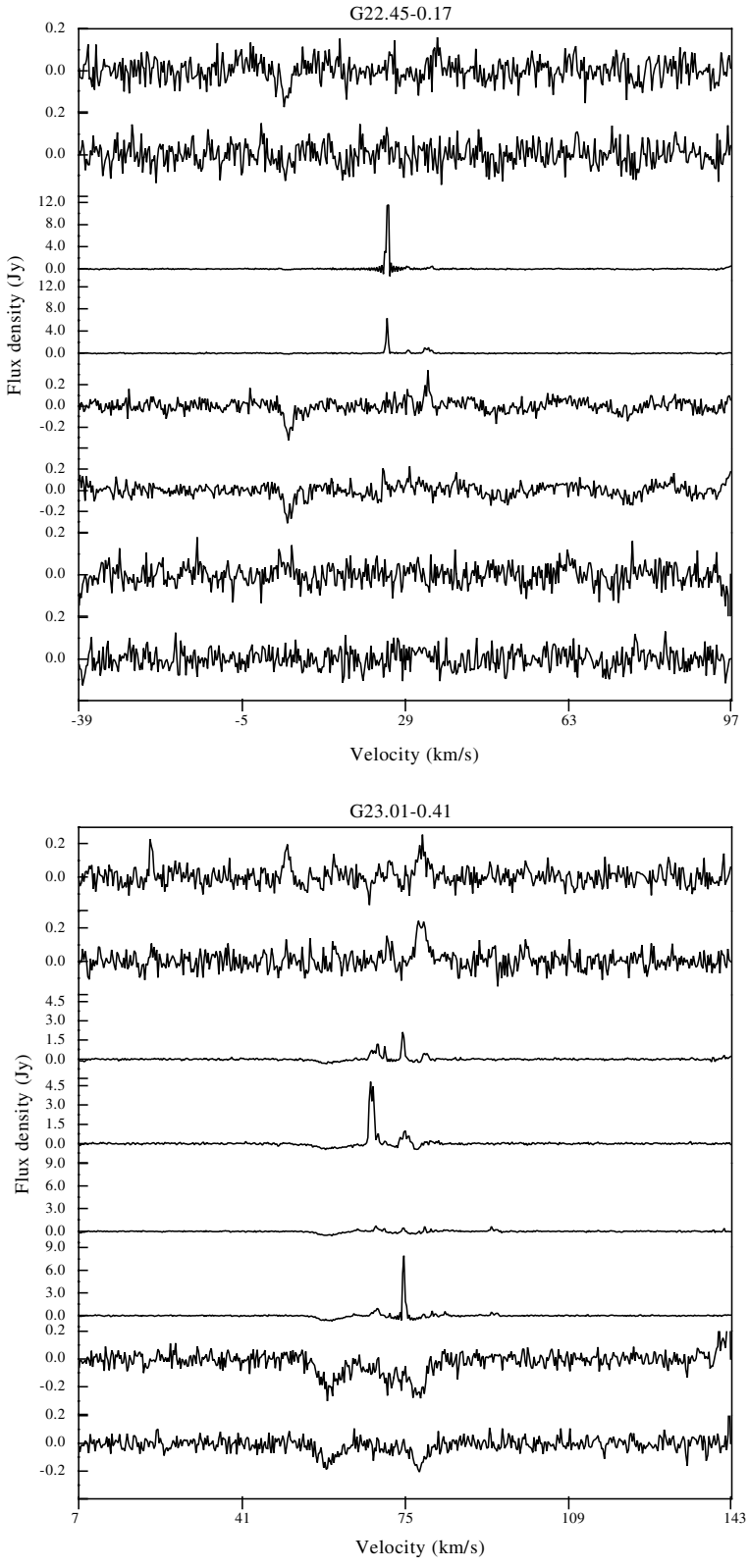

Fig. A.1. continued.

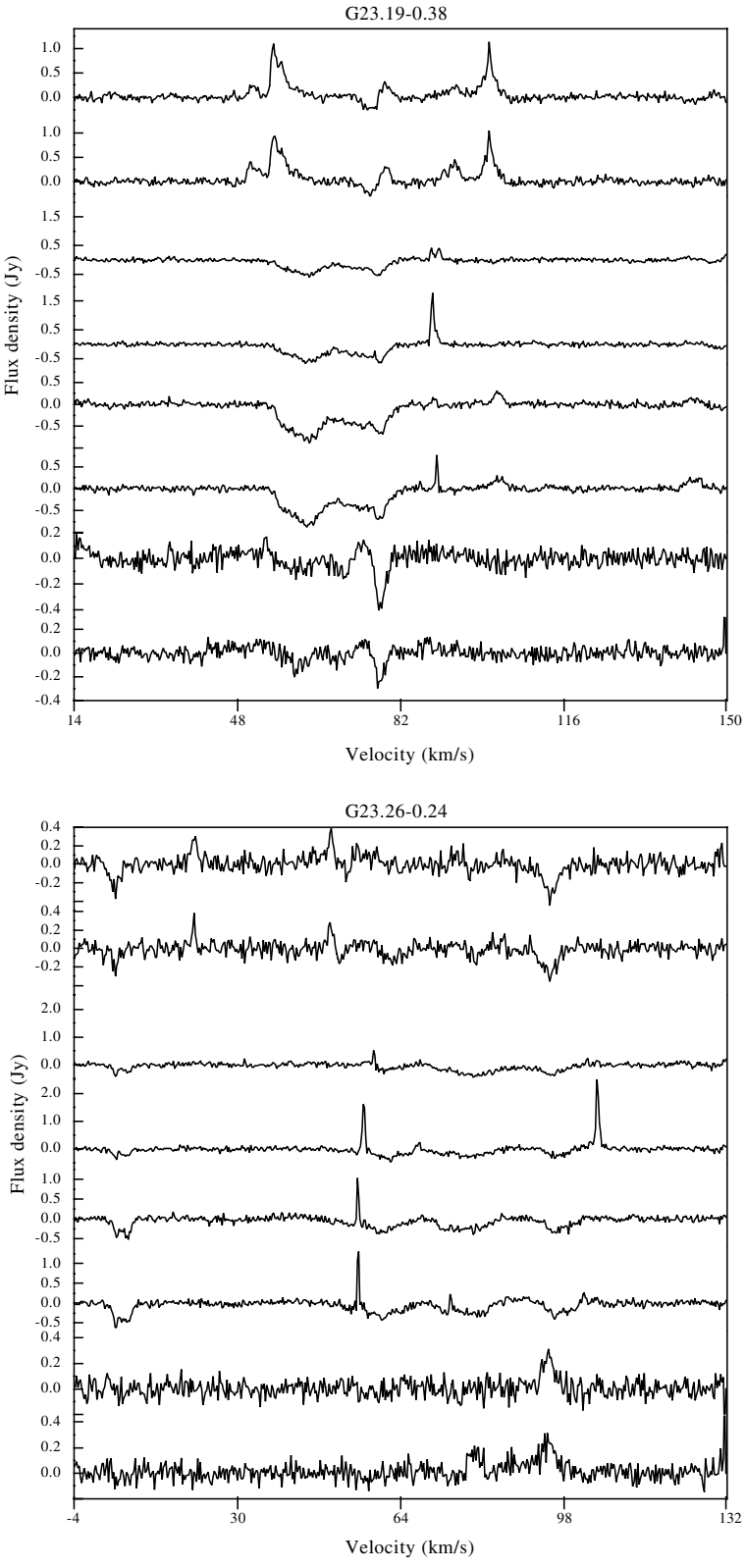

Fig. A.1. continued.

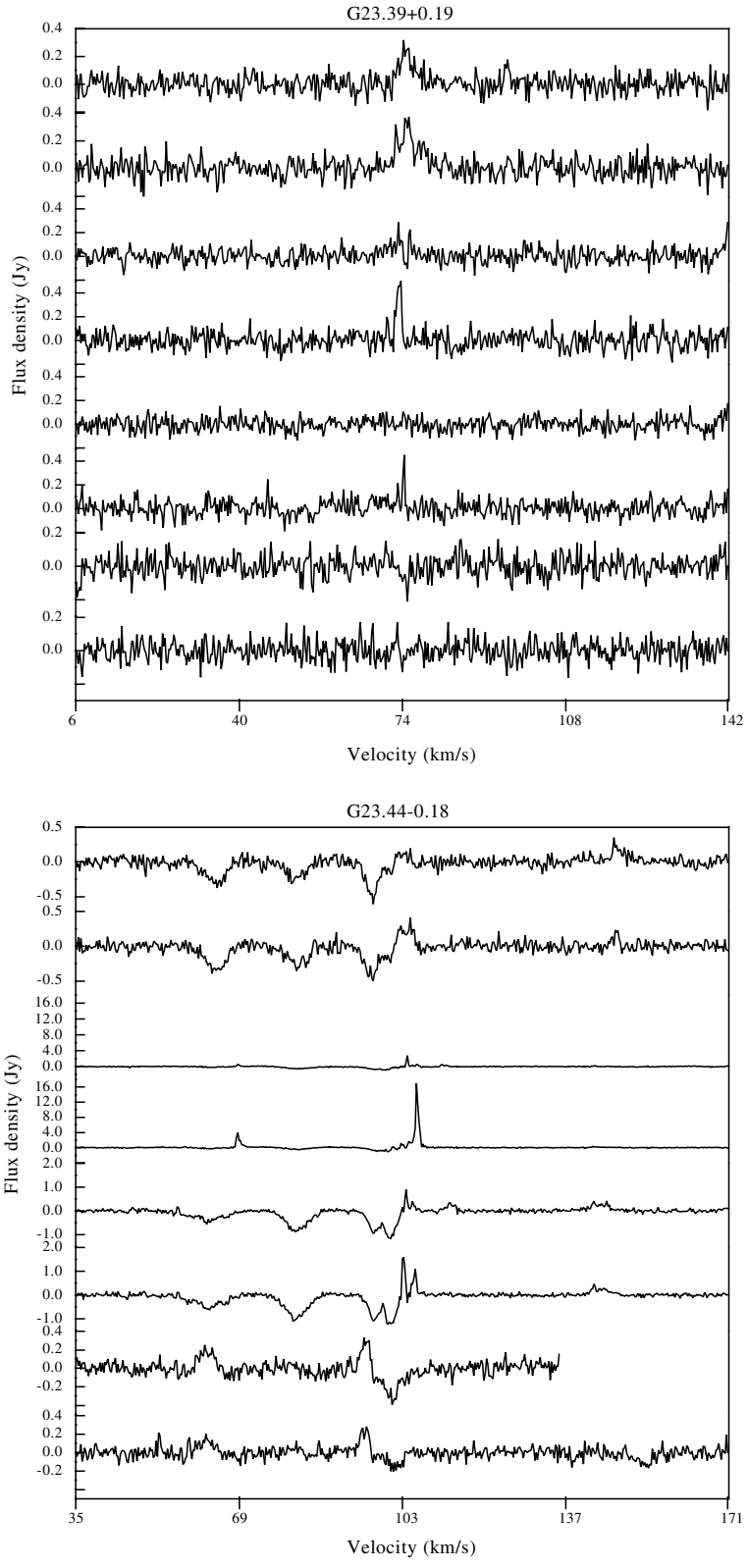

Fig. A.1. continued.

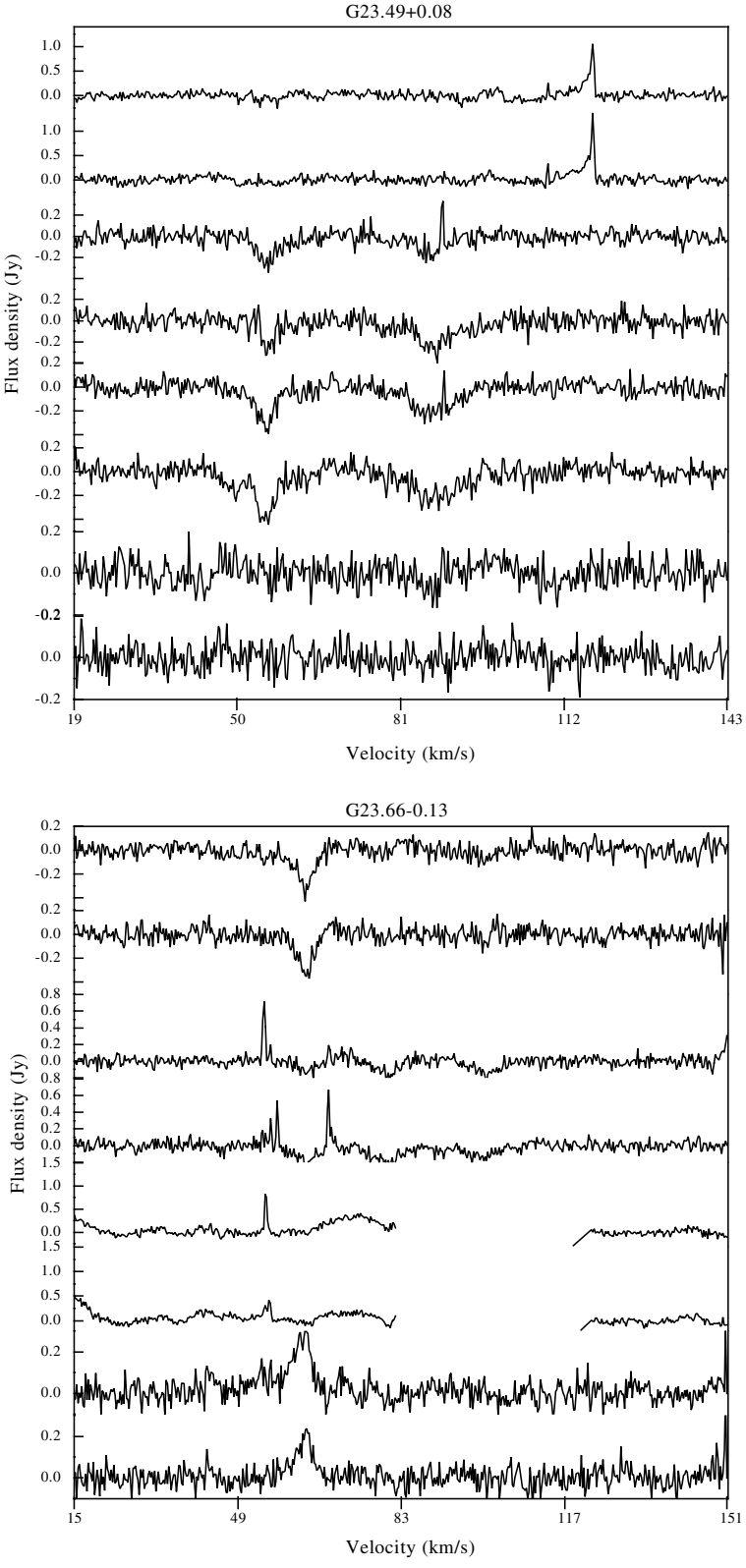

Fig. A.1. continued.

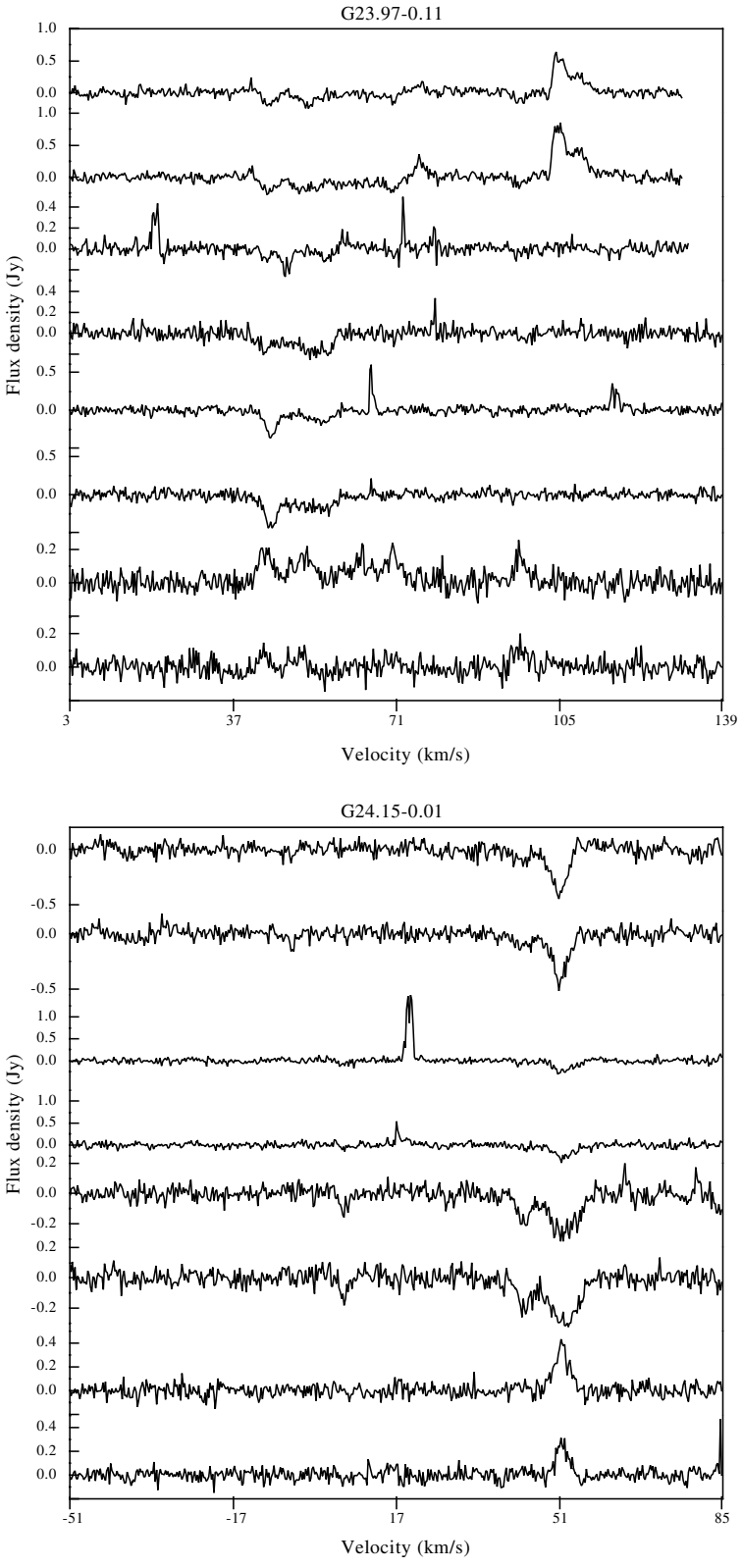

Fig. A.1. continued.

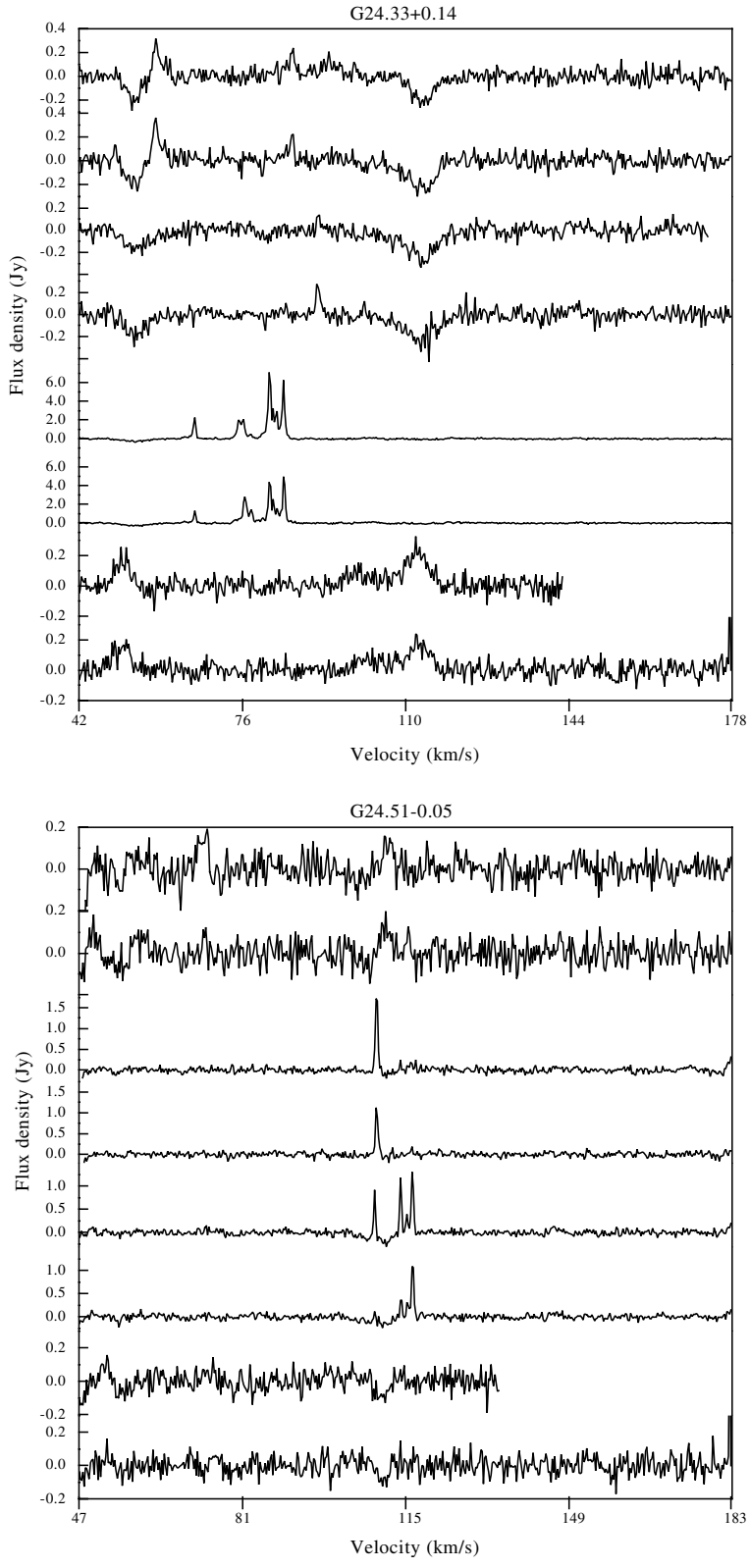

Fig. A.1. continued.

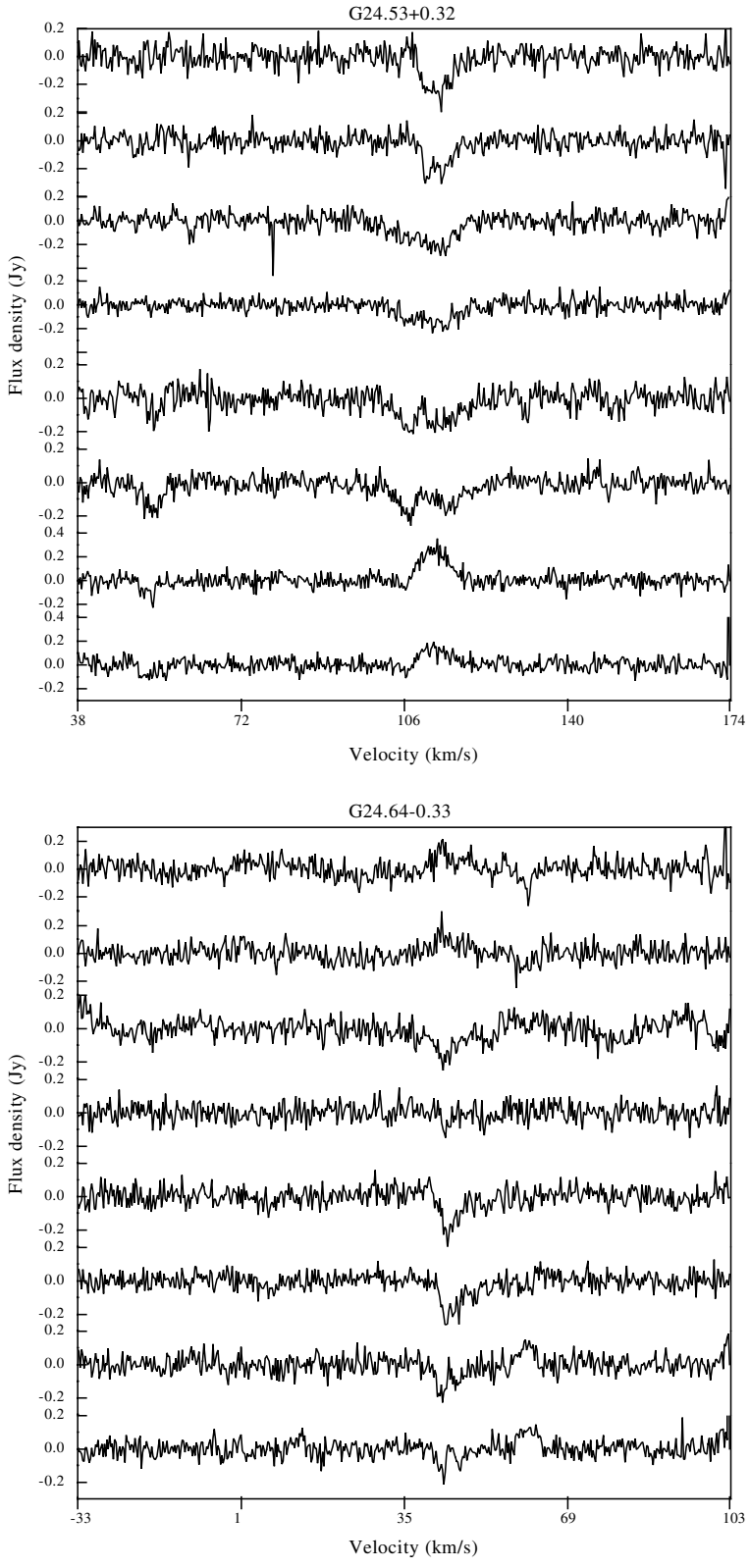

Fig. A.1. continued.

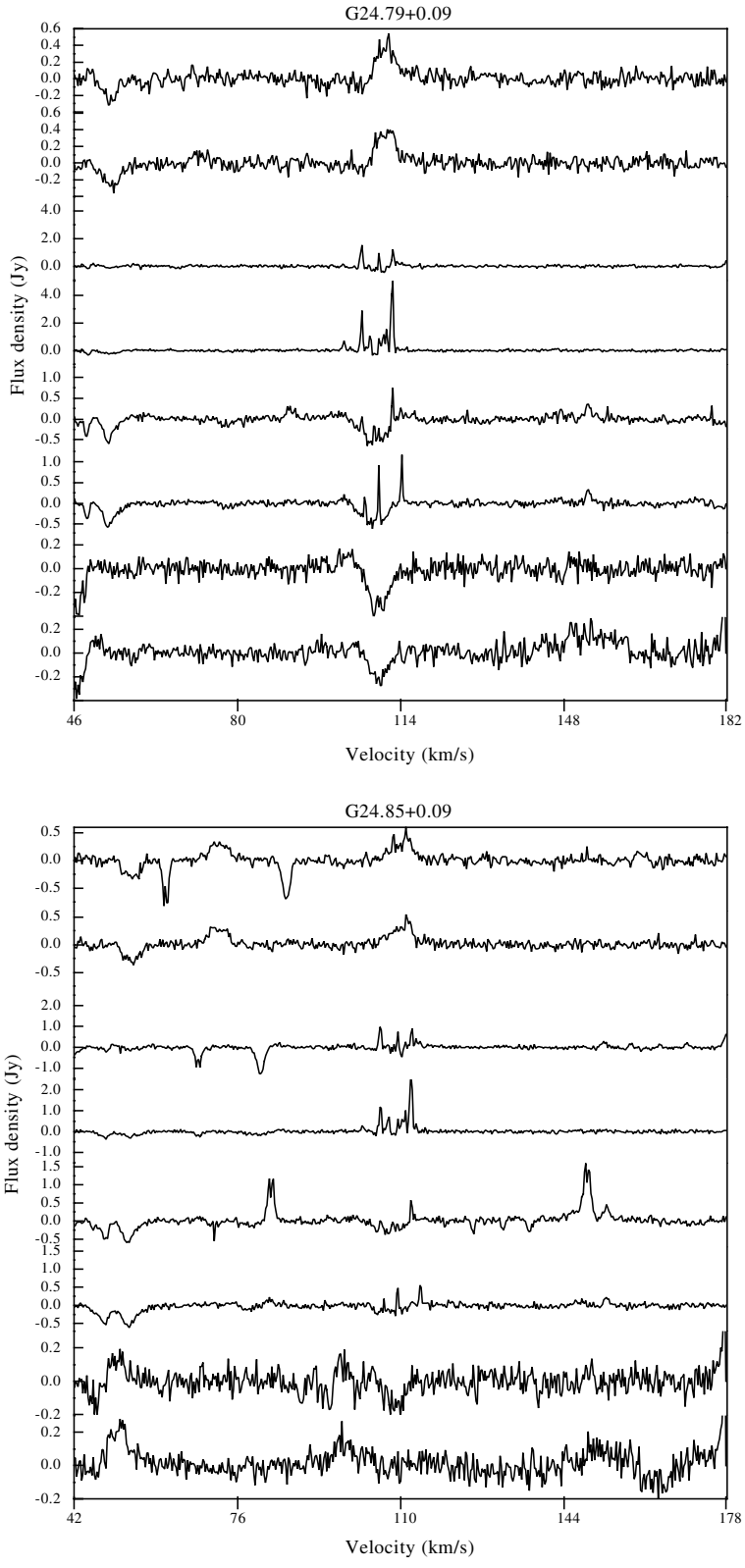

Fig. A.1. continued.

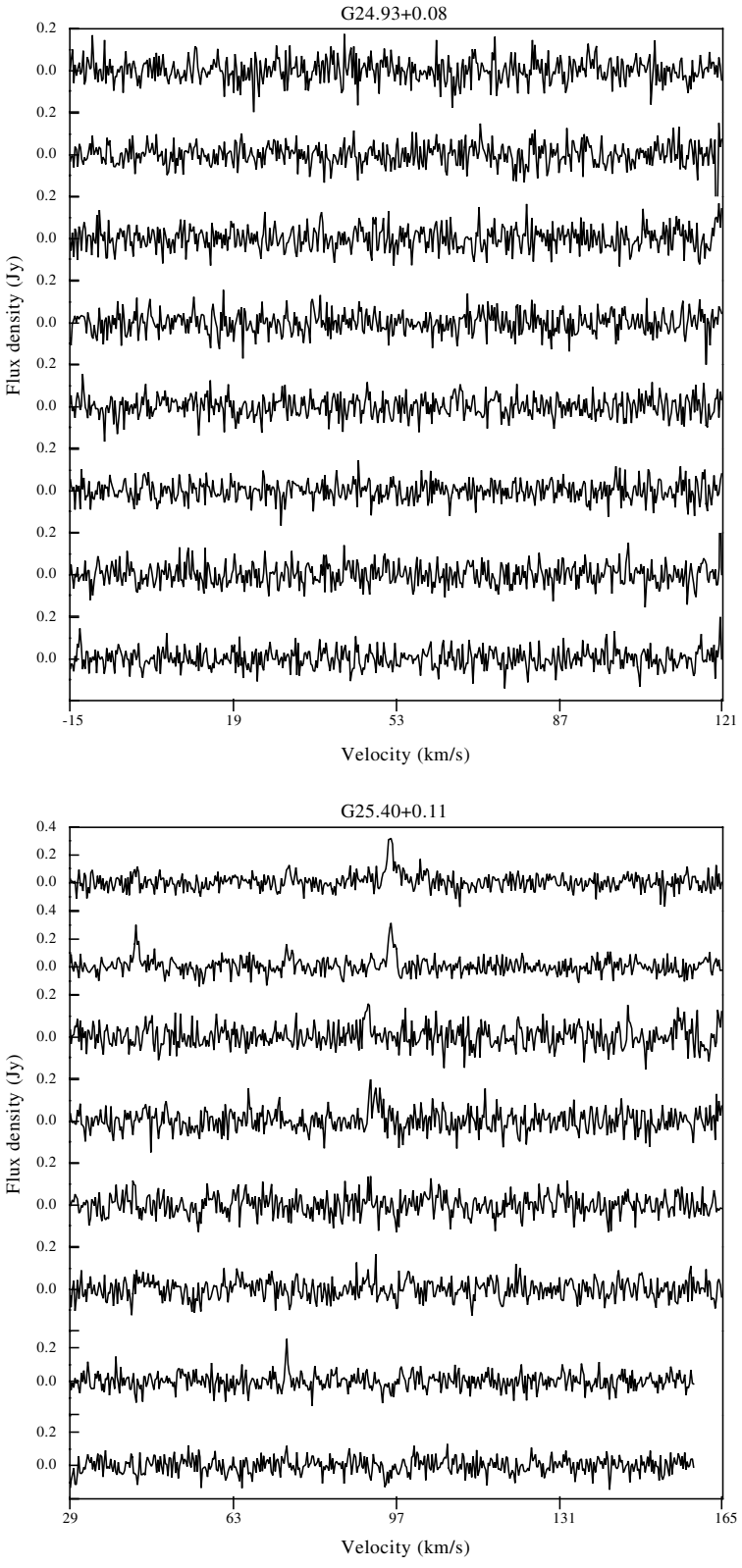

Fig. A.1. continued.

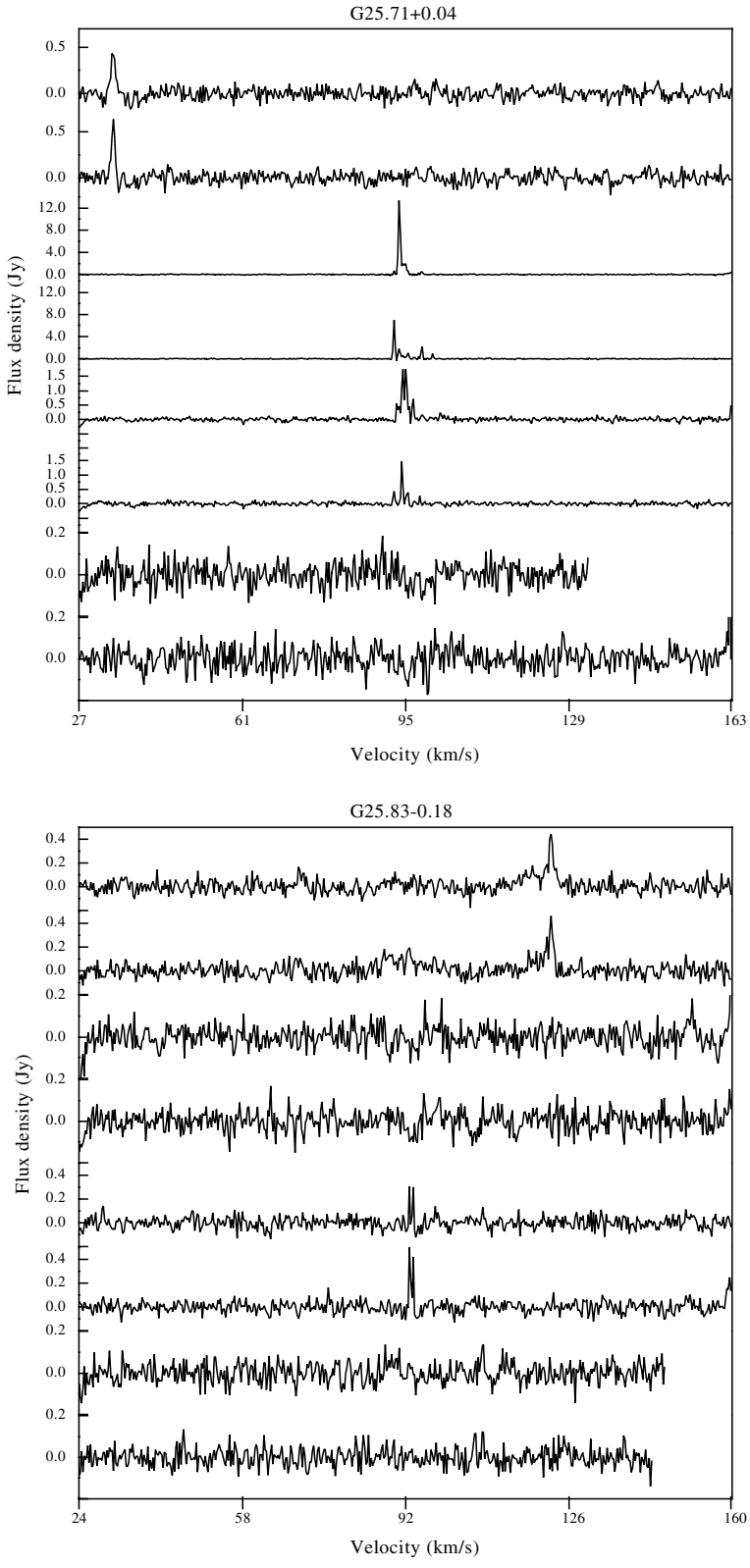

Fig. A.1. continued.

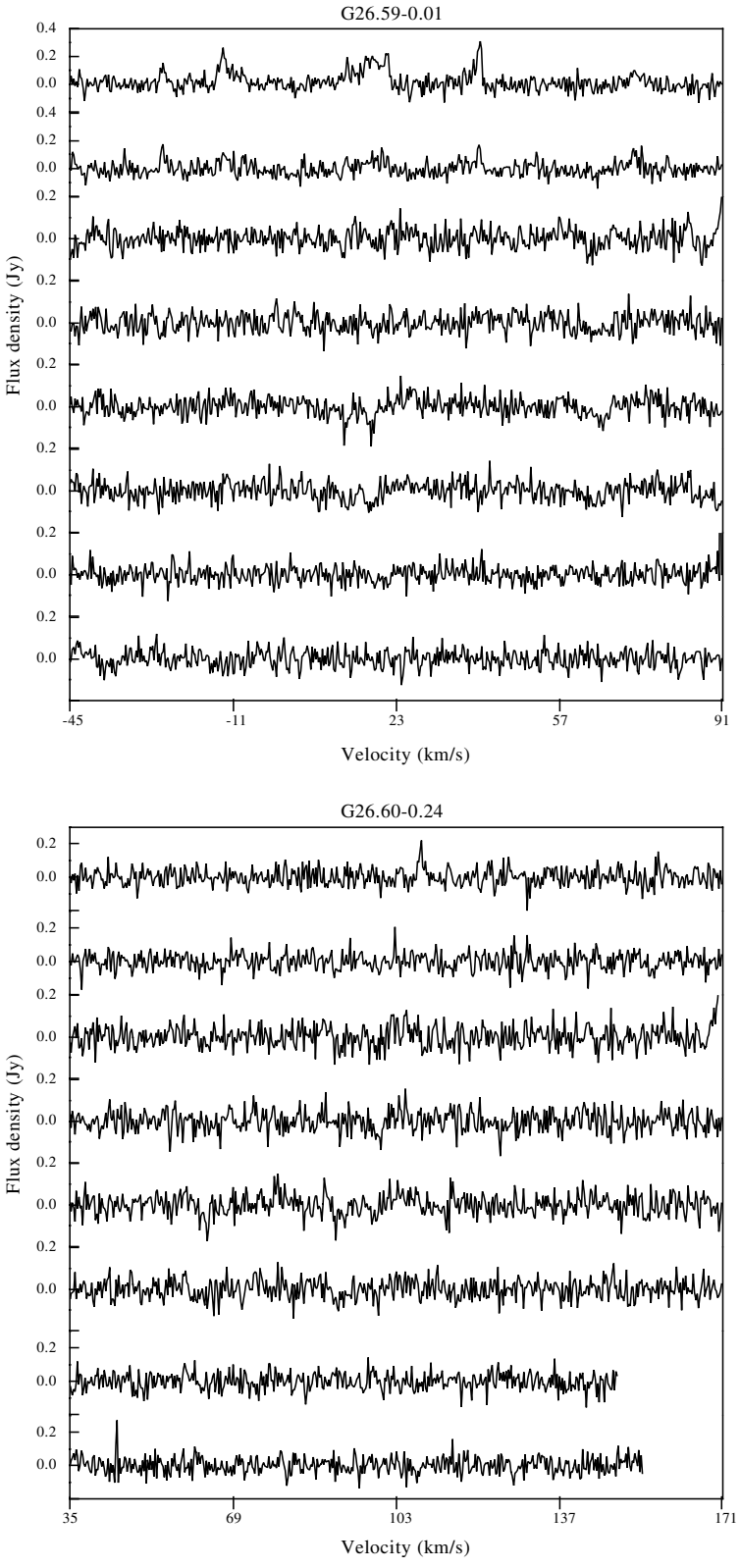

Fig. A.1. continued.

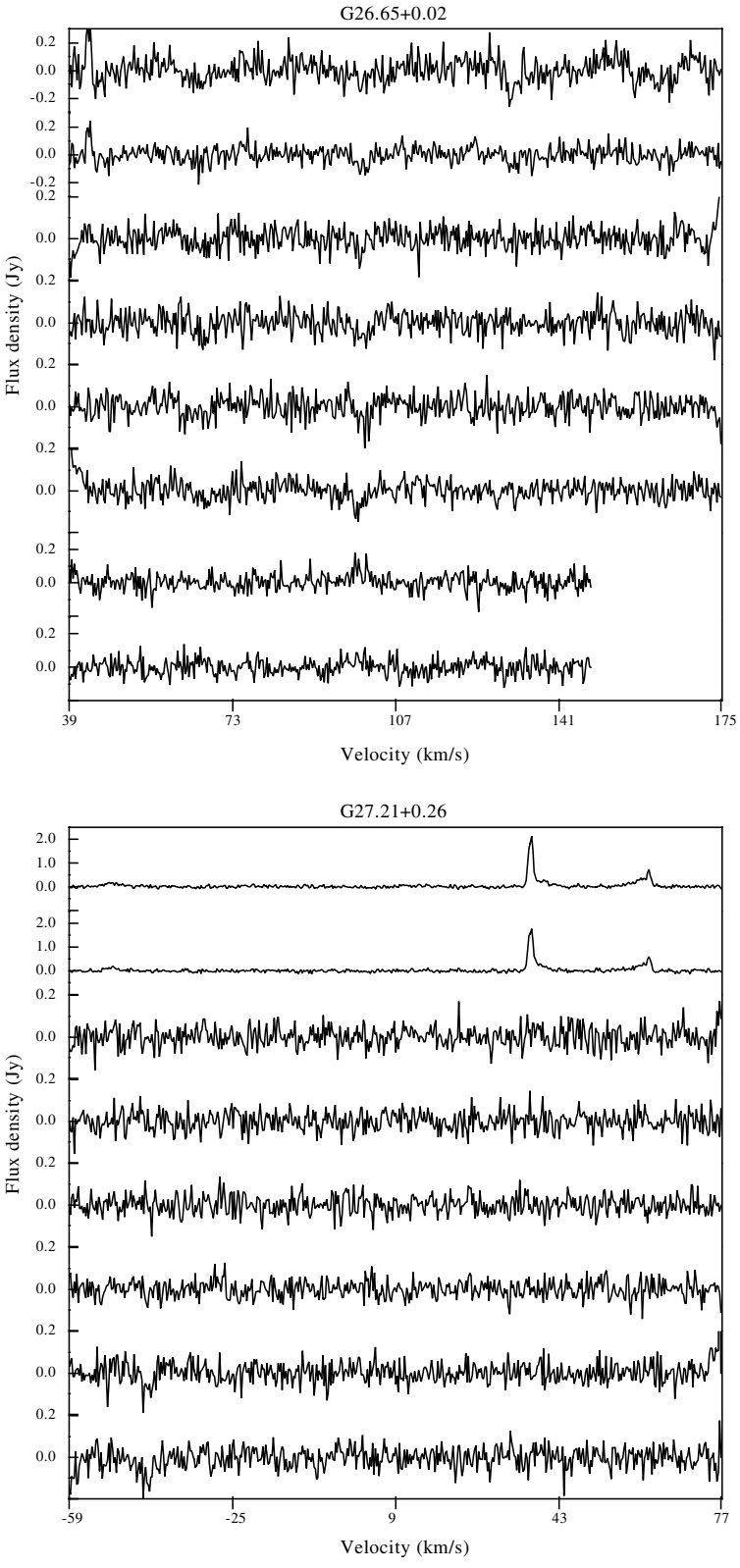

Fig. A.1. continued.

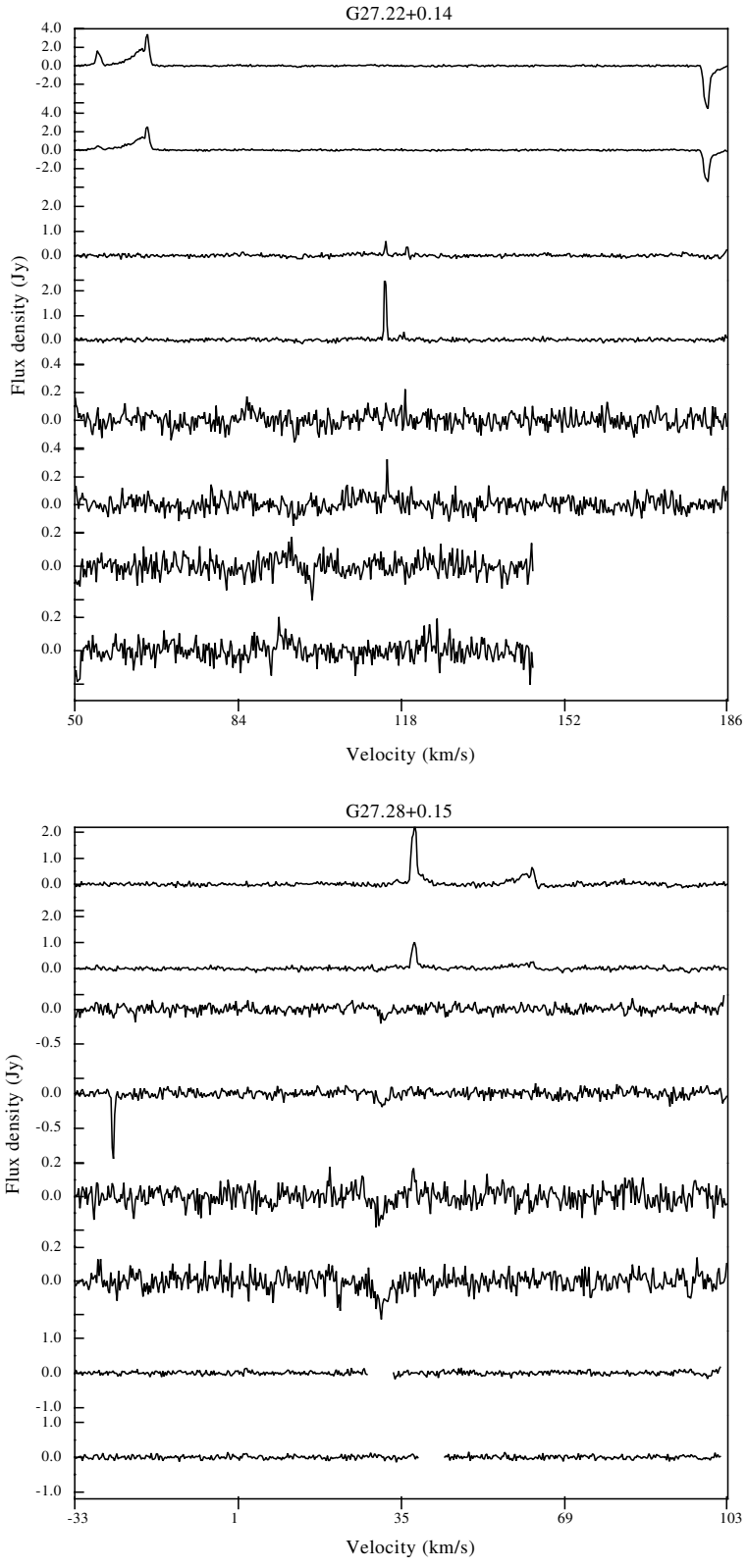

Fig. A.1. continued.

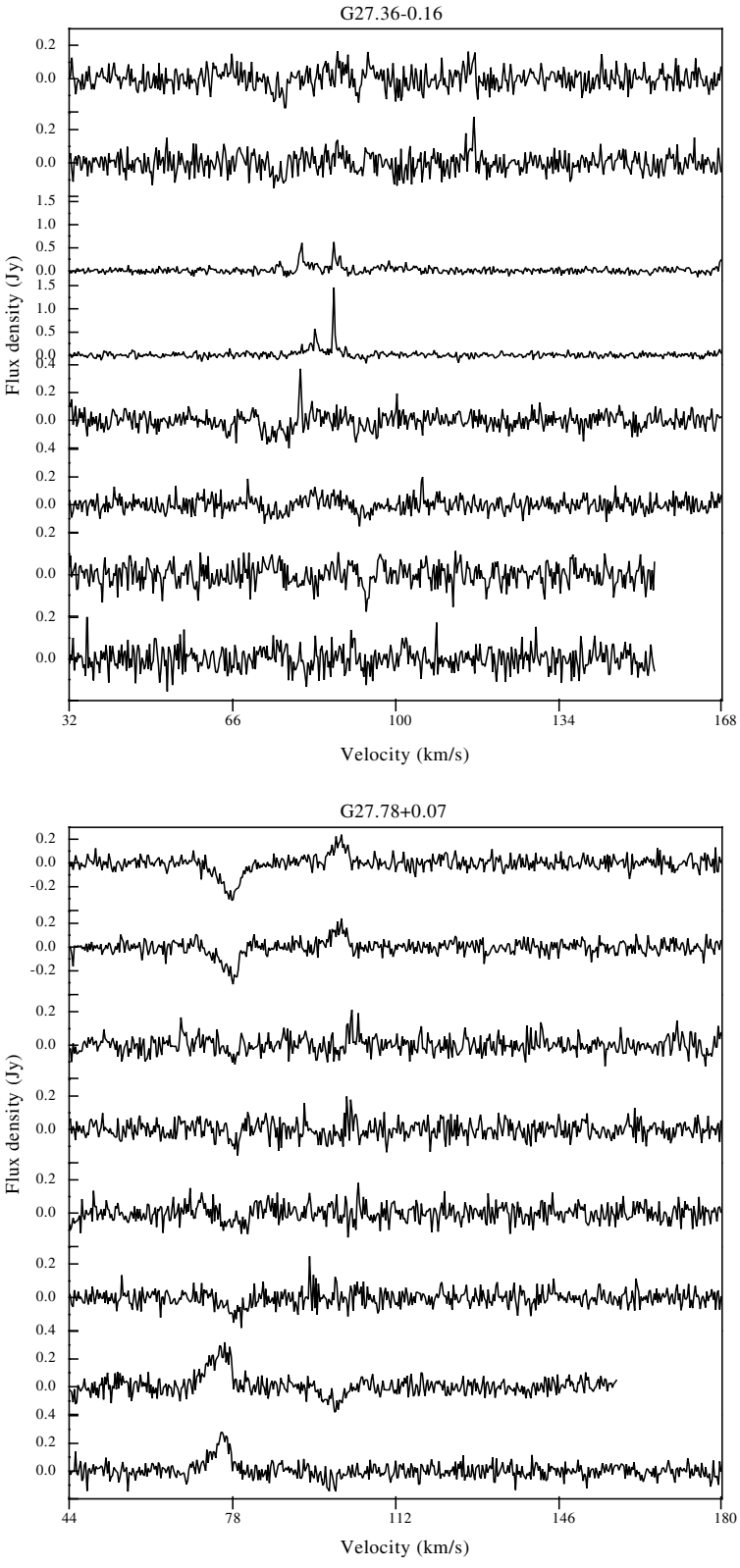

Fig. A.1. continued.

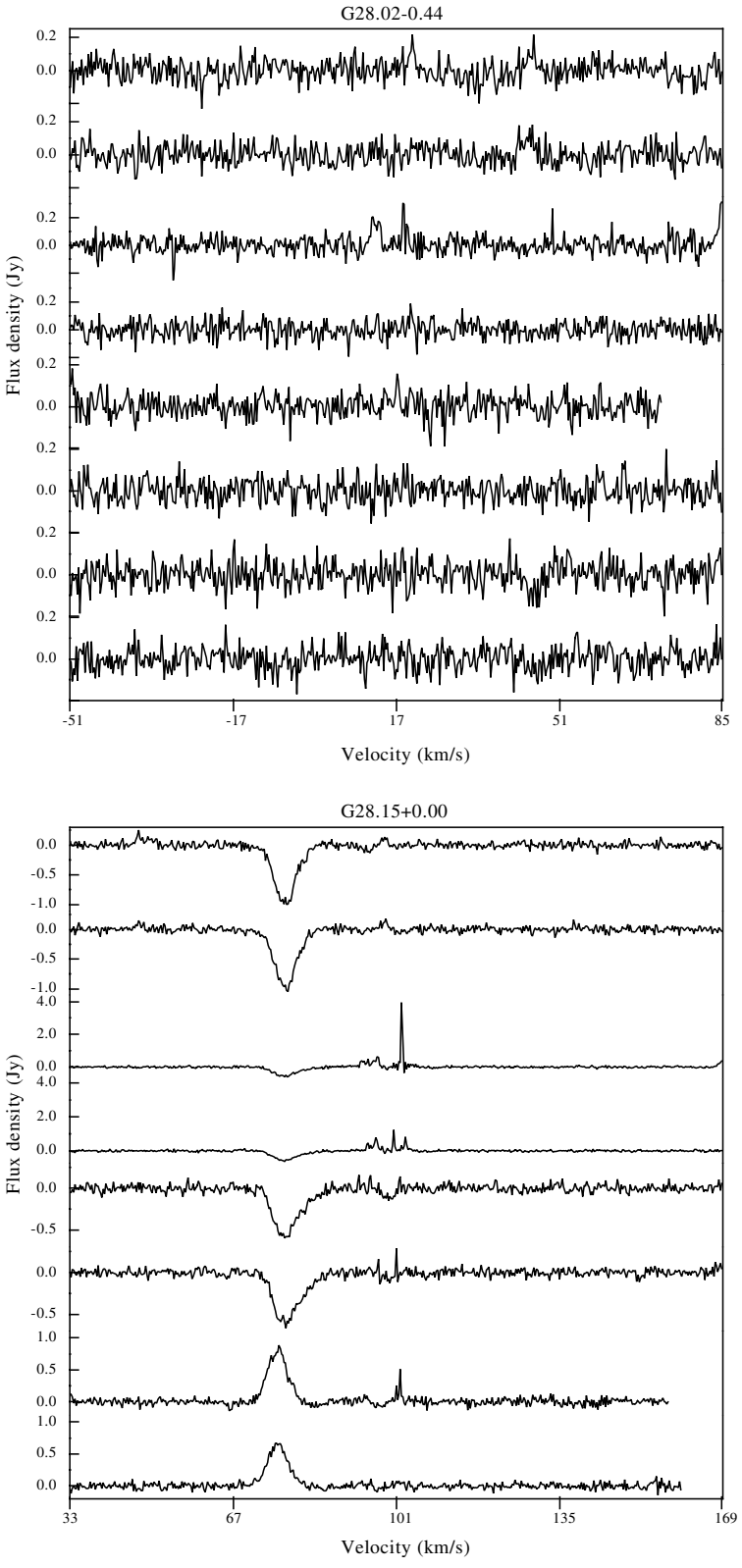

Fig. A.1. continued.

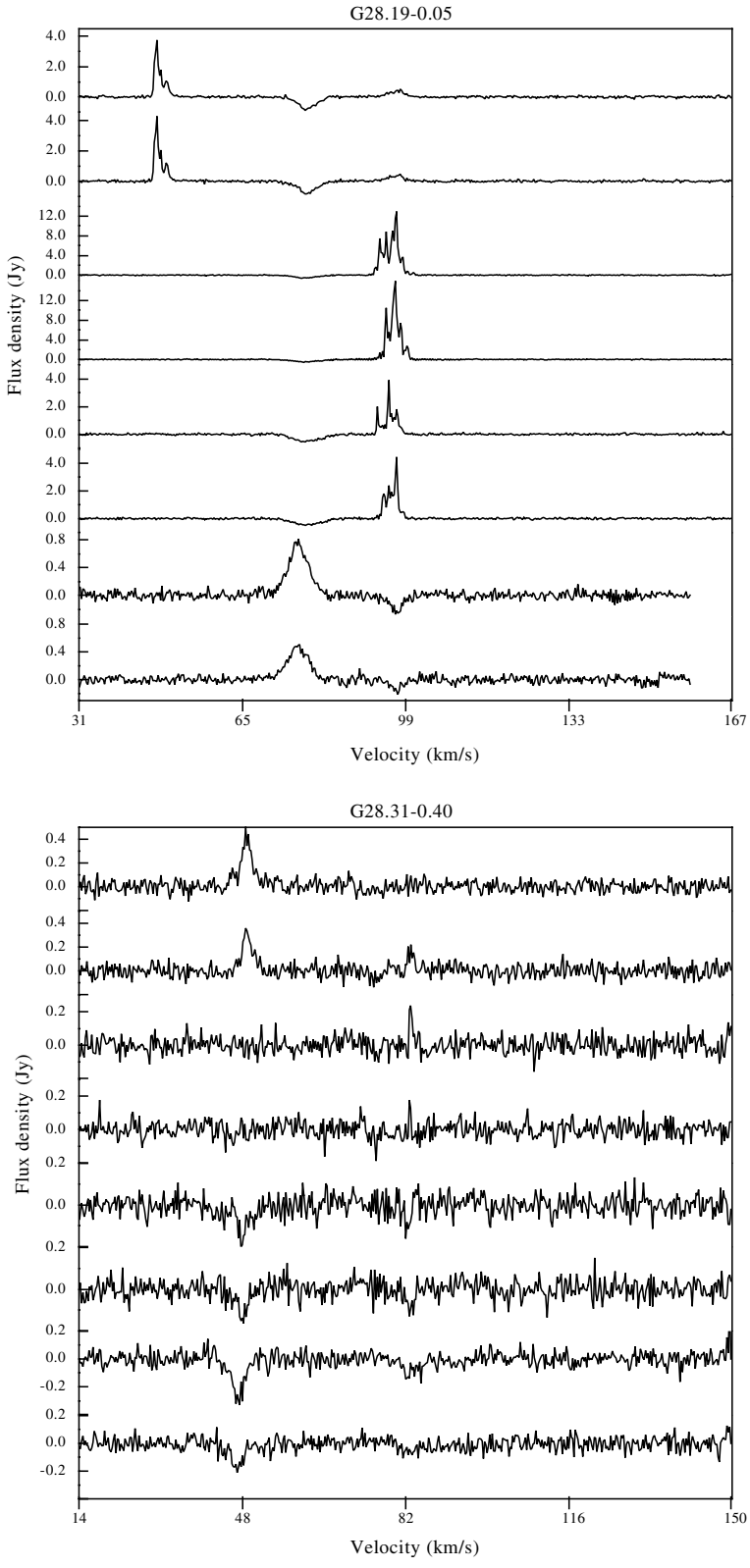

Fig. A.1. continued.

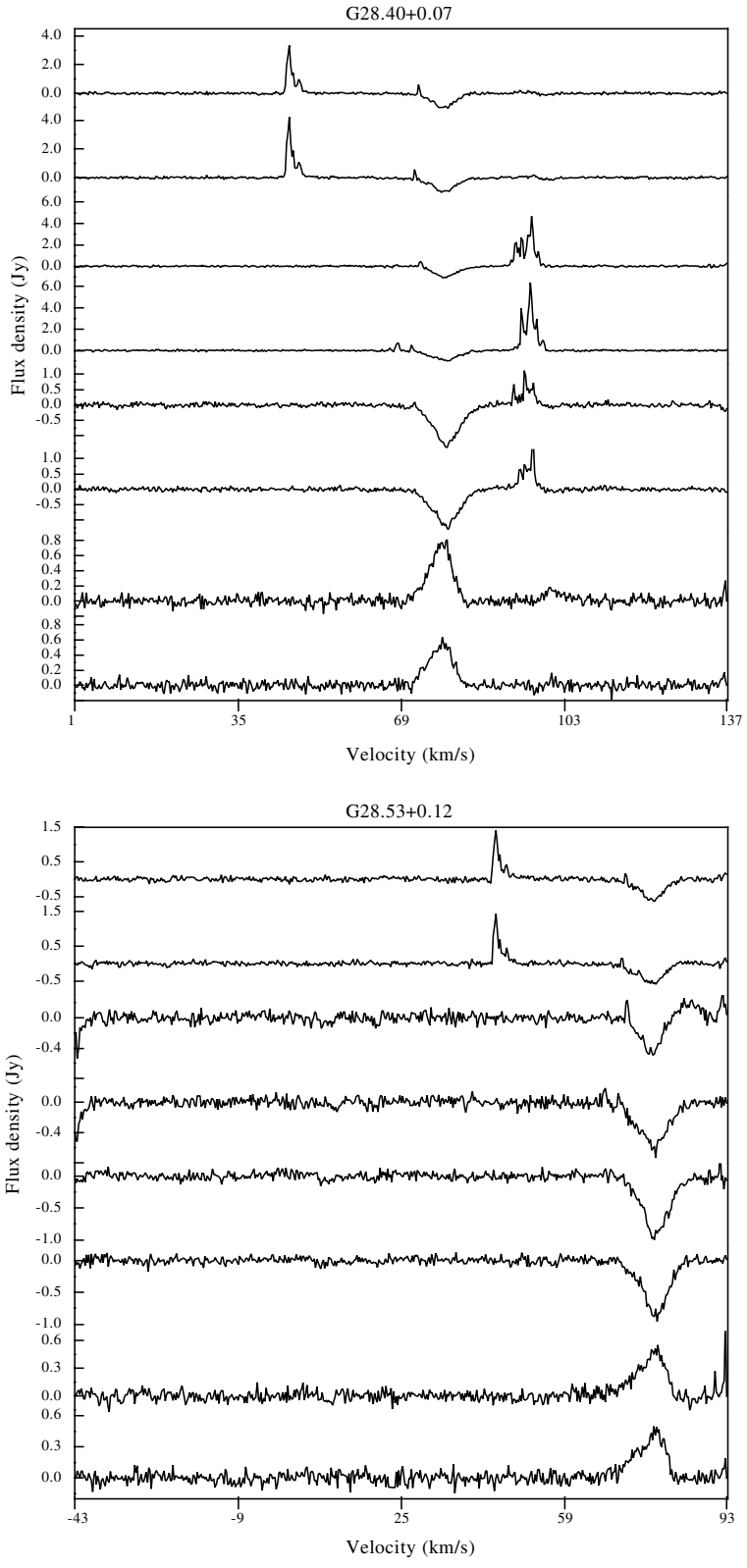

Fig. A.1. continued.

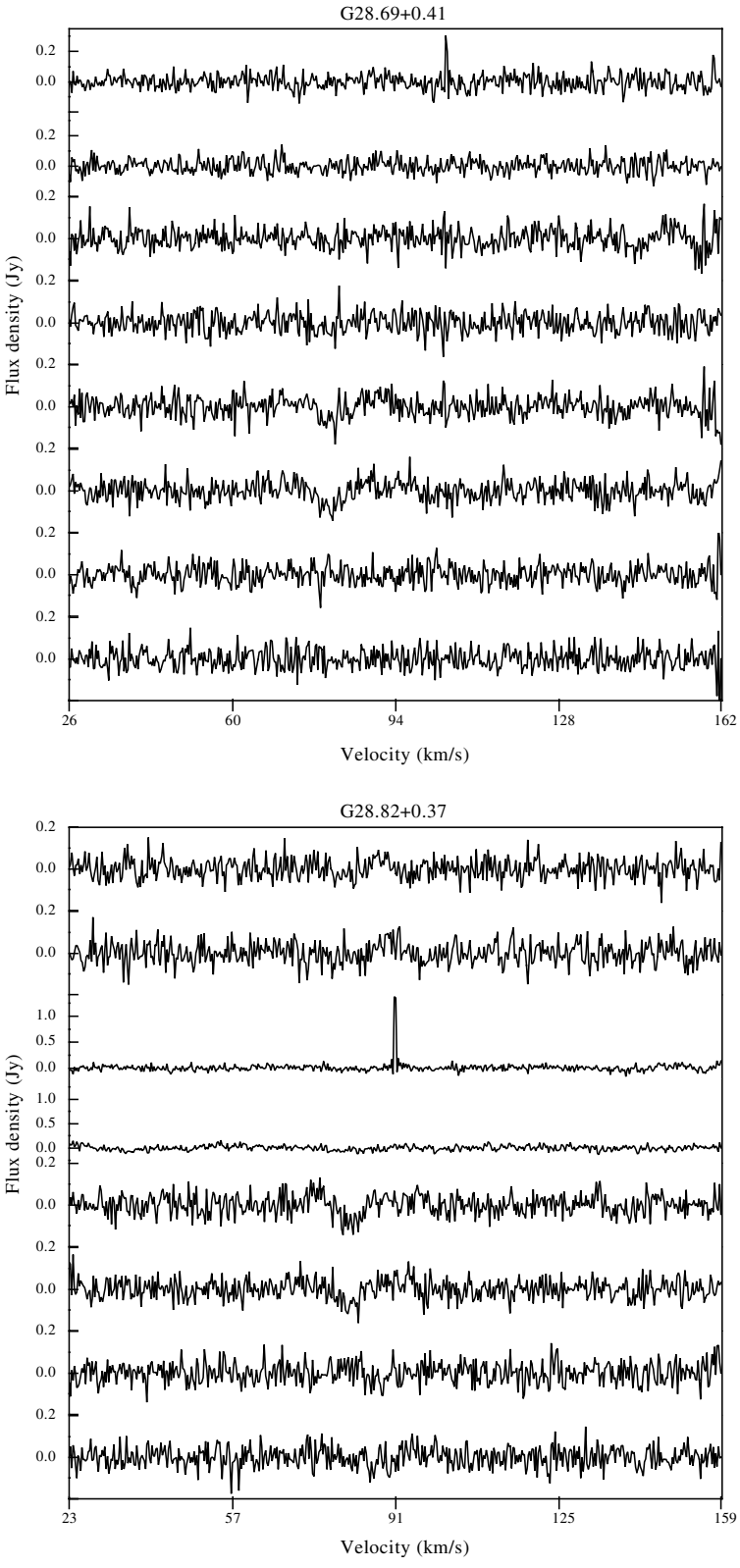

Fig. A.1. continued.

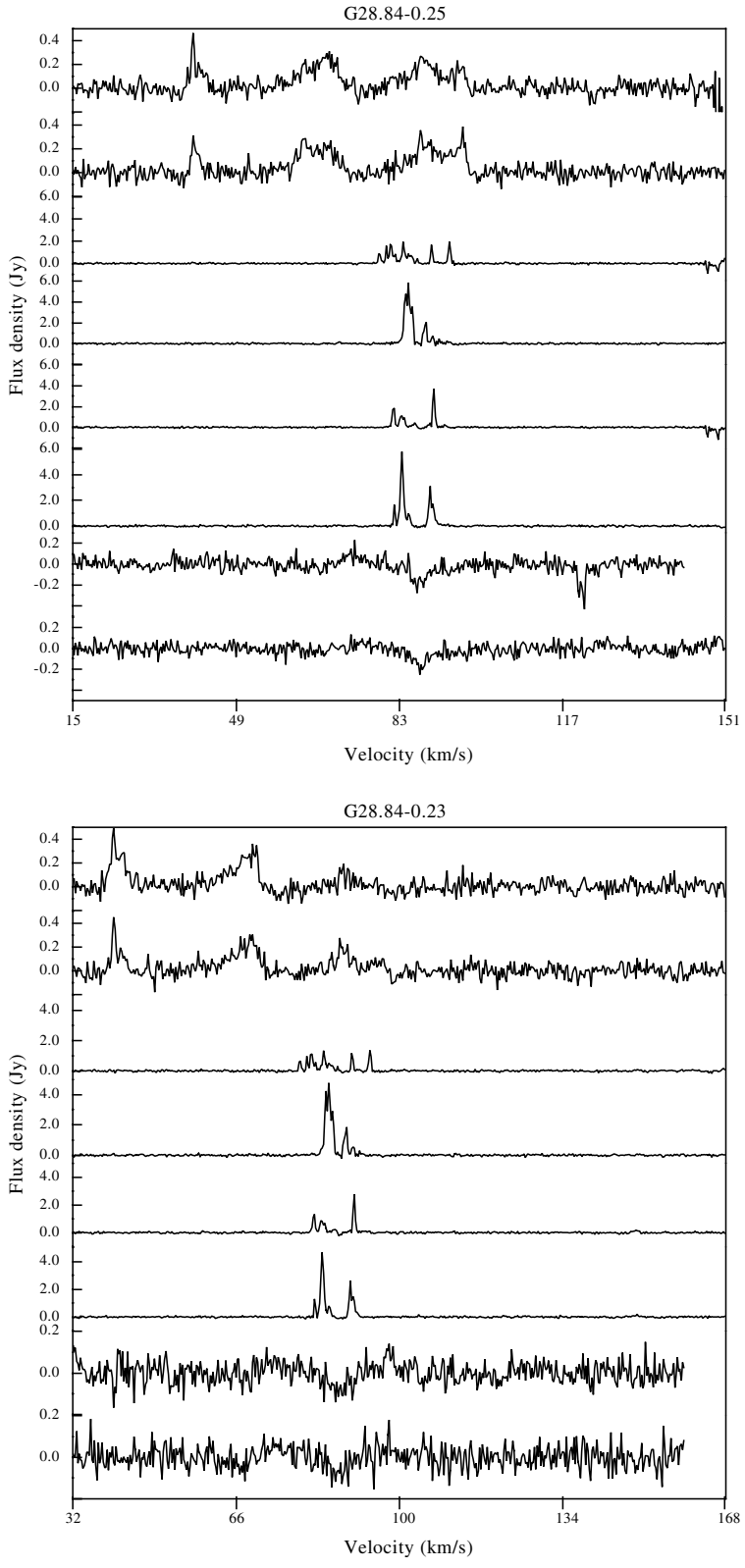

Fig. A.1. continued.

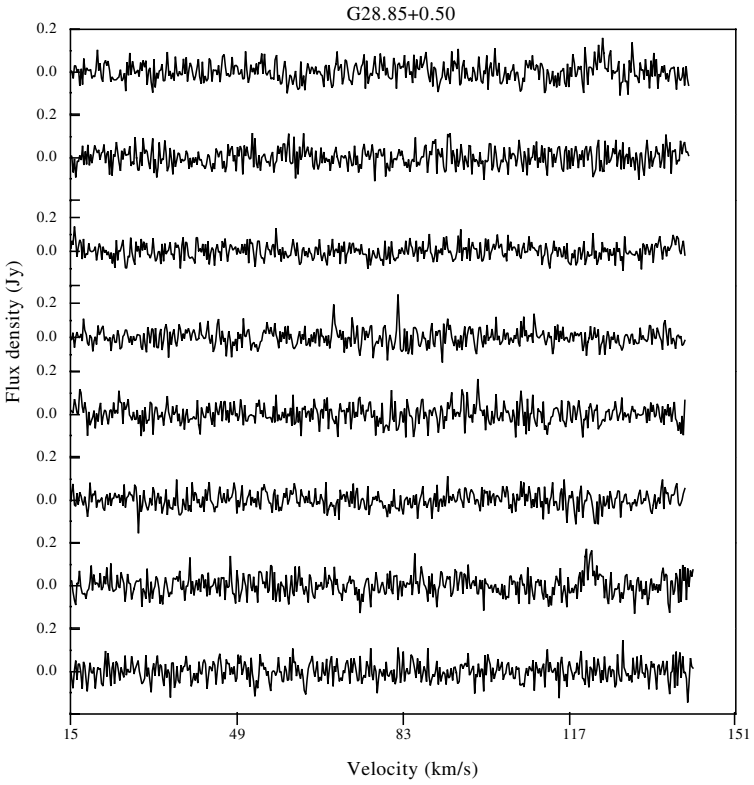

Fig. A.1. continued.

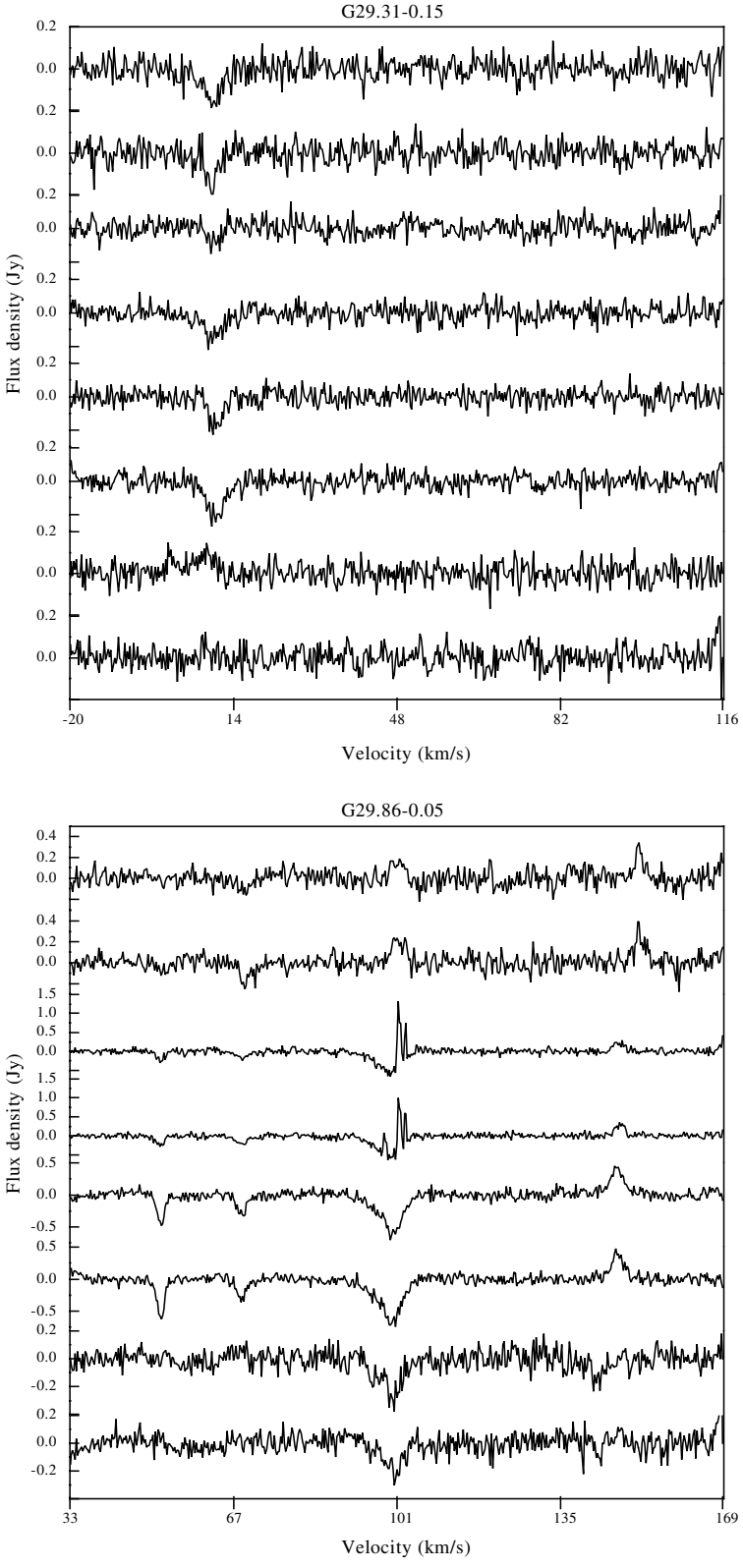

Fig. A.1. continued.

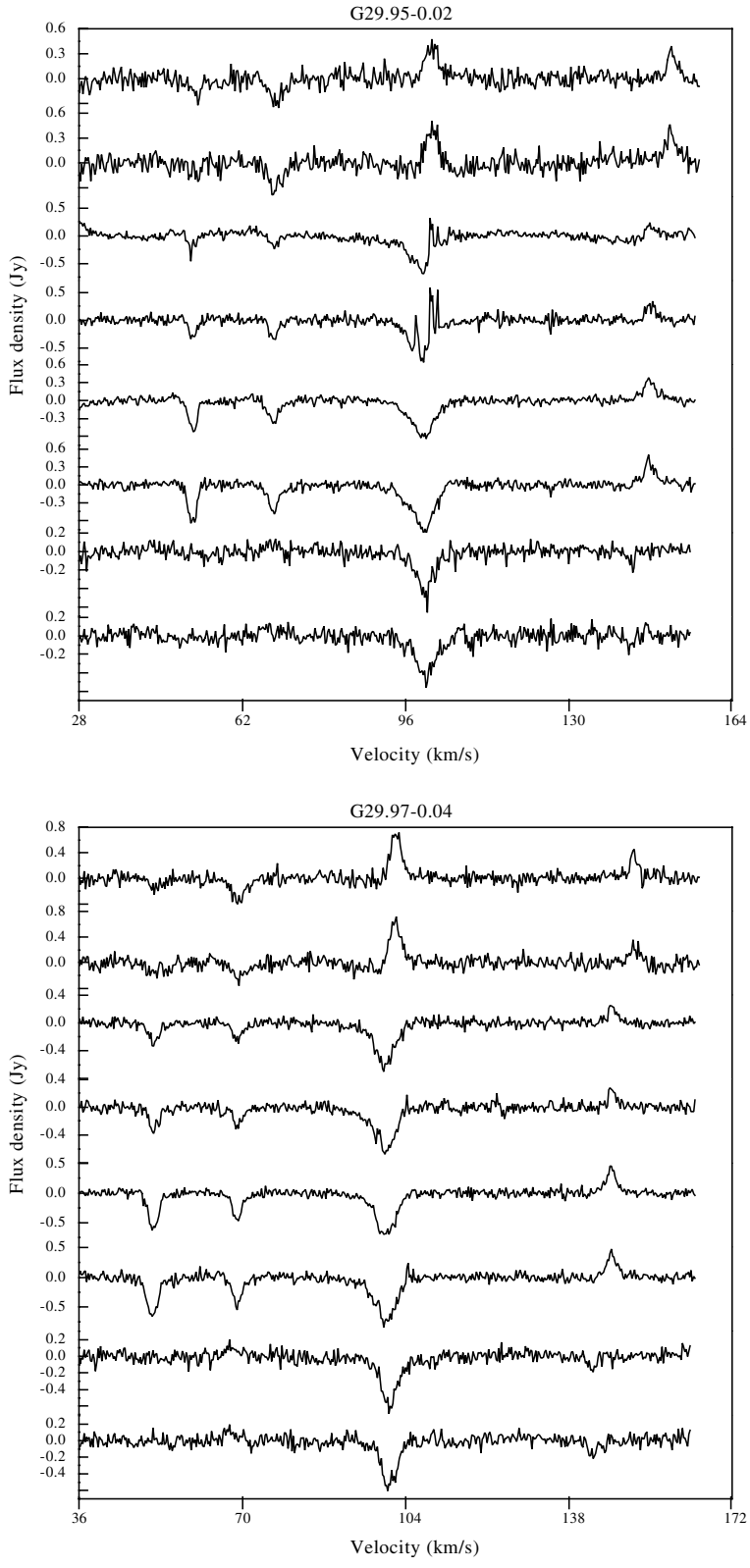

Fig. A.1. continued.

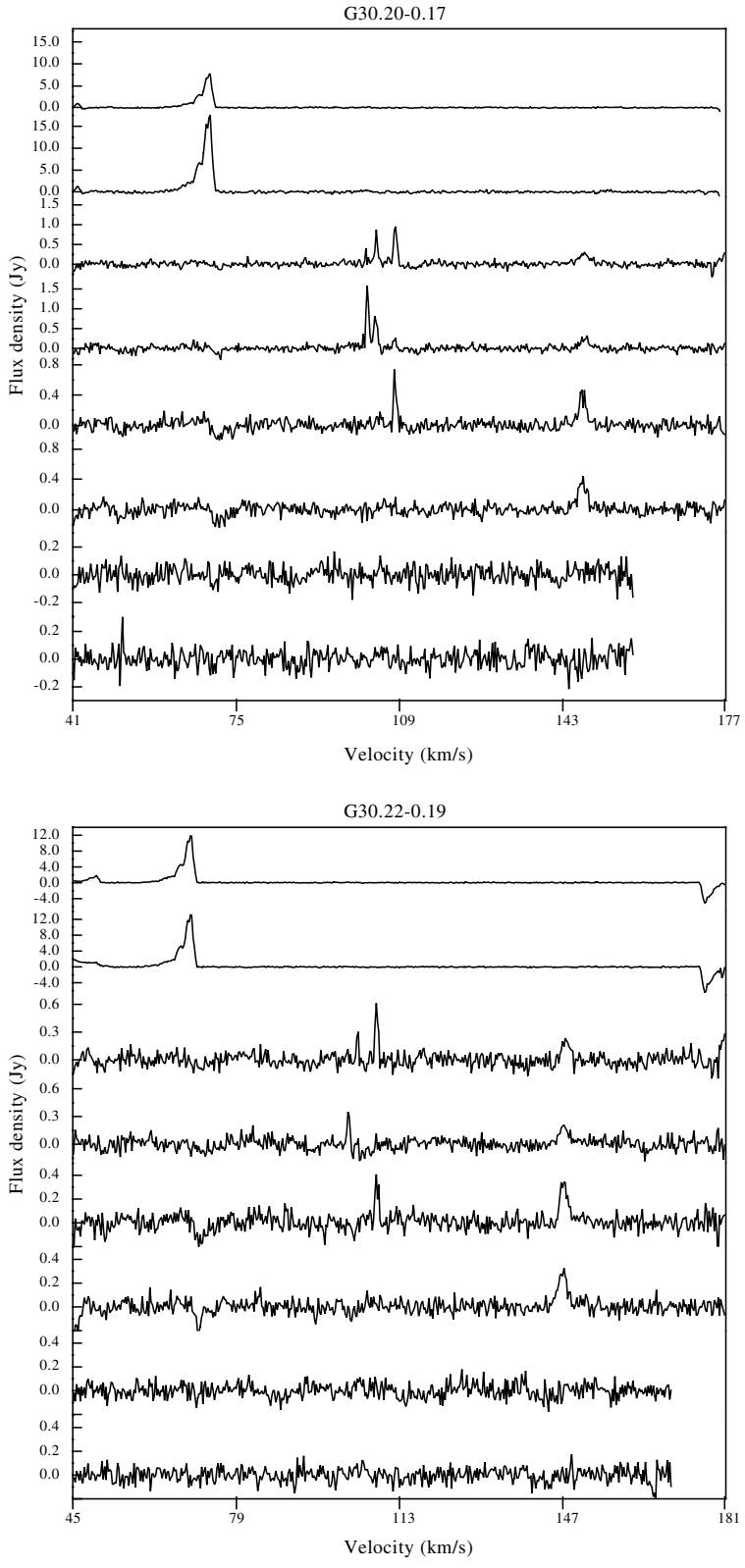

Fig. A.1. continued.

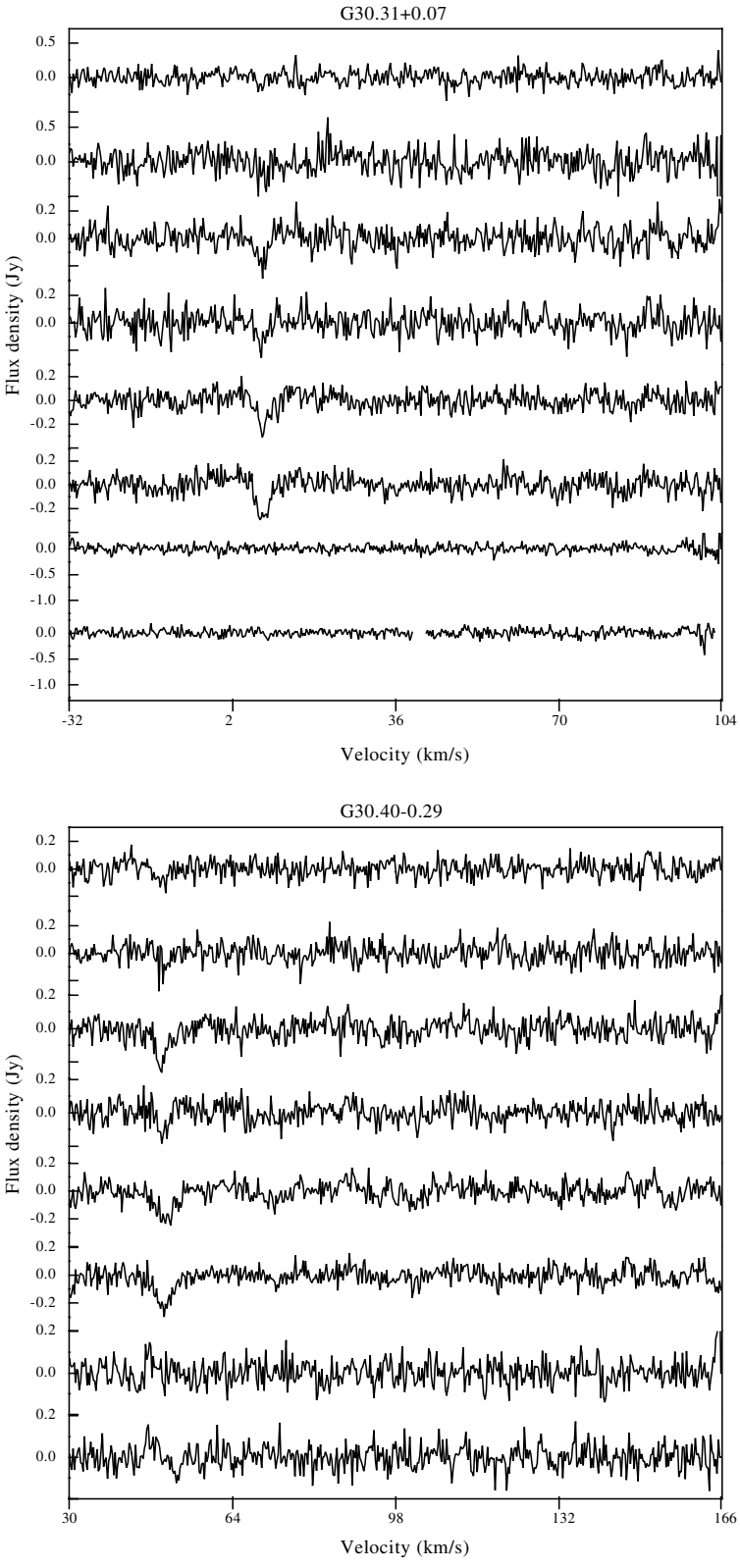

Fig. A.1. continued.

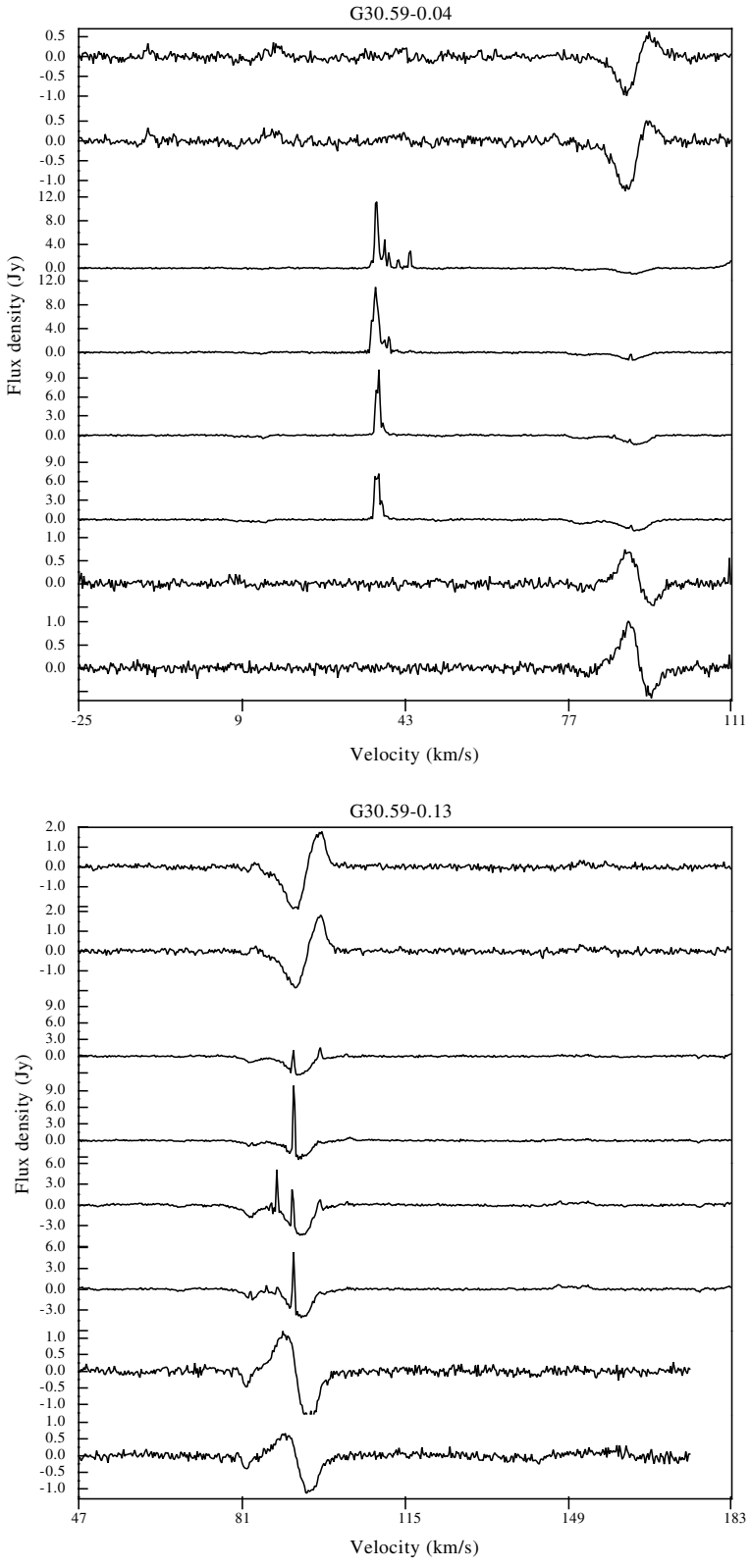

Fig. A.1. continued.

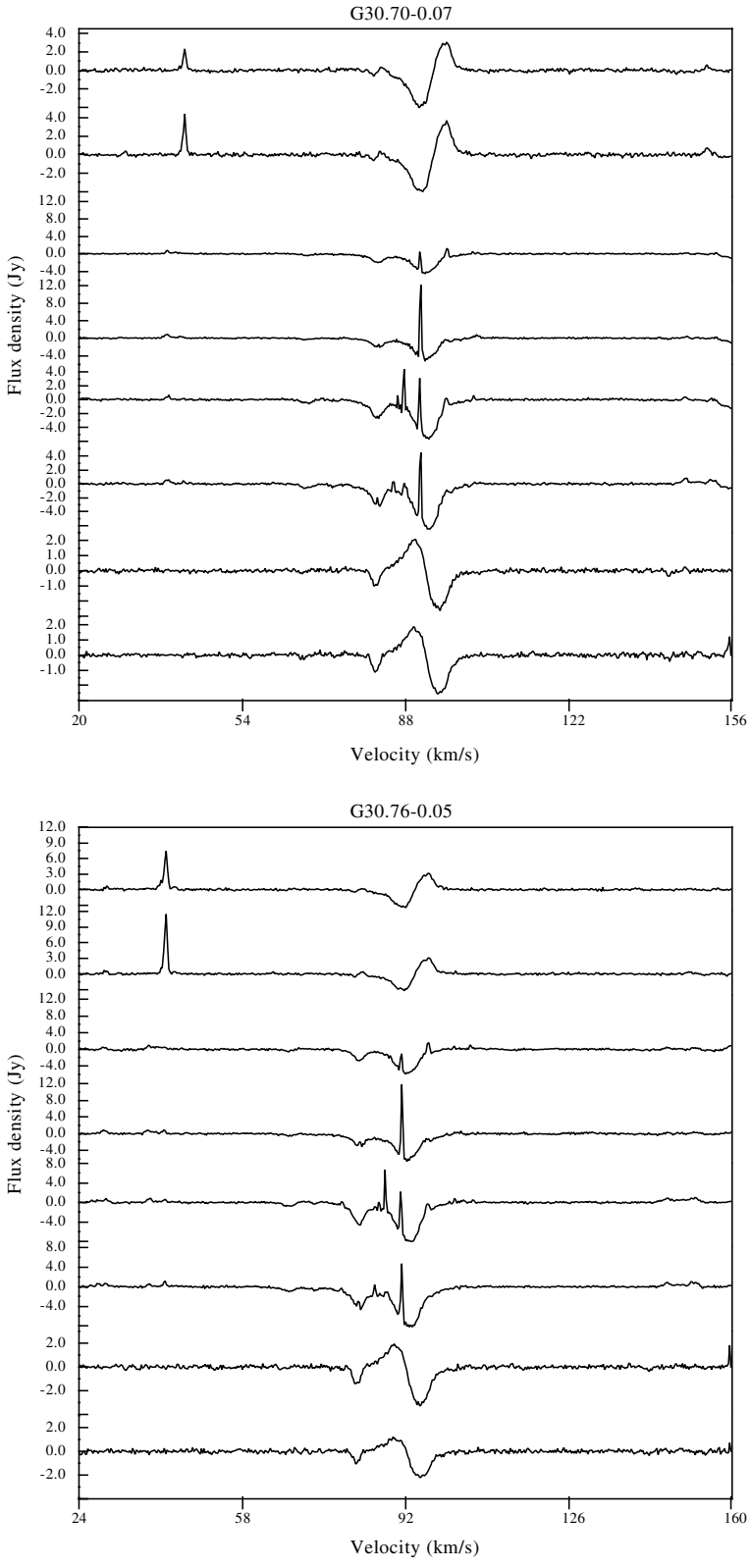

Fig. A.1. continued.

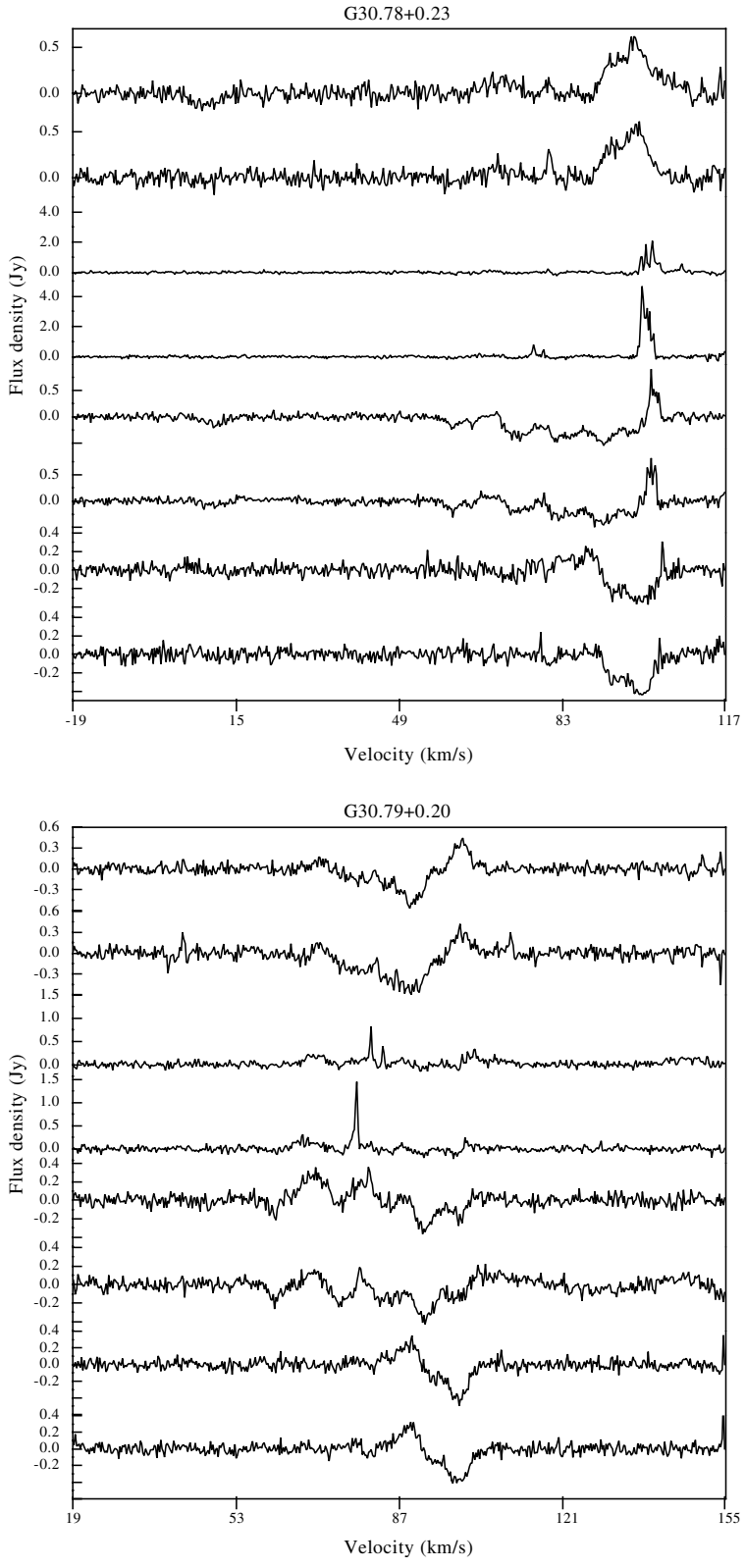

Fig. A.1. continued.

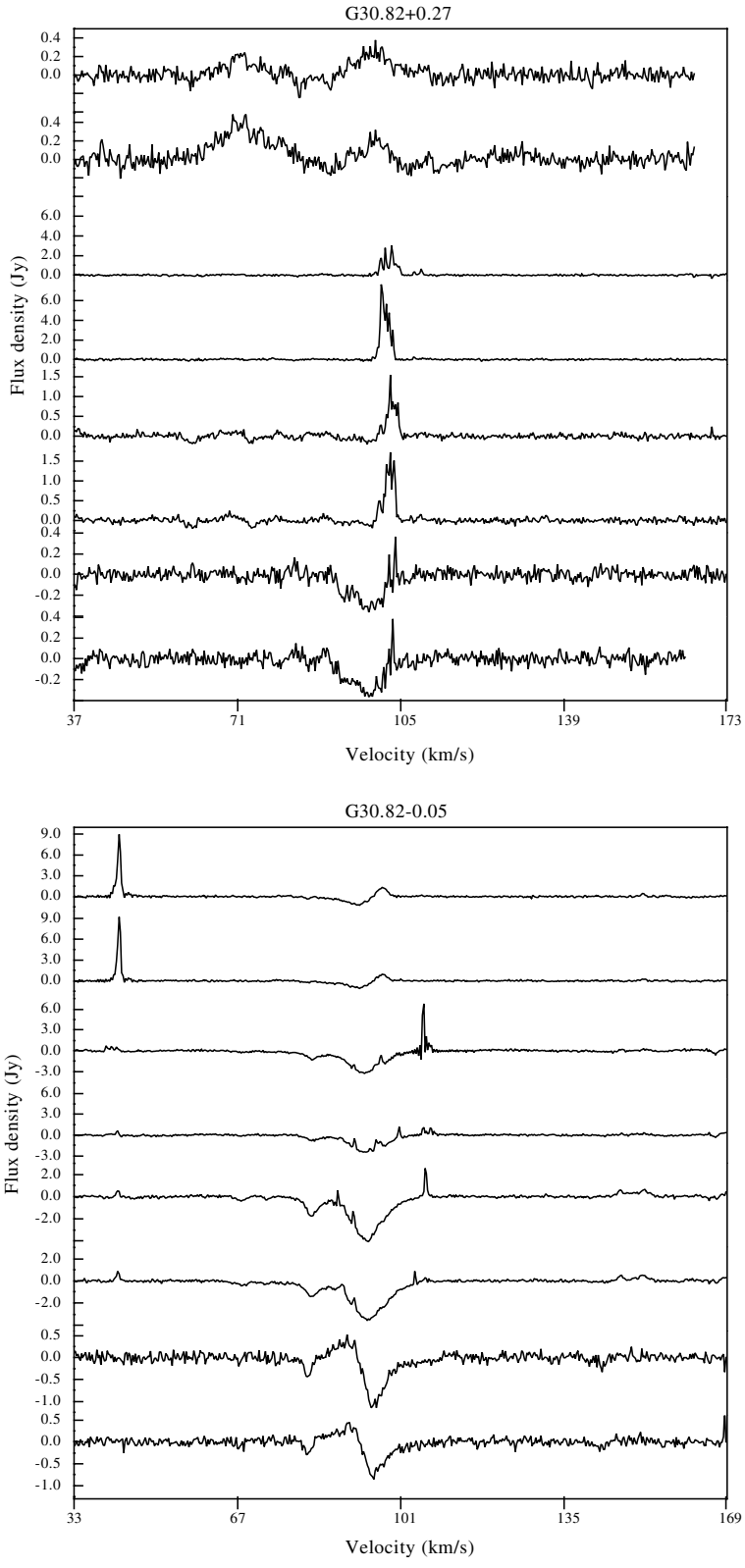

Fig. A.1. continued.

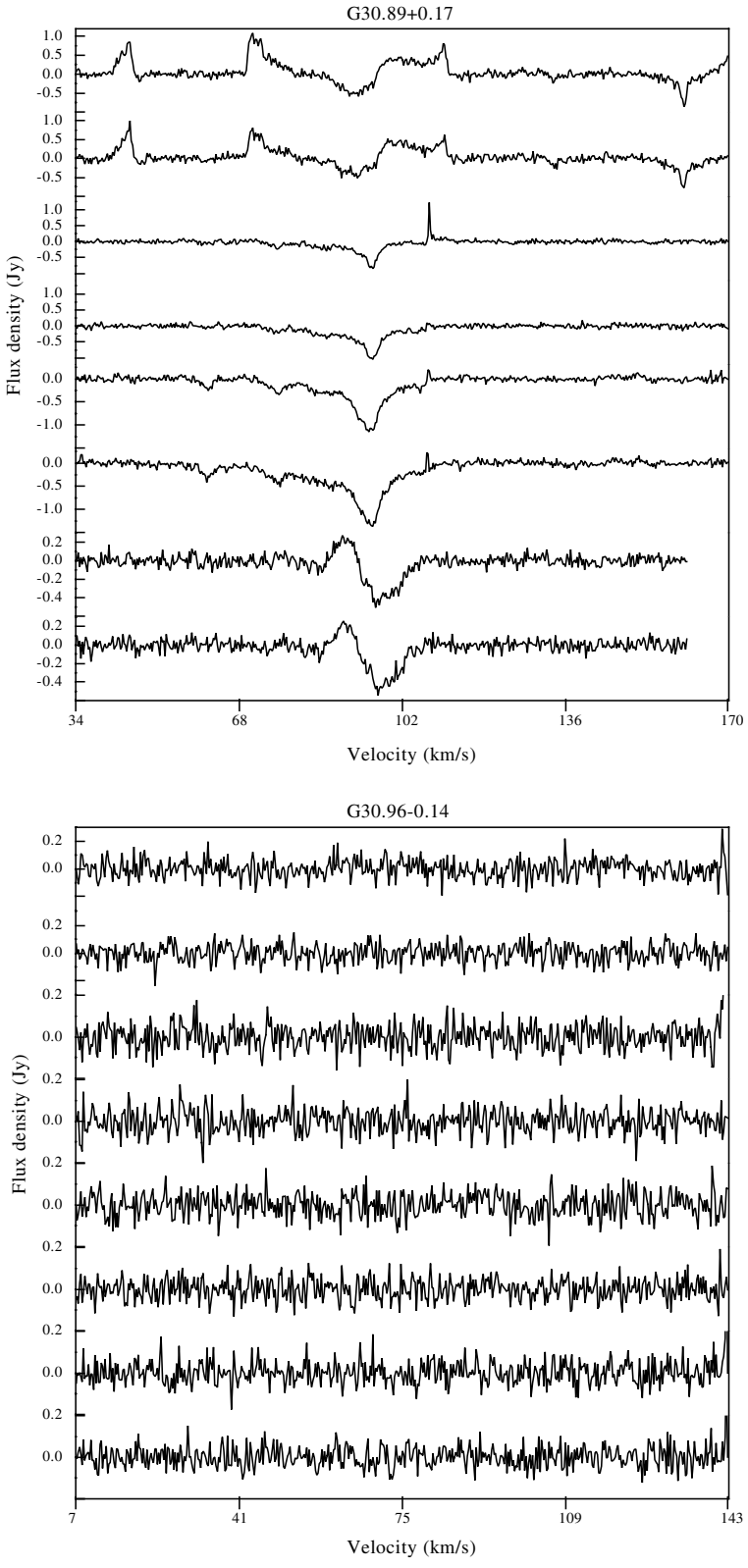

Fig. A.1. continued.

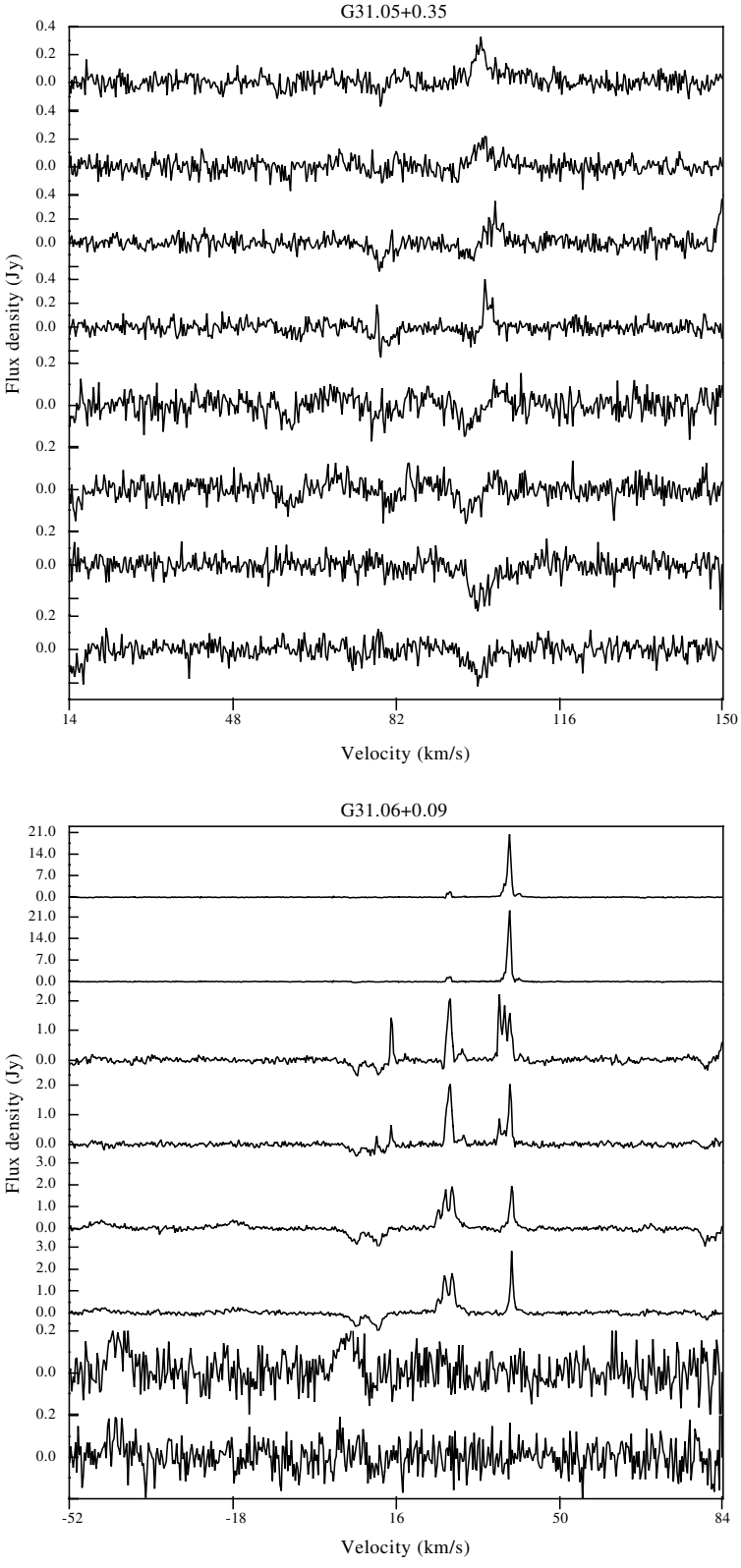

Fig. A.1. continued.

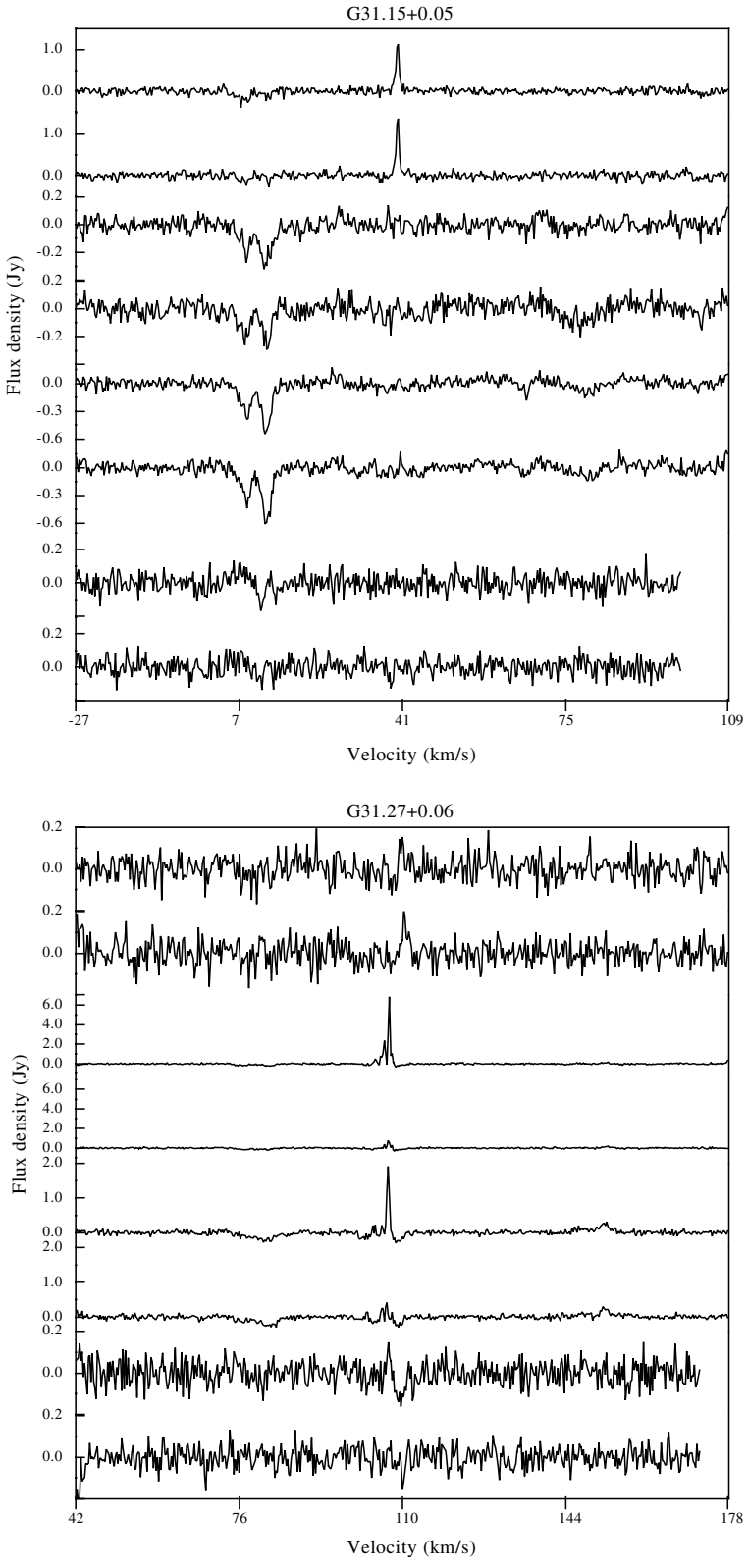

Fig. A.1. continued.

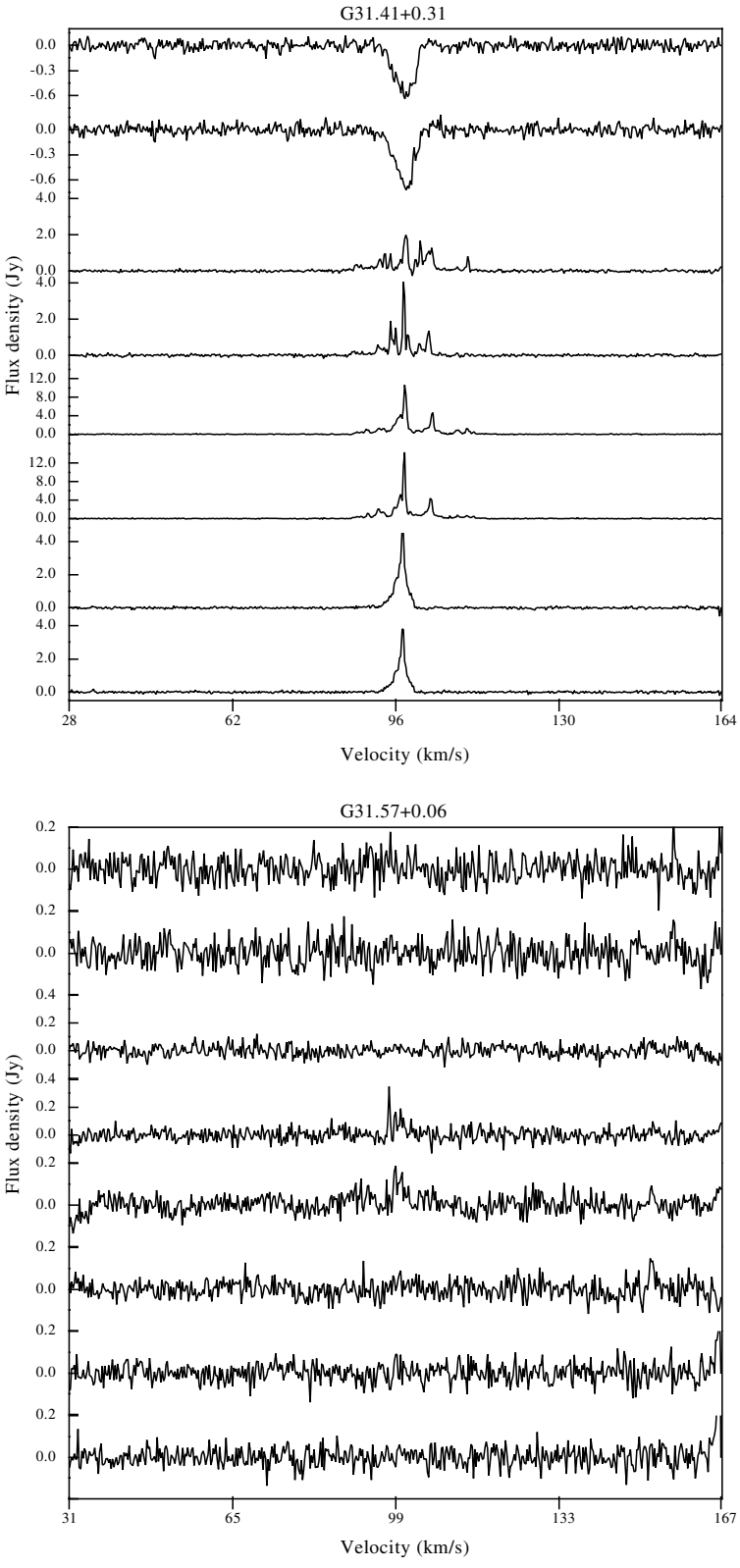

Fig. A.1. continued.

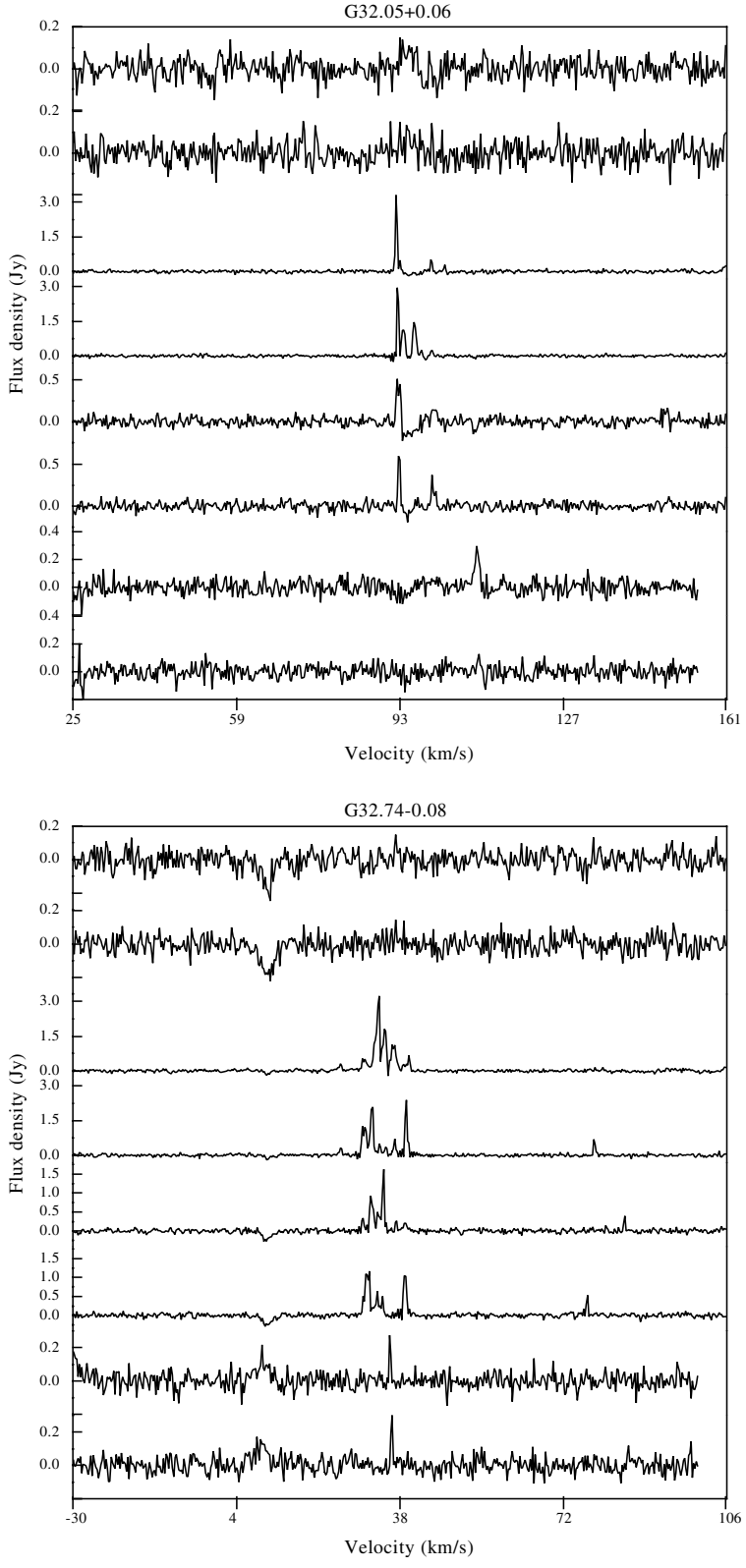

Fig. A.1. continued.

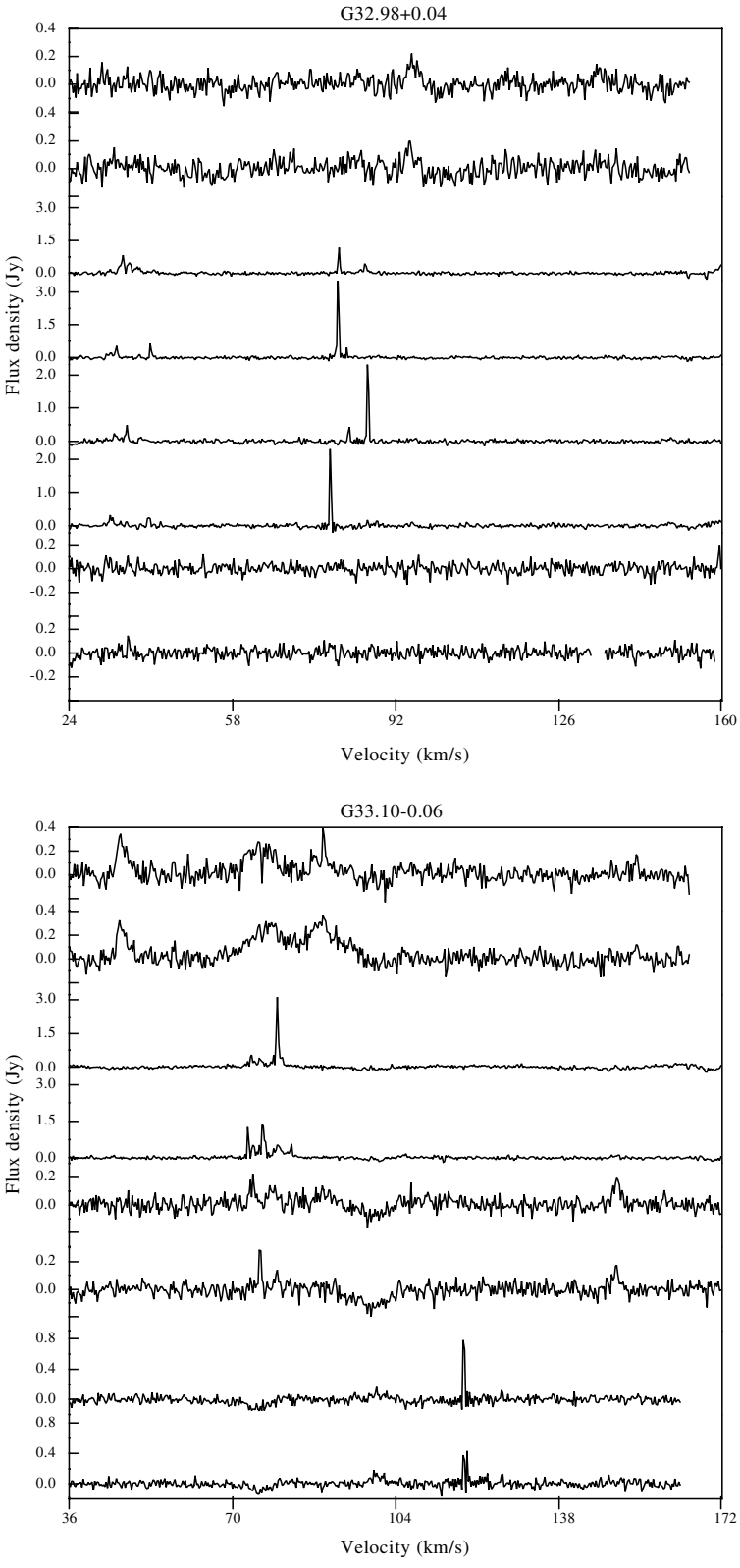

Fig. A.1. continued.

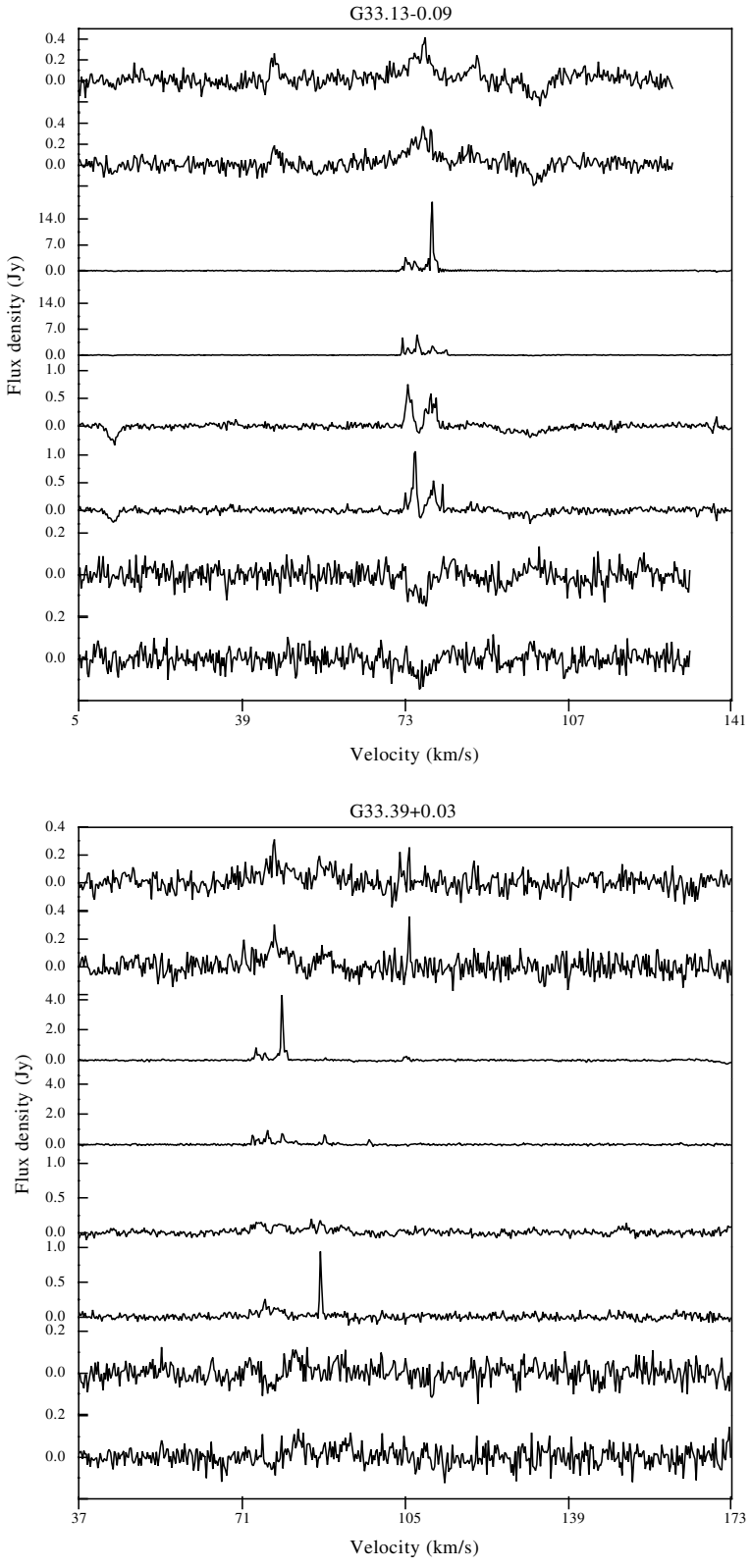

Fig. A.1. continued.

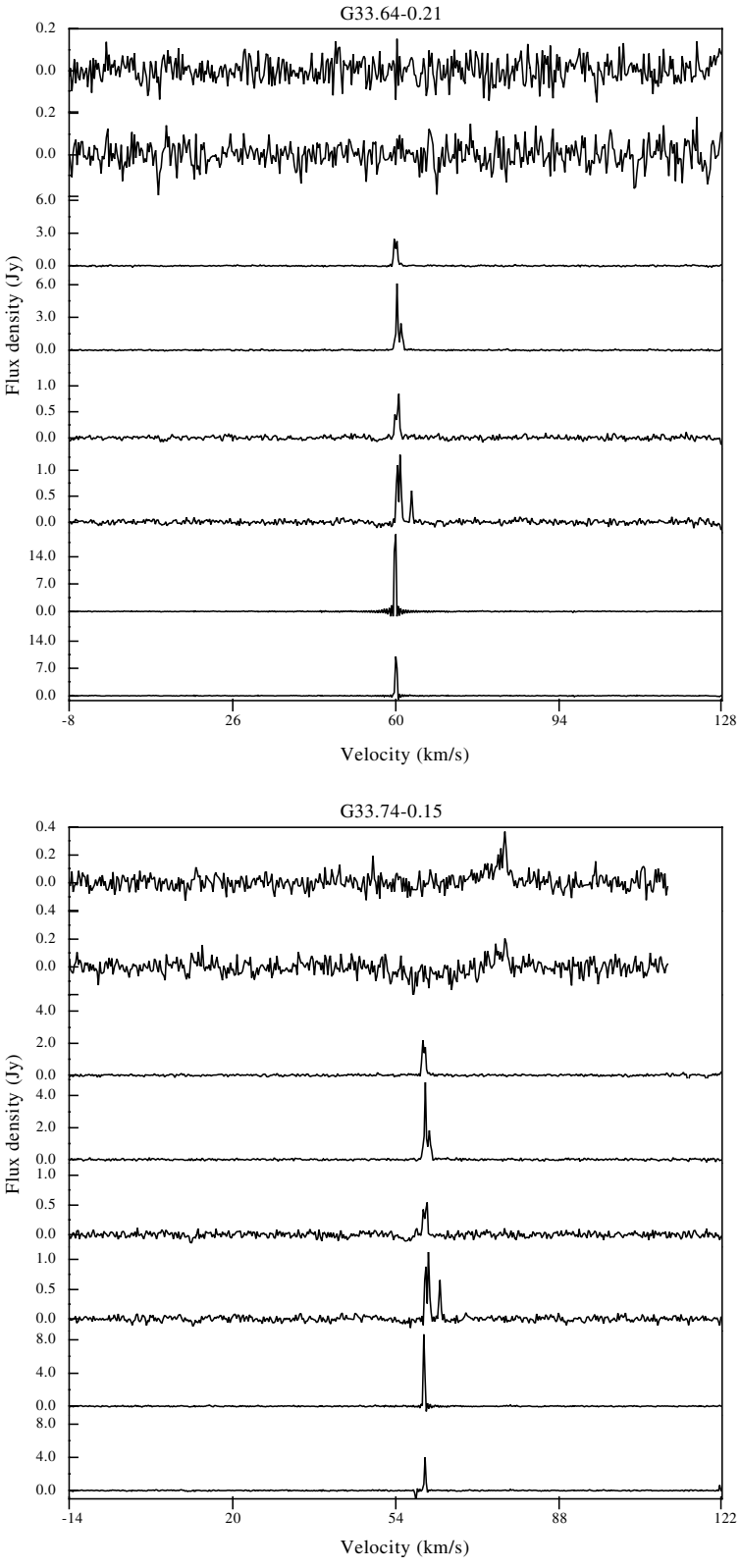

Fig. A.1. continued.

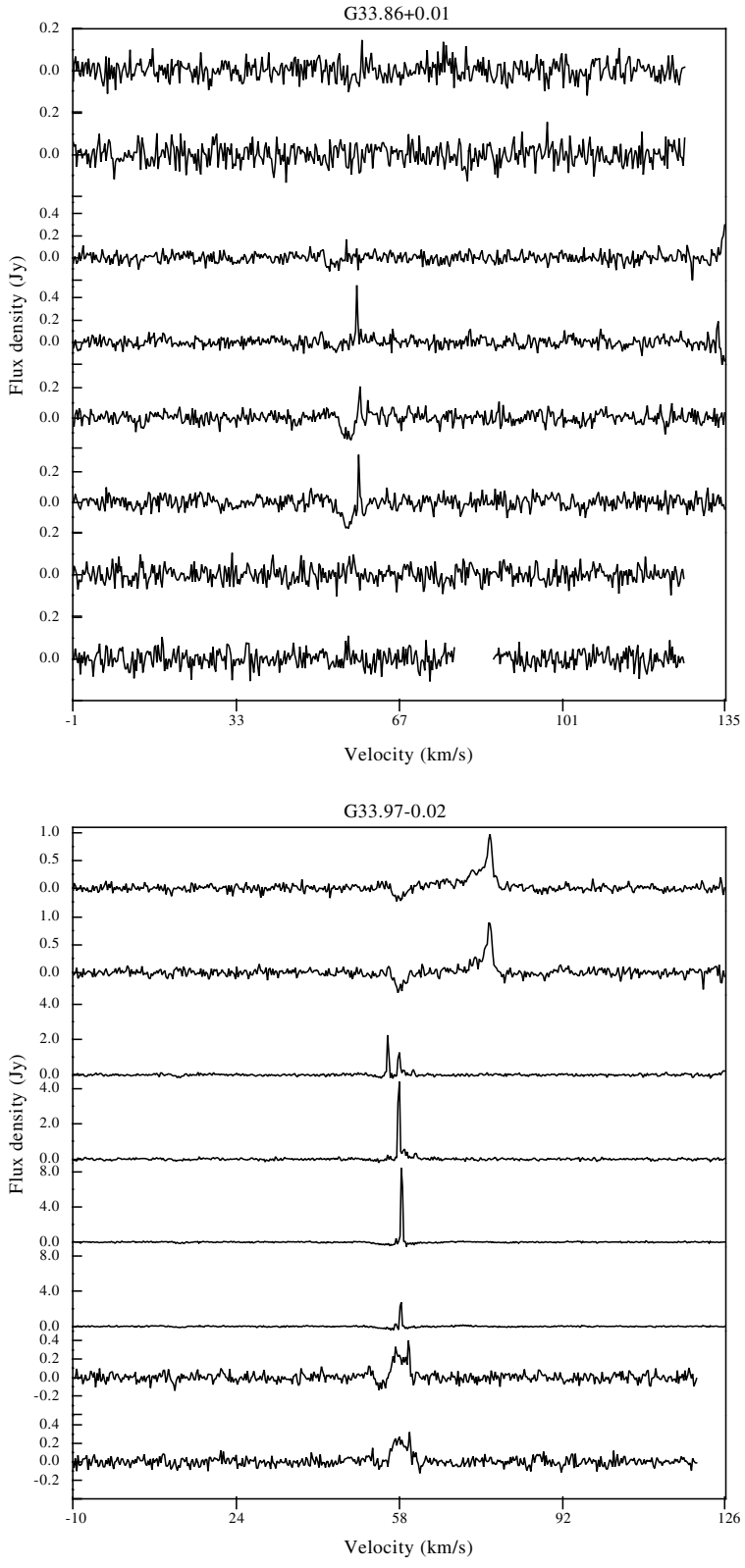

Fig. A.1. continued.

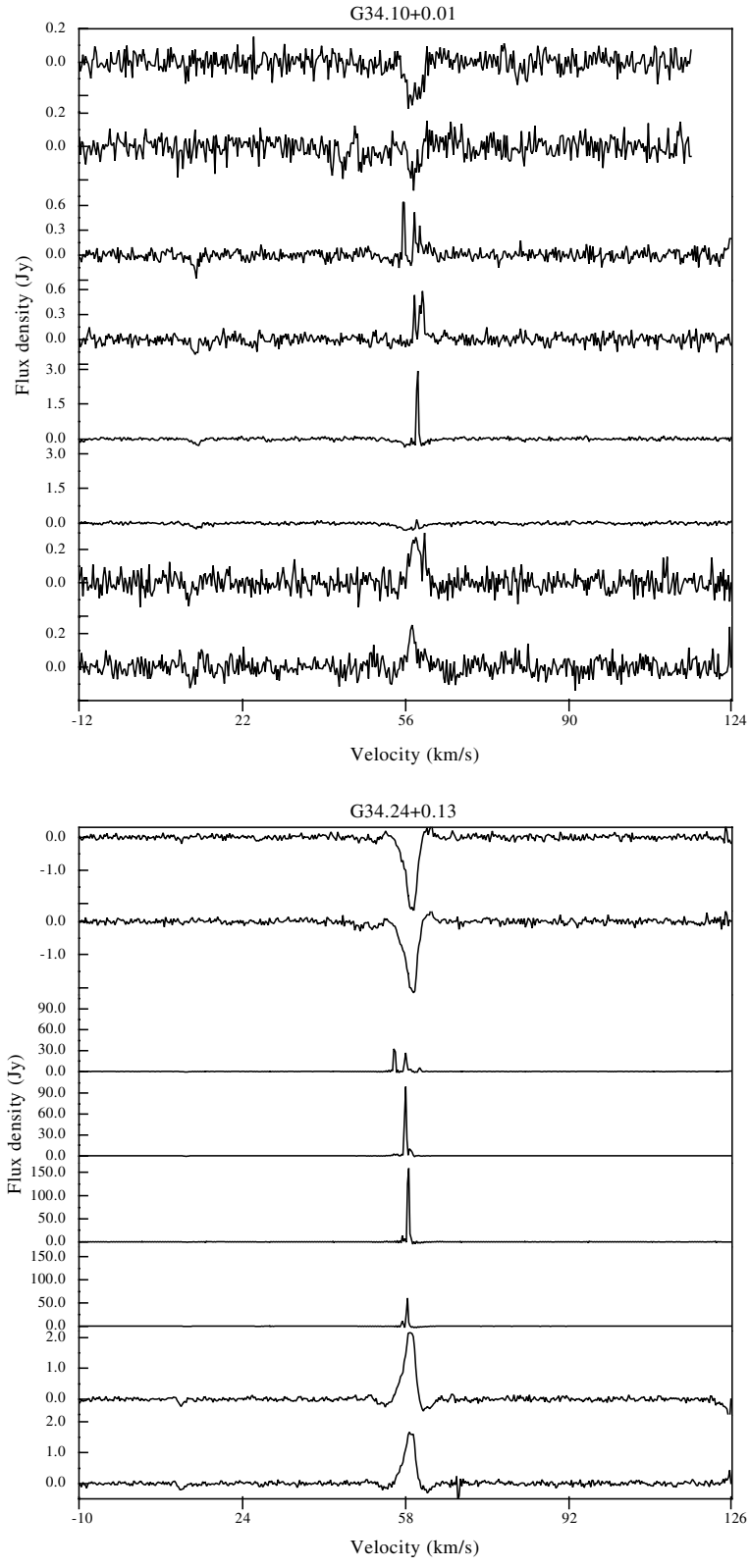

Fig. A.1. continued.

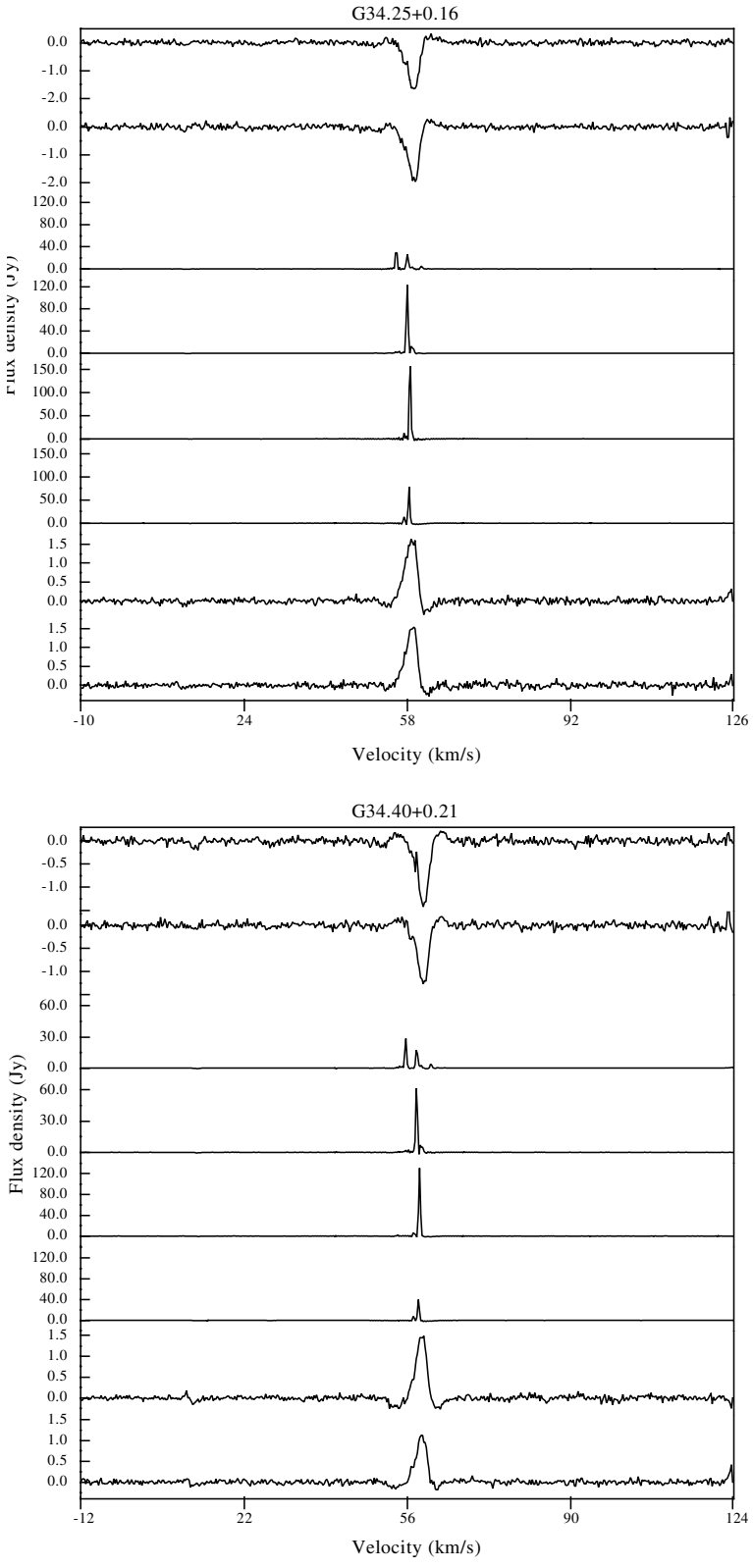

Fig. A.1. continued.

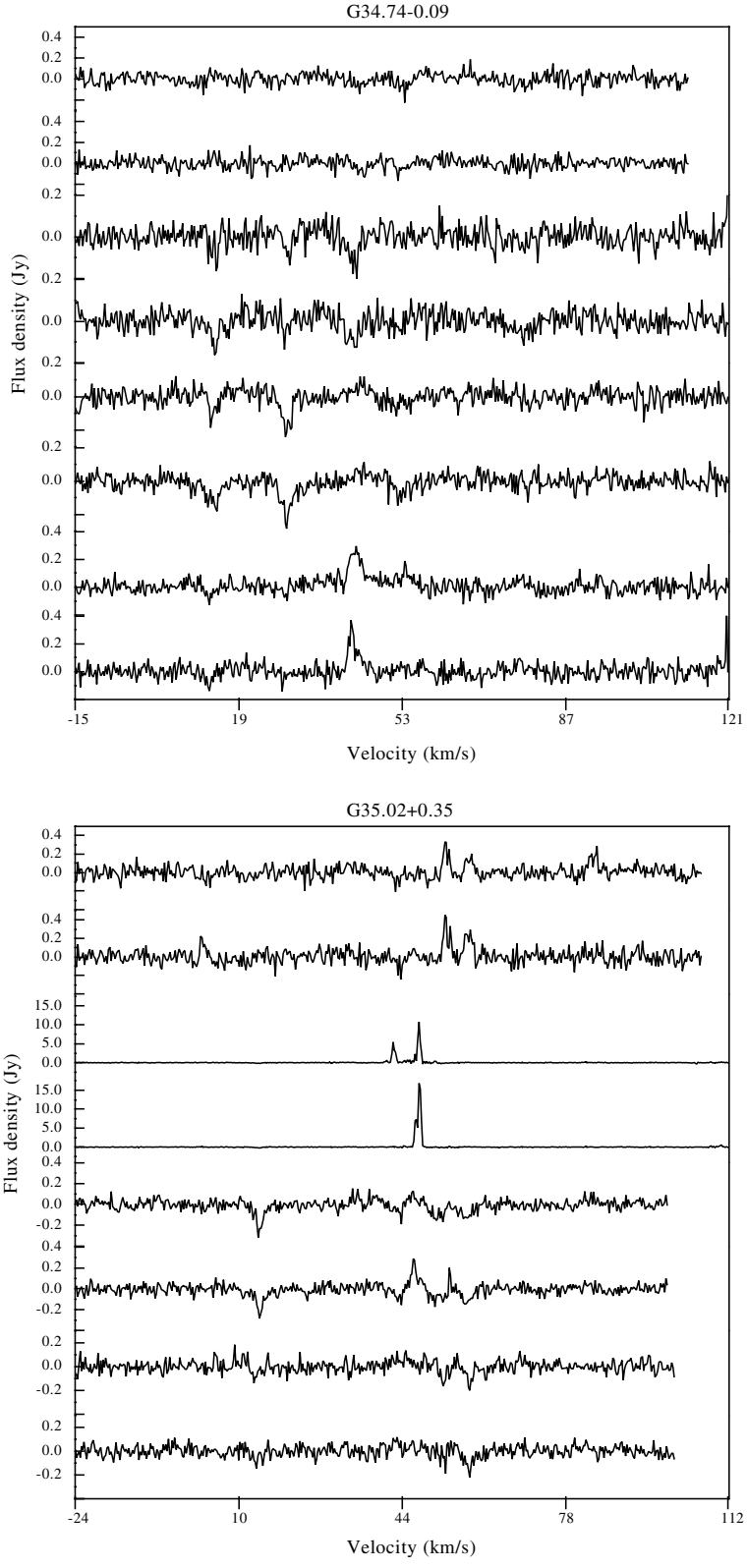

Fig. A.1. continued.

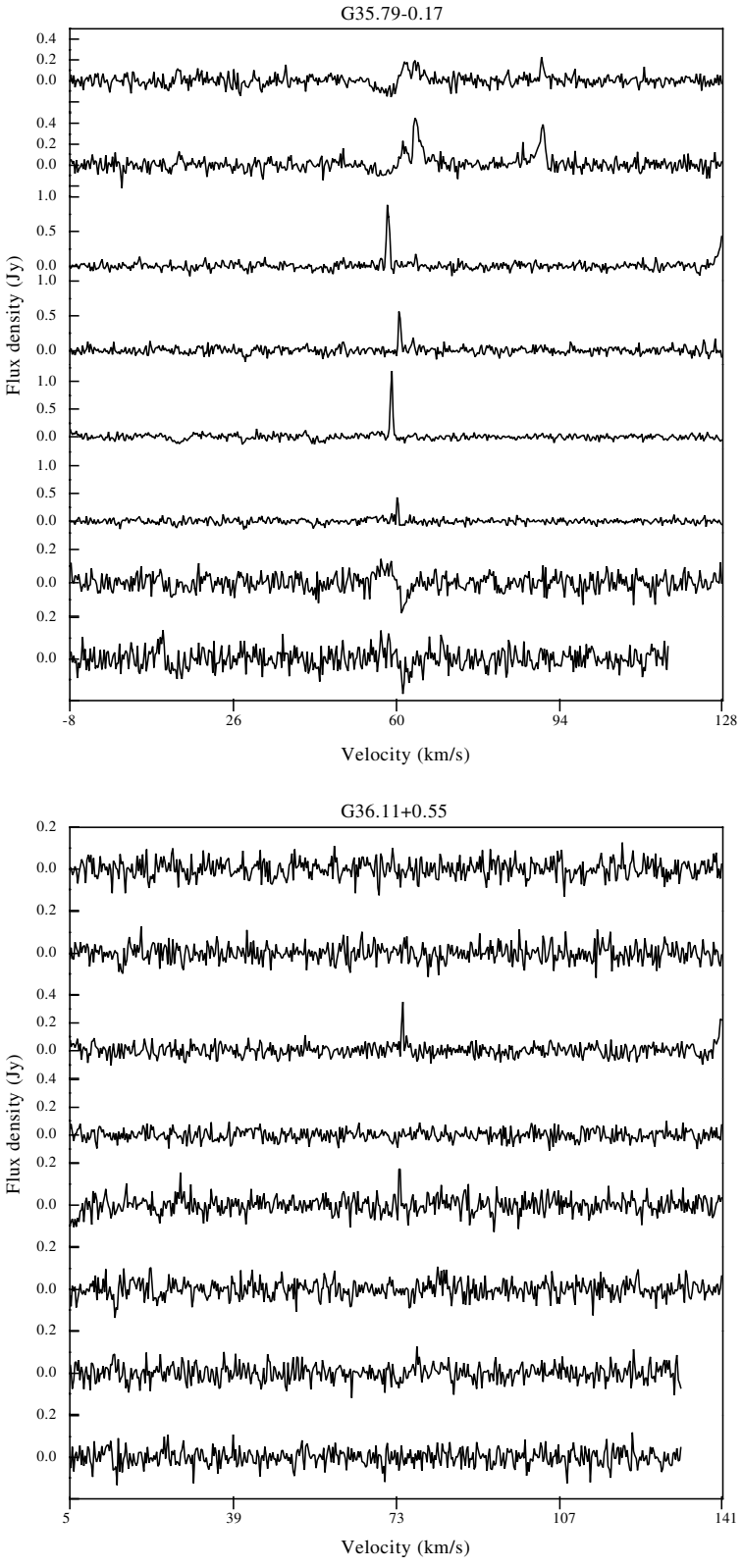

Fig. A.1. continued.

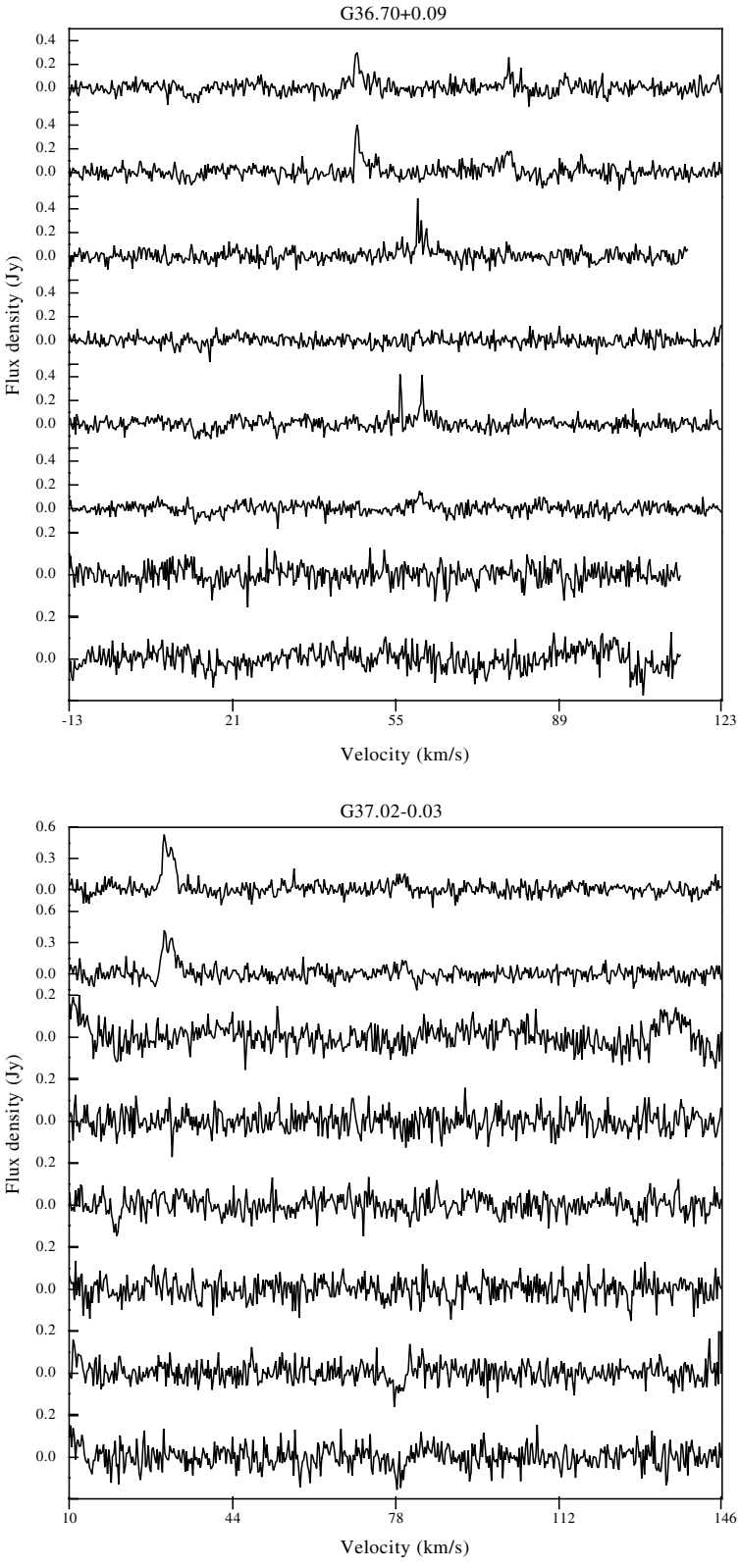

Fig. A.1. continued.

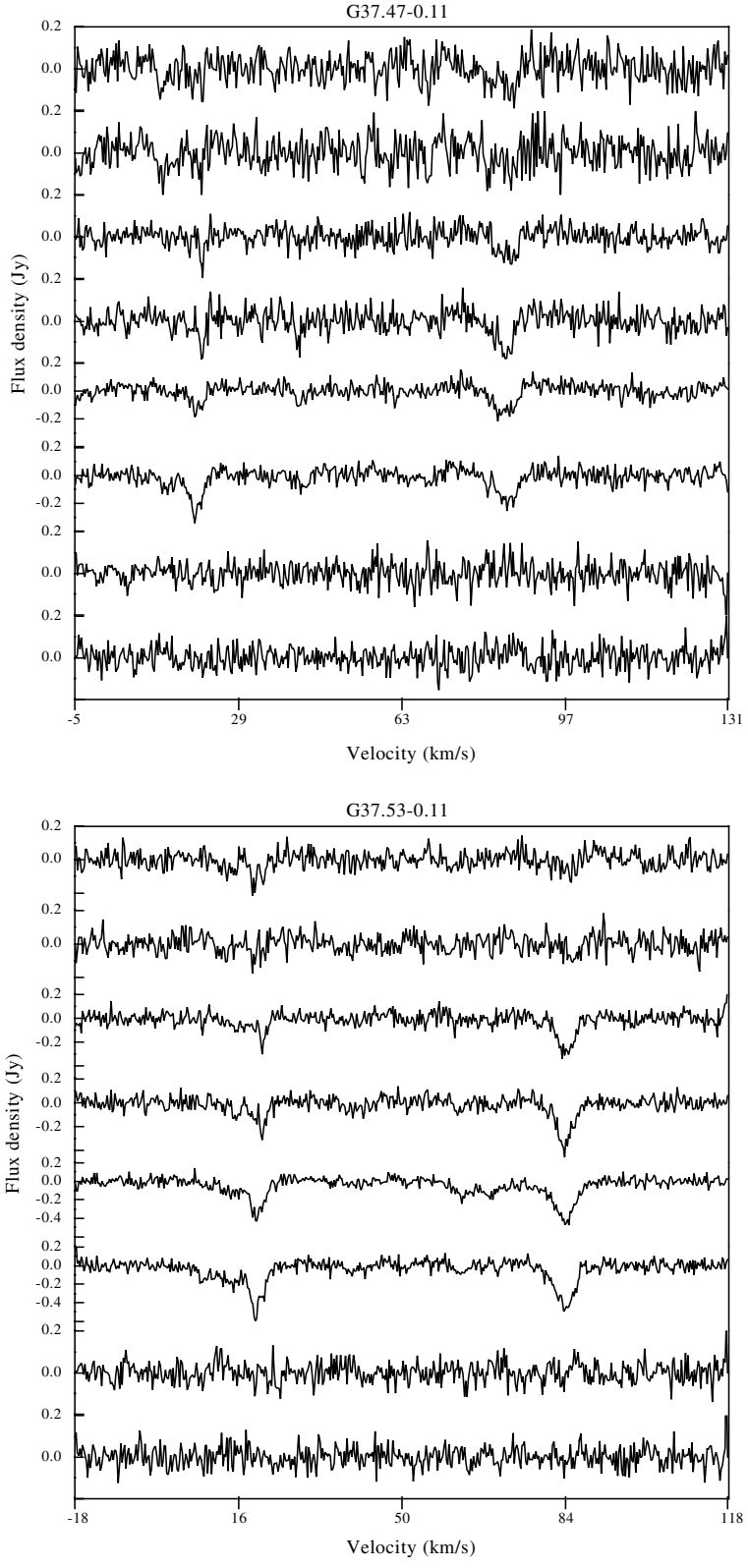

Fig. A.1. continued.

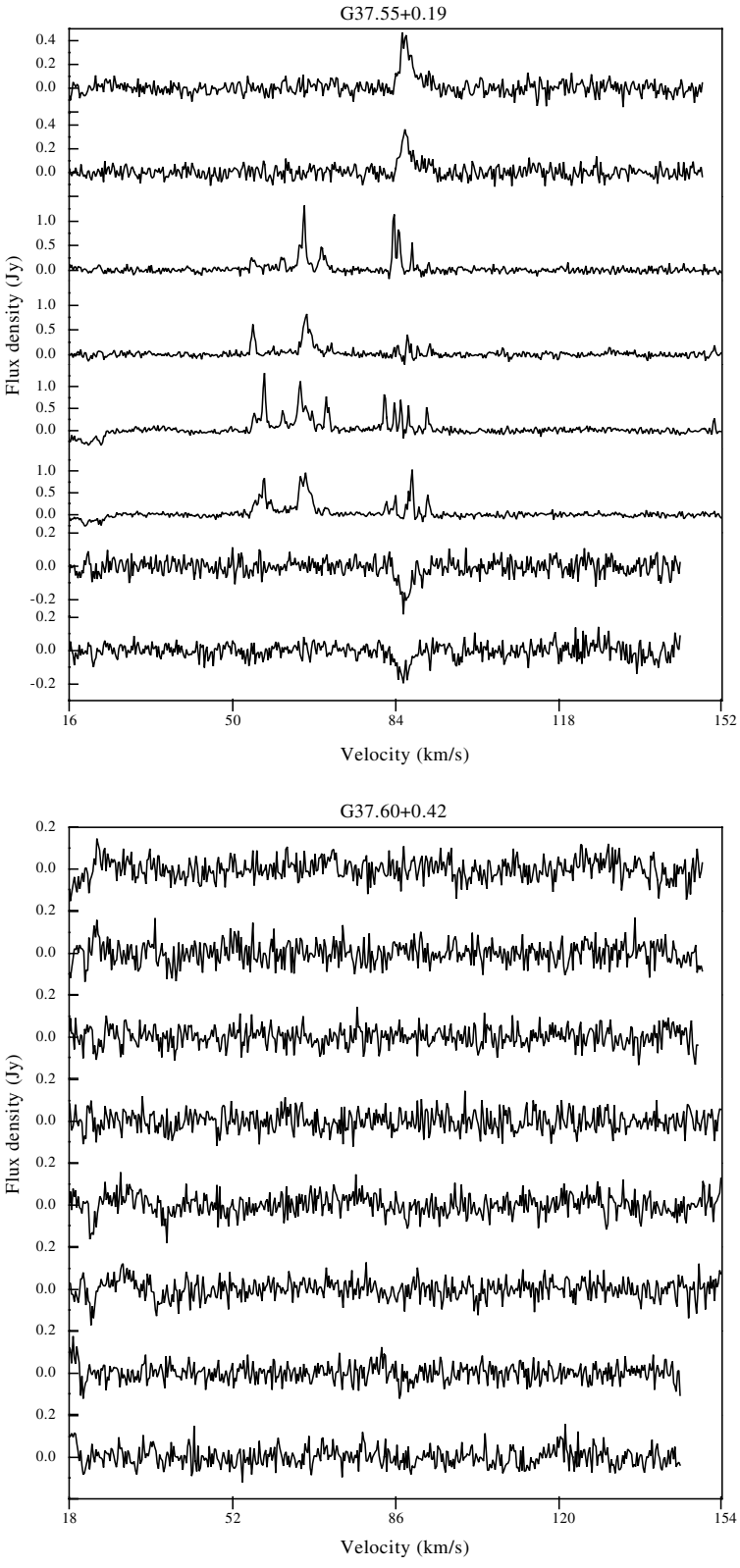

Fig. A.1. continued.

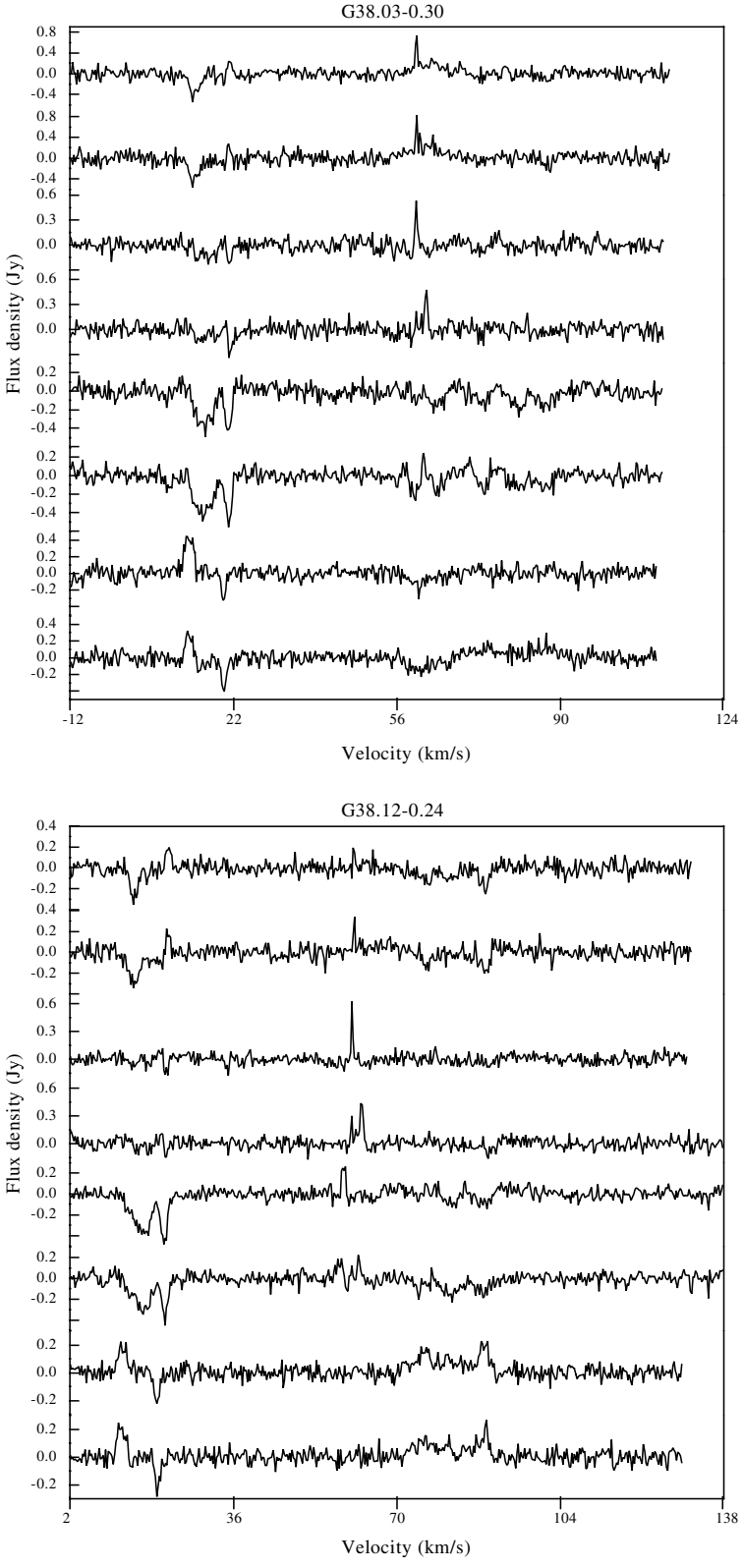

Fig. A.1. continued.

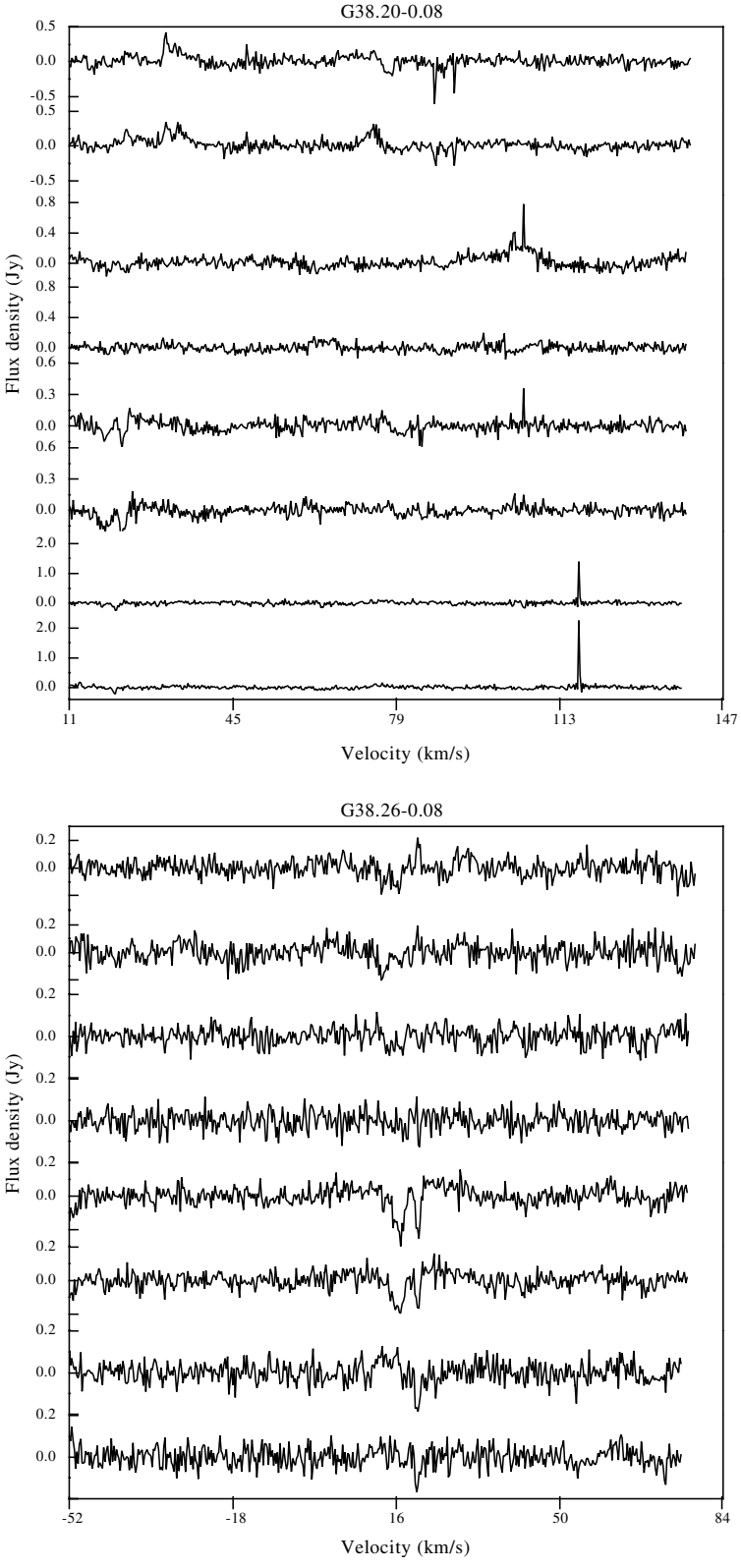

Fig. A.1. continued.

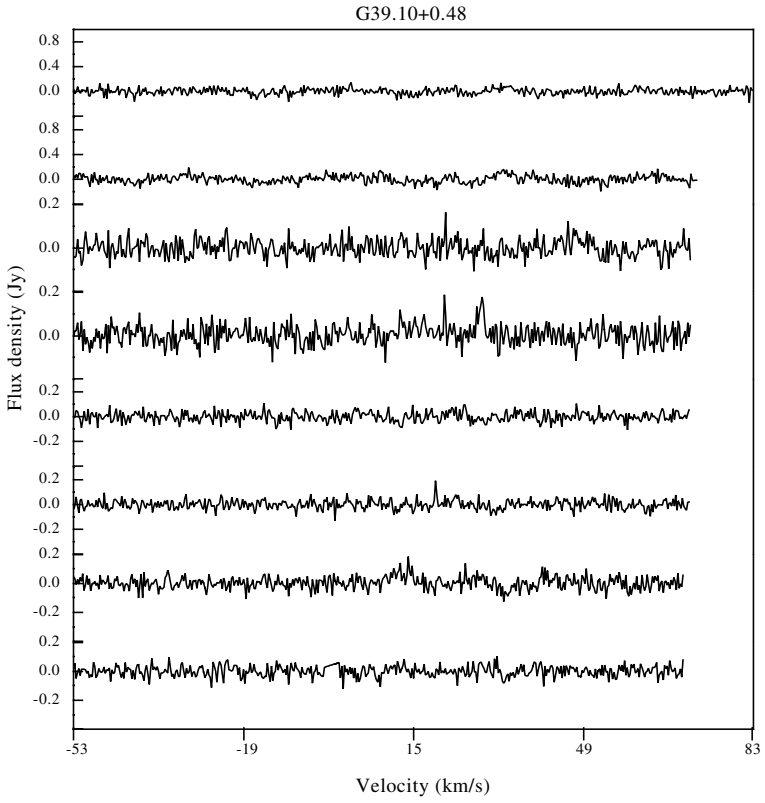

Fig. A.1. continued.